



TESIS TK092305

**PREPARASI DAN KARAKTERISASI 'FEW-LAYER  
MoS<sub>2</sub> NANOSHEETS'**

MOHAMMAD SHOLEH

2313201909

DOSEN PEMBIMBING

Dr. Ir. KUSWANDI, DEA

Prof. MING-HSI CHIANG

PROGRAM MAGISTER

BIDANG KEAHLIAN TEKNOLOGI PROSES

JURUSAN TEKNIK KIMIA

FAKULTAS TEKNOLOGI INDUSTRI

INSTITUT TEKNOLOGI SEPULUH NOPEMBER

SURABAYA

2015



THESIS TK092305

**PREPARATION AND CHARACTERIZATION OF  
FEW-LAYER MoS<sub>2</sub> NANOSHEETS**

MOHAMMAD SHOLEH

2313201909

SUPERVISOR

Dr. Ir. KUSWANDI, DEA

Prof. MING-HSI CHIANG

MASTER PROGRAM

PROCESS TECHNOLOGY

CHEMICAL ENGINEERING DEPARTMENT

FACULTY OF INDUSTRIAL TECHNOLOGY

INSTITUT TEKNOLOGI SEPULUH NOPEMBER

SURABAYA

2015

## MASTER THESIS RECOMMENDATION FORM

In partial fulfillment of the requirements for the degree of master engineering

In

Institut Teknologi Sepuluh Nopember

By:

MOHAMMAD SHOLEH

Student I.D. No. : 2313 201 909

Examination Date : July 10<sup>th</sup>, 2015

Graduation Period : September 2015

Approved by:

1. Prof. Ming-Hsi Chiang (Advisor/Examination Committee)
2. Prof. Shawn D. Lin (Co-advisor/Examination Committee)
3. Prof. Ling-Kang Liu (Examination Committee)

Director of Postgraduate Program  
Institut Teknologi Sepuluh Nopember



Prof. Dr. Ir. Adi Suprijanto, M.T.

NIP. 0064104 05 1990 02 1001



M10306821

Thesis Advisor: Shawn D. Lin



# 碩士學位考試委員會審定書

## Qualification Form by Master's Degree Examination Committee

Department: Department of Chemical Engineering

Student's Name: MOHAMMAD SHOLEH

Thesis Title:

Preparation and Characterization of few-layer MoS<sub>2</sub> Nanosheets

This is to certify that the dissertation submitted by the student named above, is qualified and approved by the Examination Committee.

### Degree Examination Committee

Members' Signatures:

林昇陽

江明銘

劉凌崗

Advisor:

林昇陽

江明銘

Program Director's Signature:

陳華炎

Department/Institute Chairman's Signature:

Date: 2015 / 07 / 10 (yyyy/mm/dd)

# Preparation and Characterization of Few-layer MoS<sub>2</sub> Nanosheets

Name : Mohammad Sholeh (2313201909)

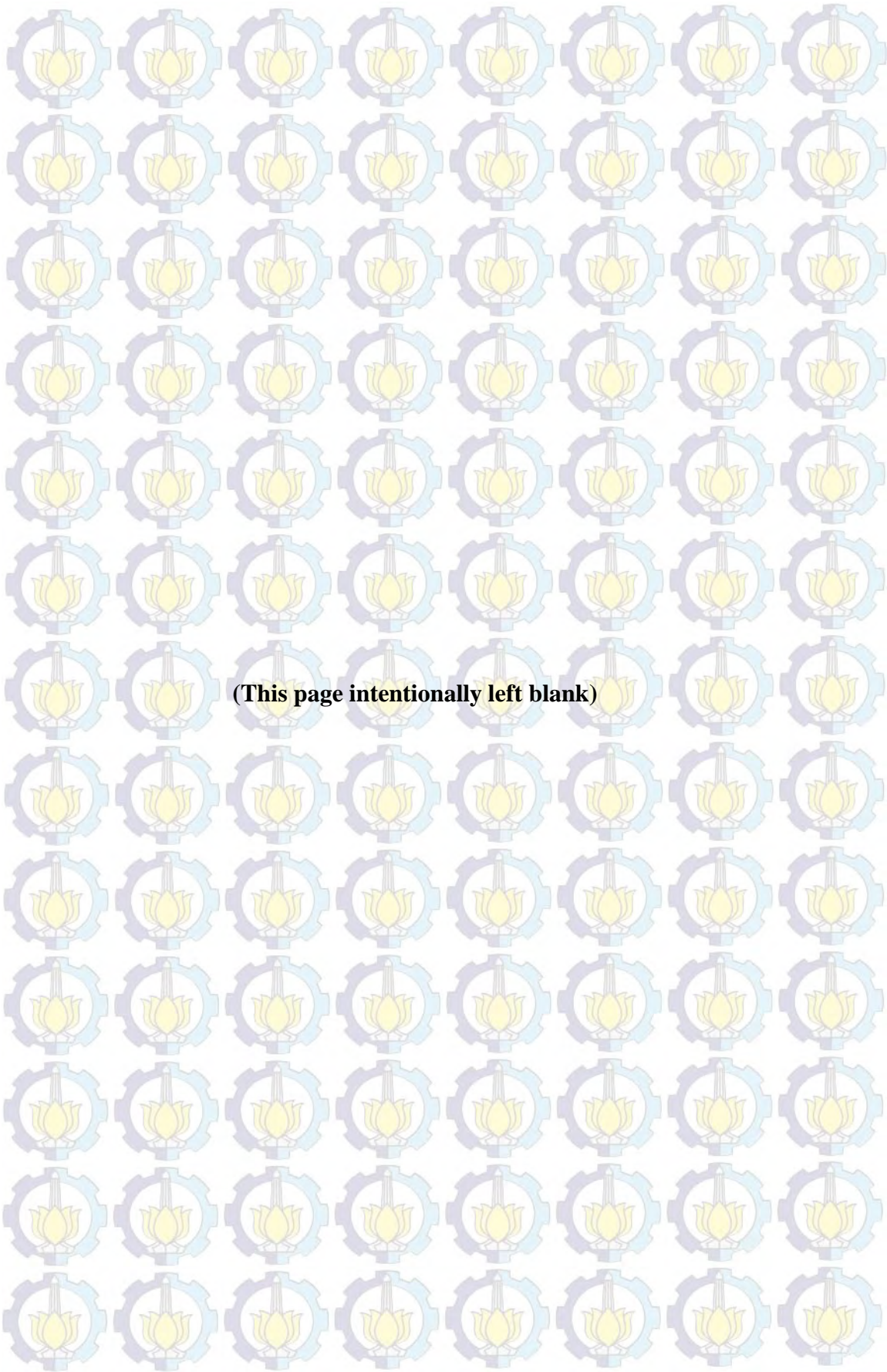
Department : Teknik Kimia FTI-ITS

Supervisor : Dr. Ir. Kuswandi, DEA  
Prof. Ming-Hsi Chiang

## ABSTRACT

*Exfoliation of bulk MoS<sub>2</sub> via Li intercalation is an attractive route to large-scale preparation of MoS<sub>2</sub> few-layers and it can be used to realize their unique properties in practical applications. In general, solution-based exfoliation of layered materials results in flakes with lateral sizes of one micron or less on average. In this report, we performed the various preparations using a Li-intercalation method at room temperature to prepare MoS<sub>2</sub> few-layers with various flake sizes according to dynamic light scattering (DLS) analysis. MoS<sub>2</sub> few-layers with particle sizes ranging 85 to 145 nm are reported. We also characterize the few-layer MoS<sub>2</sub> nanosheets by various microscopic and spectroscopic techniques.*

**Keyword :** MoS<sub>2</sub>, nanosheets, , intercalation, exfoliation.



**(This page intentionally left blank)**

## Preparasi dan karakterisasi 'Few layer MoS<sub>2</sub> Nanosheets'

Nama : Mohammad Sholeh (2313201909)

Jurusan : Teknik Kimia FTI-ITS

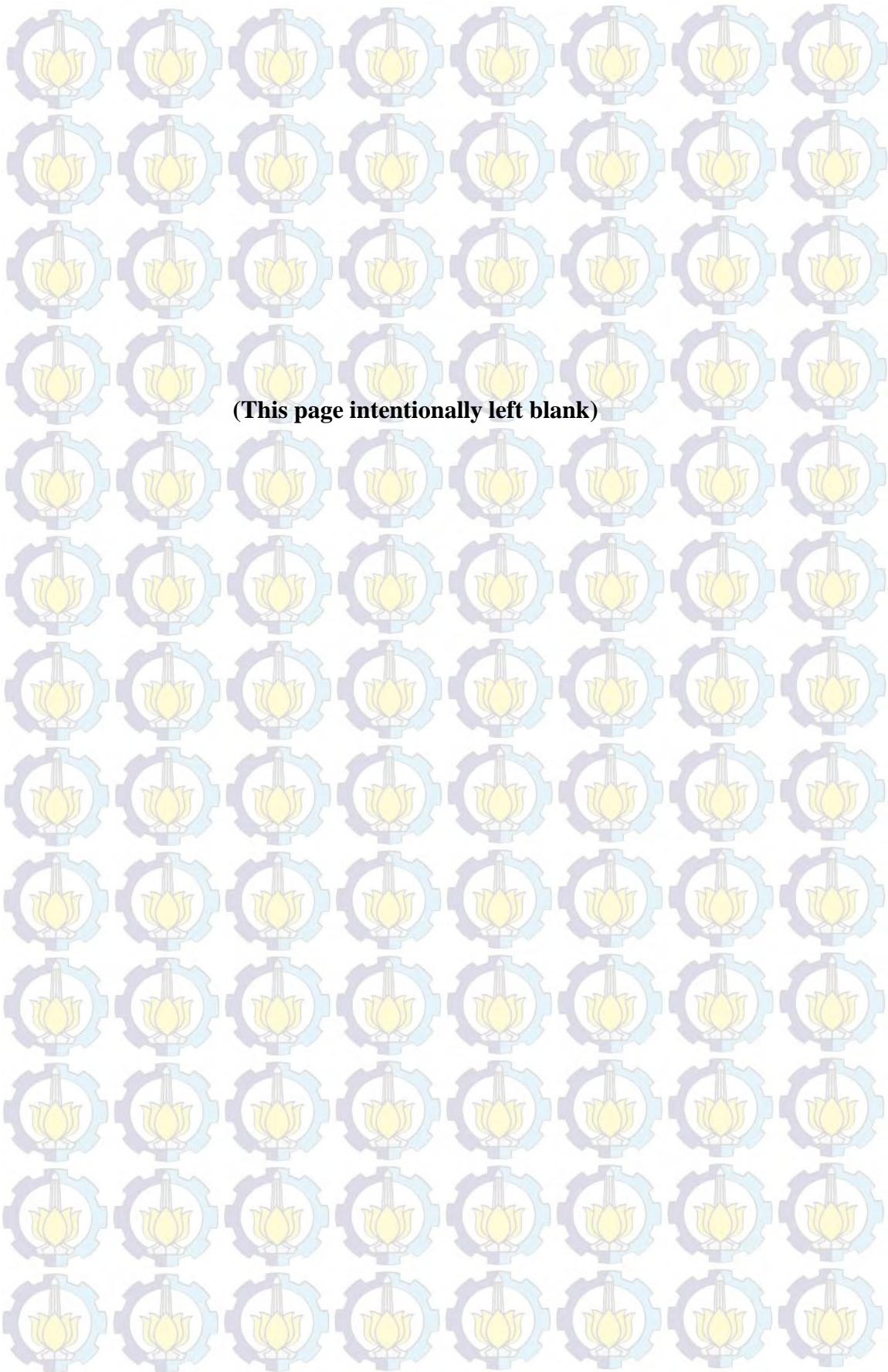
Pembimbing : Dr. Ir. Kuswandi, DEA

Co-Pembimbing : Prof. Ming-Hsi Chiang

### ABSTRAK

Pengelupasan *bulk MoS<sub>2</sub>* dengan menggunakan metode interkalasi lithium adalah metode yang menarik untuk preparasi *MoS<sub>2</sub> few-layers* dalam skala besar dan dapat digunakan untuk merealisasikan porperti-properti unik dari *MoS<sub>2</sub> few-layers* dalam aplikasi nyata. Pada umumnya, pengelupasan material berlapis yang didasarkan pada pengelupasan dengan menggunakan larutan menghasilkan serpihan dengan ukuran satu mikrometer atau masih jauh dari rata-rata. Di laporan ini, kita menunjukkan macam-macam preparasi nanosheet dengan menggunakan metode interkalasi lithium pada temperatur ruang untuk menyiapkan *MoS<sub>2</sub> few-layers* dengan variasi ukuran serpihan berdasarkan analisa *dynamic light scattering* (DLS). *MoS<sub>2</sub> few-layers* yang kita peroleh mempunyai ukuran dengan range 85-145 nm. Kita juga melakukan karakterisasi terhadap *MoS<sub>2</sub> few-layers* dengan menggunakan berbagai teknik mikroskopik dan spektroskopik.

**Kata kunci:** MoS<sub>2</sub>, Nanosheets, Interkalasi, Pengelupasan.



**(This page intentionally left blank)**



## ACKNOWLEDGEMENT

All Praises to Allah SWT who has given His blessing and guidance so that I can finish this research. I would like to express my deepest thanks to my mother Sriyati, my father Karsidi, my younger sister Desy Retno Juwita, and all of my family members. I got a lot of guidance, encouragement, and great support from them at the time I felt down. Their support have given me the spirit to continue and finish my thesis.

I sincerely thank Prof. Ming-Hsi Chiang for his wise guidance and useful advice during my dual degree study at National Taiwan University of Science and Technology (NTUST) and research at Institute of Chemistry, Academia Sinica. Also I sincerely thank Prof. Shawn D. Lin and Prof. Ling-Kang Liu for kindly serving on my thesis graduate committee and I would like to thank them for providing valuable input and comments on my work. I would like to thank to Dr. Ir. Kuswandi, DEA, as my advisor at Sepuluh Nopember Institute of Technology (ITS-Indonesia) and Prof. Dr. Ir. Gede Wibawa, M.Eng, as the head of thermodynamics laboratory in ITS for their guidance and support during my master degree study at ITS and NTUST. I have learned a lot of things and got a lot of knowledge, information, and everything about science, especially in thermodynamics from all of them. I also thank Dr. Joyce Liu as postdoctoral in Bio-inorganic laboratory (Chiang's lab) Institute of Chemistry, Academia Sinica for the sharing, cooperation, and support during my research.

I earnestly thank to Prof. Ir. Renanto, M.Sc, Ph.D. as chairman of chemical engineering Graduate Study Program at ITS and Prof. Jhy-Chern Liu as chairman of Chemical Engineering Department at NTUST and also Elyse Huang as Administrative personnel for their help since I have taken entrance administration and registration of dual degree program. I would like to thank Ms. Chung, Mei-Ying and Mr. Chiao-Wei Tseng for having provided me with the microscopy facilities and equipment which enabled me to carry out the research work.

Special thanks to my labmates Sunny who help me in everything and support to keep me focused and motivated on my research work and special for

helping me in doing synthesis. And Finally, I thank to all of my lab mates at Chiang's group, James, Agus Riyanto, Sebastianus Adip, Ivy, Elphis shu, Chris, Kai-Ti Chu, Grace, Mars, and my new labmates Adhya from Hindia that always supports and gives suggestion to improve my research. And my friend that also research in Institute of Chemistry, Academia Sinica from Indonesia Ade Sonya, Devi Wahyuningtyas, Prestika, Nia Nurfitri, Dianita, Albertus Andrian, Victor Purnomo for their help, and all of my lab mates at thermodynamics laboratory ITS, Stella Veronika, Didik Agus, Wiryawan, Faris Alnafi, Iqwal Zulfetra, Firda Nuharani, Rizki Aulia Rahman, Asti And Also special thanks to Asalil Mustain and Rizqy Romadona Ginting that always support and give me suggestion, information about thermodynamic area and for all whom I cannot mention one by one for their warm supports and sharing during my master degree study.

## TABLE OF CONTENTS

APPROVAL SHEET .....	i
ABSTRAK .....	iii
ABSTRACT .....	v
ACKNOWLEDGEMENT .....	vii
TABLE OF CONTENTS .....	ix
LIST OF FIGURES .....	xi
LIST OF TABLES .....	xiii
CHAPTER 1 .....	1
1.1 Research Background .....	1
1.2 Previous Studies .....	3
1.3 Problem Statement .....	5
1.4 Research Objective .....	5
1.5 Research Organization .....	5
CHAPTER 2 .....	7
2.1 Bulk Molybdenum Disulfide .....	7
2.2 Exfoliation of Molybdenum Disulfide .....	9
2.3 Exfoliated Molybdenum Disulfide .....	10
2.4 Properties of Molybdenum Disulfide .....	10
2.5 Potential Applications of Intercalation-Exfoliated Nanosheets .....	13
CHAPTER 3 .....	15
3.1 Synthesis .....	15
3.1.1 Materials .....	15
3.1.2 Preparation of MoS <sub>2</sub> nanosheets .....	15

3.2.3 Preparation of few-layers MoS <sub>2</sub> with specific flakes dimension.....	16
3.2 Characterization Method.....	17
CHAPTER 4.....	19
4.1 Intercalation of Lithium.....	19
4.2 Exfoliation of Molybdenum disulfide.....	22
4.3 Few-layer Molybdenum disulfide with Specific Flake Dimensions. ....	33
CHAPTER 5.....	43
REFERENCES.....	45
APPENDIX A.....	55
APPENDIX B.....	59





## LIST OF TABLES

**Table 4.1.** Summary of EDS-SEM analysis from different method .....37

**Table A.1.** Summary of zeta potential in each of experiments ..... 55

**Table A.2.** The frequency difference ( $\Delta k$ ) of MoS<sub>2</sub> nanosheets as the function of layer number.....56

# CHAPTER 1

## INTRODUCTION

### 1.1 Research Background

In recent decades, nanomaterials have attracted major attentions due to their fascinating properties and wide ranges of applications. There are two categories of nanomaterials: organic (mostly carbon allotropes) and inorganic nanomaterials, such as iron, silver, gold, boron nitride nanosheets (BNNs), molybdenum disulfide ( $\text{MoS}_2$ ), tungsten disulfide ( $\text{WS}_2$ ), etc. Inorganic nanomaterials, especially two-dimensional (2D) nanomaterials, have received tremendous attention in recent years because of unique both chemical and physical properties. The two-dimensional nanomaterials have completely different properties compared to the bulk materials (the quintuple layers). These properties includes high surface areas, mobility, conductivity, mechanical strength, transparency, electronics and optoelectronics. As one of the 2D nanomaterials, molybdenum disulfide possesses a sandwich structure which consist of covalent bonds in S-Mo-S structures that form by weak Van Der Waals forces between sheets. Therefore, it is probably easy to peel  $\text{MoS}_2$  nanosheets from bulk material (Novoselov et al., 2005). Bulk  $\text{MoS}_2$  is a semiconducting material with an indirect band gap of about 1.2 eV. When layered  $\text{MoS}_2$  pristine is peeled to single-layer, it become a semiconductor with 1.8 eV direct band gap (Wang et al., 2012a, Yoon et al., 2011). The wide band gap, which is thickness-dependent (bulk to single-layer), makes  $\text{MoS}_2$  a promising candidate for many applications, such as electronic devices (Choi et al., 2013), optoelectronic devices (Yin et al., 2012, Lopez-Sanchez et al., 2013, Fontana et al., 2013, Yu et al., 2013a), sensors (Zhang et al., 2014), and energy storage devices, like lithium ion batteries (LIB) (Park et al., 2013, Zhou et al., 2014, Li et al., 2015, Su et al., 2015), sodium ion batteries (SIB) (Bang et al., 2014), and capacitors (Cao et al., 2013). The other applications, which have become hot topics until now are utilization and optimization of exfoliated  $\text{MoS}_2$  in either hydrogen evolution reaction (HER) (Ji et al., 2013, Lukowski et al., 2013, Voiry et al., 2013) or water splitting (Yin et al., 2014,

Singh et al., 2015). If MoS<sub>2</sub>-based catalysts are to actualize their potential, there is an important need to increase the numbers of active sites and the catalytic activity by changing their electronic properties and conductivity via exfoliation of MoS<sub>2</sub> from bulk materials to nanosheets (Lukowski et al., 2013). And also the size of nanosheets is an important factor in the hydrogen evolution reaction (HER) (Varrla et al., 2015).

Recently, several methods have been reported for synthesizing single- and multi-layer MoS<sub>2</sub>. In the synthesis of 2D nanomaterials, the synthetic routes can be divided into two fundamental categories. First, top-down methods use the external energy (mechanical or ultra-sound energy) as main sources to achieve the exfoliated nanomaterials. Second, bottom-up methods are via deposition of atoms in either thermal or chemical reactions on a substrate to synthesize exfoliated 2D nanomaterials (Das et al., 2014). Until now, single-, few- and multi-layer MoS<sub>2</sub> have all been prepared by both methods. For the top-down methods, there are the mechanical exfoliation method (Lee et al., 2014, Li et al., 2014), chemical lithium intercalation and exfoliation using *n*-butyllithium (Chou et al., 2013, Xiao et al., 2010), electrochemical lithium intercalation and exfoliation (You et al., 2014), liquid phase exfoliation using solvent and surfactants (Coleman et al., 2011b), (Gupta et al., 2015) and synthesis of MoS<sub>2</sub> nanosheets via shear exfoliation (Varrla et al., 2015). For the bottom-up methods, they include the thermal chemical vapor deposition (CVD) (Zhang et al., 2011, Liu et al., 2013a) and synthesis of MoS<sub>2</sub> nanosheets via hydrothermal reaction (Ma et al., 2012, Liu et al., 2013b, Liu et al., 2014, Ye et al., 2014). Recently, many researchers made good quality MoS<sub>2</sub> monolayers using a chemical vapor deposition (CVD) or a Scotch tape-based micromechanical exfoliation method. However, a low yield is generally achieved in the Scotch tape method and a high temperature and cost of instruments are required for experiments in the CVD method. Coleman et al. reported direct exfoliation of MoS<sub>2</sub> sheets with thickness of 3–12 nm and the lateral nanosheets size of 0.1–2 μm in organic solvents through sonication (Coleman et al., 2011b). However this method leads to a low yield and the major issue is that specific nanosheet sizes cannot be obtained. It is essential for various applications. For

example, composite reinforcement requires large nanosheets (May et al., 2012) at least around 2  $\mu\text{m}$  in length, whereas a catalyst of hydrogen production requires small nanosheets with lateral size or length below 100 nm (Jaramillo and Horch, 2007). Significance of this work focuses on synthesis of few-layer  $\text{MoS}_2$  nanosheets with specific lateral size via the lithium intercalation method and characterization of the material, even though some research on the intercalation of alkali metals into bulk  $\text{MoS}_2$  has been reported (Somoano et al., 1973, Somoano and Woollam, 1979, Lacaze et al., 1997, Hara et al., 1990).

Nanotechnology and its applications are expanding in academic research and also moving into industry in recent years. The development in this area is supported by technological advancement, such as microscopy and spectroscopy. The microscopic images help us understand the morphology of nanomaterial, like lateral size, thickness, lattice, and the diffraction pattern with high resolution. The spectroscopic instruments include Raman spectroscopy, X-ray photoelectron spectroscopy, UV-vis spectroscopy, and Photoluminescence spectroscopy, which help us characterize nanomaterials, like lattice vibration of nanomaterial and excitation of electron.

## 1.2 Previous Studies

Joensen and co-workers (Joensen, 1986) have conducted experiments to prepare monolayer  $\text{MoS}_2$  via the lithium intercalation using *n*-butyl lithium dissolved in hexane. In this method, the intercalation process would be an important step because of the formation of  $\text{Li}_x\text{MoS}_2$  compound. This process can be tuned to control the yield of monolayers  $\text{MoS}_2$ . The X-ray diffraction was used to distinguish single-, bi-, tri-, and quadratic-layer of  $\text{MoS}_2$ .

Benevante and co-workers (Benevante et al., 2002) reported the successful preparation of  $\text{MoS}_2$  nanosheets using *n*-butyl lithium as the intercalating agent and also demonstrated the influences of quasi-equilibrium voltage-composition to the number of lithium inserting into 2H- $\text{MoS}_2$  (semiconducting phase of  $\text{MoS}_2$  with trigonal prismatic coordination) (Figure 2.1). Electrochemical behavior, spectroscopy and structural features, crystal structures of single-layers and



restacked MoS<sub>2</sub> were also studied. The main advantage of the lithium intercalation method is its ability to access the metallic phase (1T-MoS<sub>2</sub>) with octahedral coordination phase that is induced through charge-transfer from *n*-butyl lithium to MoS<sub>2</sub> sheets and thus the semiconducting to the metallic phase occurs.

Ambrosi and co-workers (Ambrosi et al., 2015) studied the influences of various kinds of the lithium intercalation compound on electrochemical properties of exfoliated MoS<sub>2</sub>. In this work, they used methyl lithium (Me-Li), *n*-butyl lithium (Bu-Li), and *t*-butyl lithium. The *n*-Bu-Li, and *t*-Bu-Li are more efficient than Me-Li. Based on both Raman and XPS spectra results, smaller lateral sizes and numbers of layers can be produced. Larger current signals (per unit mass) in KCl electrolyte are observed in electrochemical measurements, suggesting they are promising for the applications in rechargeable batteries and good energy storage.

Liu and co-workers (Liu et al., 2014) demonstrated the preparation of MoS<sub>2</sub> nanosheets with lithium hydroxide (LiOH) dissolved in ethylene glycol via hydrothermal exfoliation. (The materials are used as anode materials in lithium ion batteries (LIB)). This process uses lithium ion (Li<sup>+</sup>) for intercalating into MoS<sub>2</sub> layers to form Li<sub>x</sub>MoS<sub>2</sub>. It exhibited a good initial capacity of 1190 mAh/g and cyclic stability at constant current density of 50 mA/g and also still delivered reversibly sustained high capacity of 750 mAh/g after 50 cycles.

Wang and co-workers (Wang et al., 2013) demonstrated the continuous tuning of layer vertically aligned MoS<sub>2</sub> nanosheets through electrochemical intercalation of lithium ion (Li<sup>+</sup>) to different voltages vs. Li<sup>+</sup>/Li in nanofilms with perpendicular to the substrates and its application for electrochemical hydrogen evolution reaction (HER). So, the formation of Li<sub>x</sub>MoS<sub>2</sub> and the reaction process can be tuned to control the characteristic and yield of nanosheets. The layer spacing changes, oxidation state, and the ratio of semiconducting to metallic phase due to their electron transfer from Li<sup>+</sup> to MoS<sub>2</sub> layer were also studied. This paper mentioned that increasing the molar ratio of lithium in Li<sub>x</sub>MoS<sub>2</sub> caused rearrangement of the atomic structure of MoS<sub>2</sub> from 2H semiconducting to 1T metallic phase. Related to hydrogen evolution reaction, HER activities are already

enhanced along with the lowered oxidation states of Mo before transformation of semiconducting to metallic phase occurs.

### **1.3 Problem Statement**

As described previously, exfoliation of layered material via lithium intercalation method is considered as a useful method for preparation of discrete dimension of layered materials. The unique properties of MoS<sub>2</sub> nanosheets have attracted many researcher's interests in recent years to seek its applications on the lithium ion batteries (LIBs) and evolution of hydrogen. The nanosheet sizes are very important with respect to the catalytic performance. The development of nano-sized sheets as electrocatalysts for hydrogen production is a challenge for researchers. In this work we simultaneously solve that problem. We demonstrated the preparation of MoS<sub>2</sub> nanosheets with specific flake dimensions via the lithium intercalation method at room temperature with low cost, we will extend their use in applications of either LIBs or HER.

### **1.4 Research Objective**

The objective of this study is to synthesize few-layer MoS<sub>2</sub> nanosheets via lithium intercalation method with simple experiments. Their morphology, flake dimensions, and thickness are characterized. The results are compared with the previous ones.

### **1.5 Research Organization**

This thesis is divided into five parts which is organized as follows:

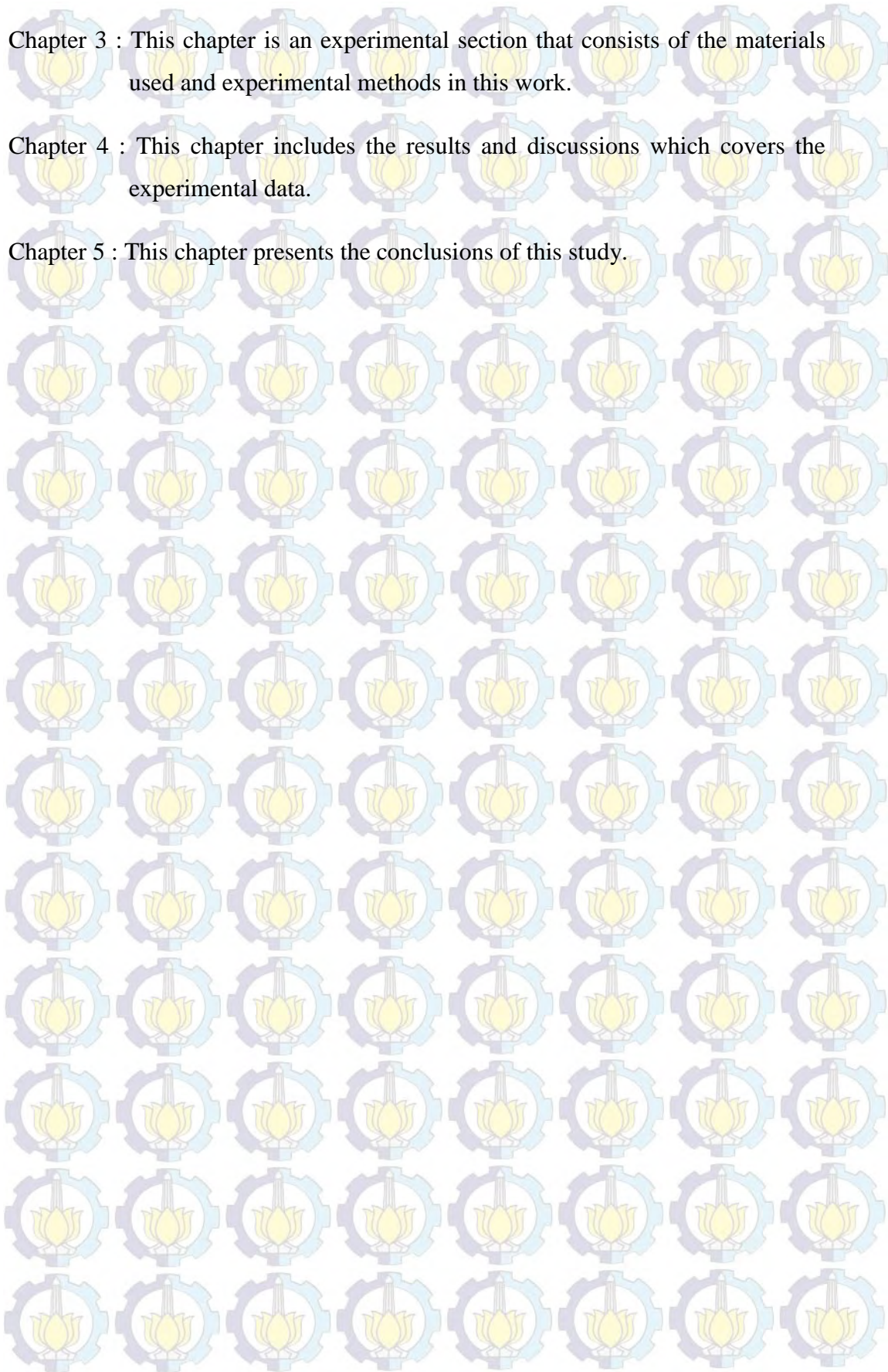
Chapter 1 : This chapter gives an introduction that provides the background of the research, previous studies, problem statement, and the objective of this study.

Chapter 2 : This chapter provides an introduction to molybdenum disulfide that presents a brief explanation about characteristics of molybdenum disulfide and potential applications of intercalation-exfoliated nanosheets.

Chapter 3 : This chapter is an experimental section that consists of the materials used and experimental methods in this work.

Chapter 4 : This chapter includes the results and discussions which covers the experimental data.

Chapter 5 : This chapter presents the conclusions of this study.





## CHAPTER 2

### INTRODUCTION TO MOLYBDENUM DISULFIDE

#### 2.1 Bulk Molybdenum Disulfide

Molybdenum disulfide ( $\text{MoS}_2$ ) in the bulk is a semiconductor that occurs naturally as the molybdenum or molybdenite. Molybdenum disulfide belongs to the family of transition metal dichalcogenides (TMDs), or a compound with the general chemical formula  $\text{MX}_2$ , where M is a transition metal and X is a chalcogen (S, Se or Te). These materials tend to have a highly anisotropic structure formed by two dimensional sheets weakly held together by Van Der Waals interactions. Each sheet consist of a central layer of M atoms sandwiched between two layers of X atoms. Therefore, it is probably easy to peel monolayer sheets from bulk material.

In general, the transition metals in TMDs ( $\text{MX}_2$  structure) have three kinds of crystal structure, 1T (Tetragonal symmetry), 2H (Hexagonal symmetry), and 3R (Rhombohedral symmetry) (see Figure 2.1). The formed tend to be semiconductors, like  $\text{MoS}_2$ , while the letter exhibit metallic behavior.

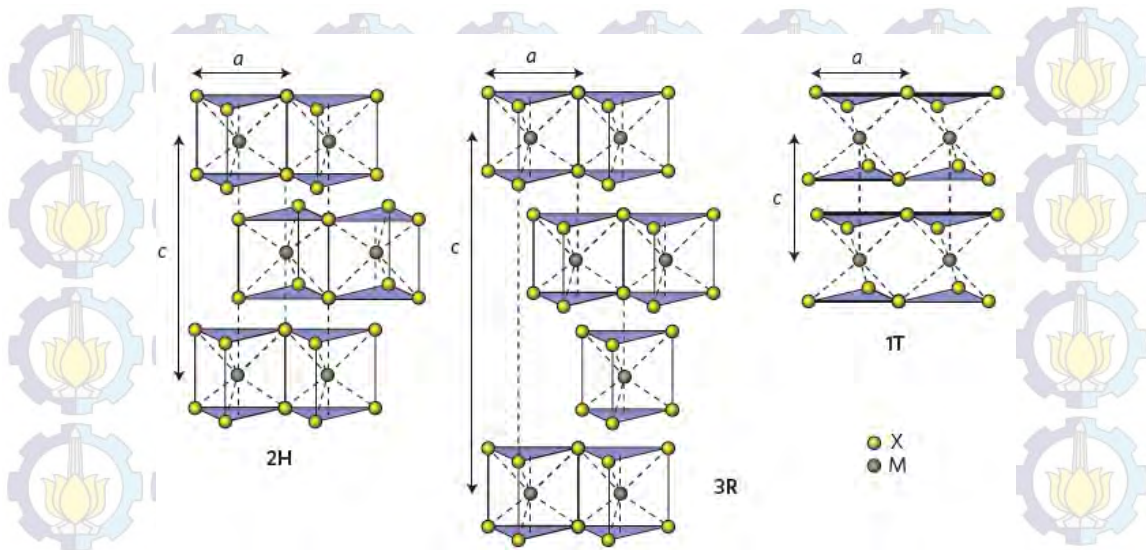


**Figure 2.1.** Schematics illustration of the structural polytypes in TMDs, with the chalcogen atoms (X) in yellow and the metal atoms (M) in grey: 2H (hexagonal symmetry, two layers per unit cell, trigonal prismatic coordination), 3R (rhombohedral symmetry, three layers per unit cell, trigonal prismatic coordination) and 1T (tetragonal symmetry, one layer per unit cell, octahedral coordination). The lattice constants  $a$  are in the range 3.1 to 3.7 Å for different materials, The stacking index  $c$  indicates the number of layers in each stacking order, and the interlayer spacing is  $\sim 6.5$  Å. (Adapted from Wang et al. Nature Nanotechnology, 2012).

In the  $\text{MoS}_2$  bulk also has three main polytypes of crystal structure: 1T, 2H and 3R, with 2H being the most stable form. This structure consists of the stacked trilayer structure with every 2 stacks offset such that two  $\text{MoS}_2$  trilayers are included in the unit cell. The Van Der Waals gap, the (002) plane, has a spacing of around 0.6 nm (Figure 2.2A). In addition, the Mo atoms have trigonal prismatic coordination relative to the S atoms, this gives rise to a hexagonal structure when viewed along the  $c$  axis (normal to layers) (Figure 2.2B). The characteristic spacing of the (100) plane in the hexagonal lattice is 0.26 nm and 0.16 nm for the (110) plane. The covalent bonding results in an oxidation state of +4 for the Mo unit and -2 for each sulfur atom.

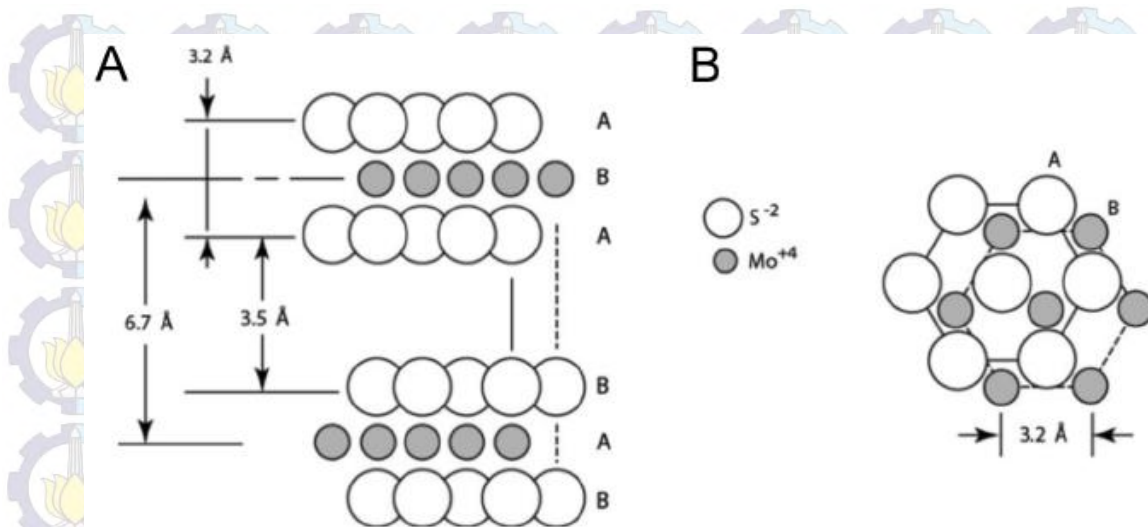


**Figure 2.2.** (A) Bulk MoS<sub>2</sub> observed parallel to basal plane shows stacked trilayer structure. (B) Perpendicular to the basal plane the trigonal crystal structure can be observed. (Adapted from W. G. S. B. C. Windom, and D. W. Hahn, Tribology Letters, 2011).

An interesting feature of many MX<sub>2</sub> compounds is that the layers can be separated through a procedure known as *exfoliation*. For example, when lithium (Li) is intercalated into MoS<sub>2</sub> layers, the Li atoms move into the crystal from the edges and diffuse in between the layers to form a compound Li<sub>x</sub>MoS<sub>2</sub>, where x is typically close to 1 (Joensen, 1986). In the intercalated materials, the coordination of the Mo atom changes from trigonal prismatic to octahedral, (Py and Haering, 1983) and thus the MoS<sub>2</sub> changes from semiconducting to metallic (Lin et al., 2014).

## 2.2 Exfoliation of Molybdenum Disulfide

The Scotch-tape based on mechanical exfoliation made famous because graphene, has also been applied to MoS<sub>2</sub>. A bulk crystal is cleaved with adhesive tape repeatedly over a substrate, with single and few layers settling on the surface. The fragments or layers will be of different layer heights and lateral sizes, so this technique is not suited for producing uniform nanostructures on a large scale. This method involves locating a single nanostructure of interest on the substrate and micro-fabricating measurement electronics around it. Exfoliation of nanomaterial can be achieved by intercalation of lithium (Joensen, 1986). The MoS<sub>2</sub> is soaked

in a lithium containing solution for several hours to saturate the interlayer gaps, then exposed to water. The hydrolysis reaction produces hydrogen gas which causes the exfoliation. The suspension of few layer nanosheets can be produced in the presence of a support such as alumina to generate industrial catalyst material.

### 2.3 Exfoliated Molybdenum Disulfide

Preparation of single-layers has become increasingly in recent years. A simple mechanical exfoliation technique has been explored to prepare single-layer of MoS<sub>2</sub> (Splendiani et al., 2010). The robust enhancement of photoluminescence from few-layer to single layer of MoS<sub>2</sub> allows single-layer regions to be identified by optical microscopy. The robust enhancement is caused by a transition from an indirect bandgap of 1.3 eV from bulk material to a direct bandgap of about 1.83 eV in single-layer of MoS<sub>2</sub> (King et al., 2013, Geim and Grigorieva, 2013, Wang et al., 2012b). From single-layer to bilayer, the bandgap goes from the direct transition of 1.83 eV to indirect one of 1.6 eV (Mak et al., 2010). However from bilayer to hexa-layer, the bandgap changes slowly from 1.6 to 1.4 eV (Mak et al., 2010). Increasing to original multiple layers changes bandgap ultimately to 1.3 eV (Mak et al., 2010). Therefore, the value of the indirect bandgap depends on the number of layers within nanosheets. The simplicity of fabrication and analysis, as well as the high impact from such a novel material has made their study attractive. As graphene, single and few-layer of MoS<sub>2</sub> nanosheets were also produced by lithium intercalation.

### 2.4 Properties of Molybdenum Disulfide

**Crystal structure.** Layered molybdenum disulfide is made of stacked plane of covalently bonded Mo and sulfur atoms, and the neighboring layers are connected by weak Van Der Waals interactions. There are three main polytypes of bulk crystal structure: 1T (tetragonal symmetry, one layer per repeat unit, octahedral coordination), 2H (hexagonal symmetry, two layers per repeat unit, trigonal prismatic coordination) and 3R (rhombohedral symmetry, three layers per repeat unit, trigonal prismatic coordination), where 2H is the most stable form in nature. Powder X-ray diffraction and TEM are direct method to study the crystal structure, and TEM can be used to study additionally the morphology of MoS<sub>2</sub>.

However, we only can use TEM to identify the difference of diffraction pattern of single- and few-layer MoS<sub>2</sub>. As we know that the 2H can transformed to 1T phase through lithium intercalation method. The lattice symmetry changes from 2H to 1T phase is followed by the change of density of state (DOS). Thus MoS<sub>2</sub> changes from the semiconducting (2H) to metallic (1T) phase (F. Wypych and R. Schollhorn, 1992).

**Mechanical properties.** Pristine graphene is one of strongest material that has been measured before, with having a breaking strength of 42 N/m and the Young's modulus of 1000 GPa (Huang et al., 2011). Therefore, it is to be a great interest and importance to examine the mechanical properties of the other 2D layered nanomaterials. Castellanos-Gomez *et al.* have measured the elastic properties of freely suspended exfoliated MoS<sub>2</sub>, which have thickness ranging from 5 to 25 layers (Castellanos-Gomez et al., 2012). They reported that the average Young's modulus of suspended MoS<sub>2</sub> nanosheets is relatively high,  $Y = 330 \pm 70$  GPa, which is comparable to that of graphene oxide. The Young's modulus of MoS<sub>2</sub> nanosheets is also higher than bulk MoS<sub>2</sub>,  $Y = 240$  GPa. The individual single-layers of MoS<sub>2</sub> have comparatively high values of both stiffness ( $Y \approx 300$  GPa) and tensile strength ( $\sigma_B \approx 23$  GPa) (Bertolazzi et al., 2011, Castellanos-Gomez et al., 2012), which are lower than graphene ( $Y \approx 1000$  GPa,  $\sigma_B \approx 130$  GPa) (Huang et al., 2011) but extremely higher than macroscopic materials such as steel ( $Y \approx 200$  GPa,  $\sigma_B \approx 1$  GPa). The superior elastic properties of single- and few-layer MoS<sub>2</sub> make them attractive semiconductors for both of electronic and optoelectronic devices, as well as for nanocomposite films (O'Neill et al., 2012).

**Optoelectronic properties.** MoS<sub>2</sub> nanosheets possess different optical and electrical properties than bulk form. For an example, MoS<sub>2</sub> nanosheets are semiconducting, with a direct electronic bandgap of  $\sim 1.9$  eV, while the bulk material exhibits an indirect bandgap of 1.2 eV (Figure 2.3). The bulk material shows an indirect bandgap since the bottom of the conduction band and the top of the valence band is situated at different reciprocal lattice points (K, M, and  $\Gamma$ ). Nevertheless, for single-layer MoS<sub>2</sub>, the position of bottom of conduction band



and the top of the valence band are at the same K point of the x (wave factor) axis. Since this material exhibits direct bandgap behavior, it exhibits strong photoluminescence (Splendiani et al., 2010) and spin polarization (degree of alignment of electron's spin) (Mak et al., 2012). The unique optoelectronic properties of this material make it suitable for photovoltaics in which it can be used as absorber materials in thin film solar cell (Aruchamy, 1992). In addition, it has a potential applications in optoelectronic devices.

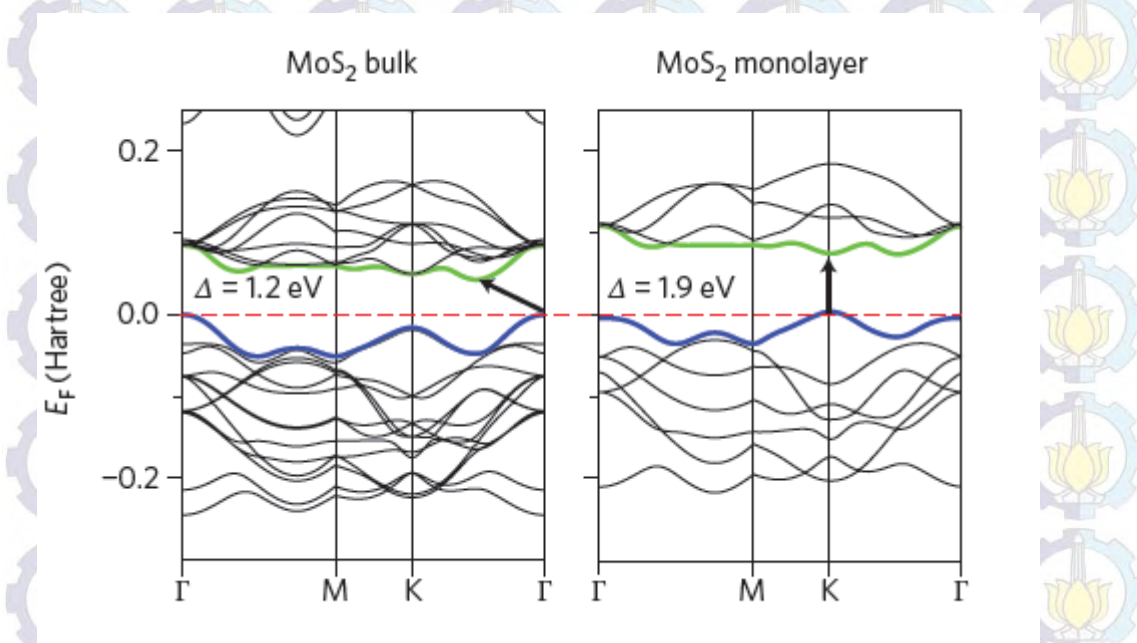


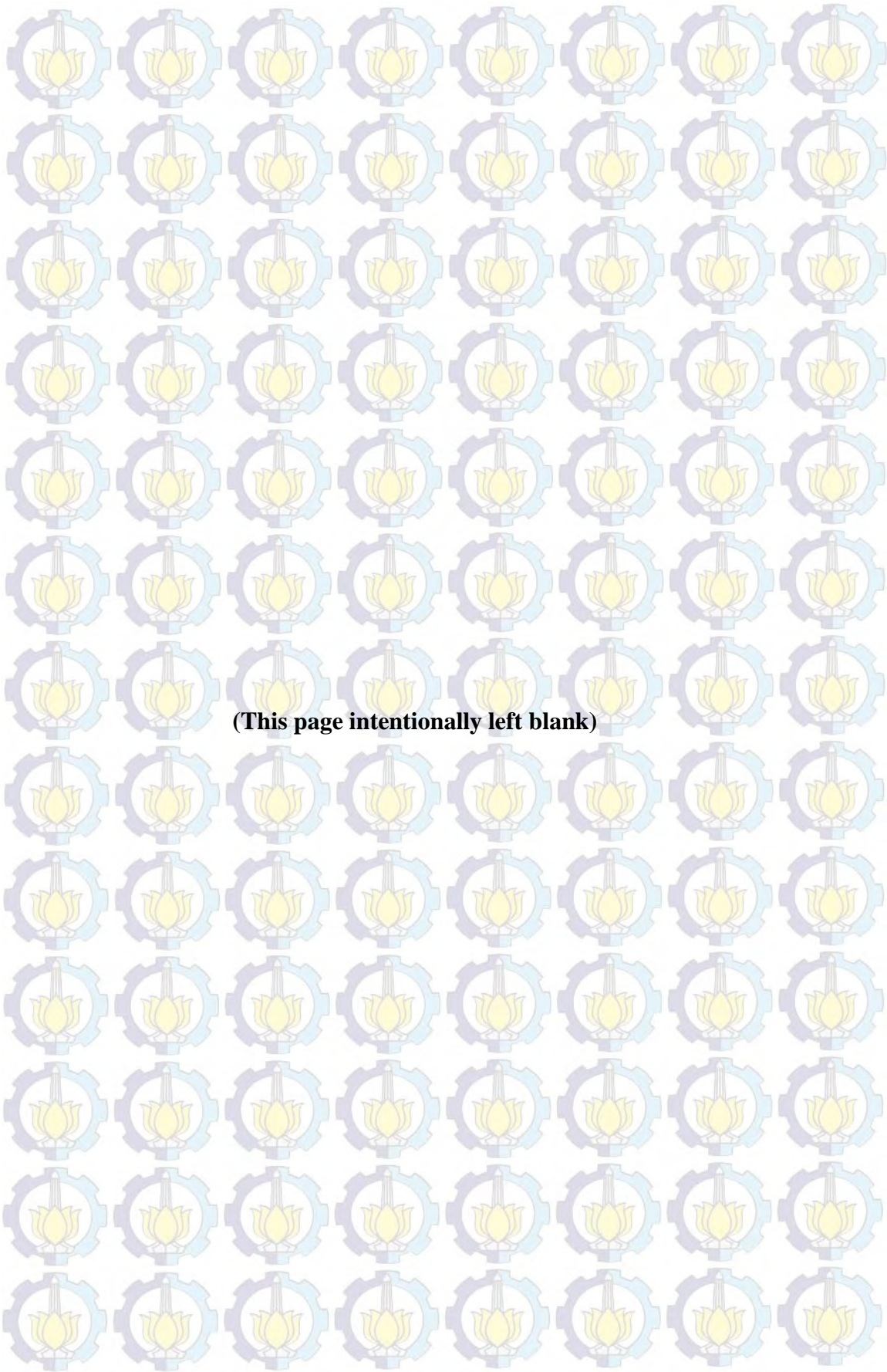
**Figure 2.3.** Electronic bandgap of bulk and monolayer MoS<sub>2</sub> (Adapted from Wang et al, Nature Nanotechnology, 2012).

**Catalytic properties.** When MoS<sub>2</sub> is exfoliated into sheets, the prismatic edge and basal plane are exposed. Many forms of MoS<sub>2</sub> are important in several catalytic reactions. The catalytic activity of the molybdenum disulfide is closely related to the structural properties of the material. As we know that the photoluminescence increases very significantly from an indirect bandgap to a direct bandgap which is followed by changes in orbital hybridization. The edge molybdenum and sulfur sites are highly active for hydrogen evolution reactions and thus are being considered as electrodes for water splitting by using sunlight.

**Lubricant properties.** The main industrial use of MoS<sub>2</sub> in addition to being catalysts as a dry lubricant where graphite is impractical. The lubrication is achieved by the easy shearing plane of the Van Der Waals interlayer gap. Graphite functions best when the graphene layers are lubricated by water vapor, whereas it is opposite for MoS<sub>2</sub>. MoS<sub>2</sub> finds its use in space, vacuum and high temperature applications. In the form of suspended MoS<sub>2</sub> particles in micro sizes are often used in a grease for low-end applications. The high quality lubricating surfaces can be produced by coating a thin film of MoS<sub>2</sub>, usually by magnetron sputtering. For the lubricating purpose, the MoS<sub>2</sub> surface should ideally present the basal plane for shearing as opposed to the edges, which are best for catalysis.

### **2.5 Potential Applications of Intercalation-Exfoliated Nanosheets**

Lithium intercalation represents a versatile and sustainable route for production of molybdenum disulfide nanosheets. The successful intercalation is closely related to both charge transfer and diffusion rates. The high reduction potentials and mobility of lithium species are notably appropriate for such purposes. Lithium intercalates in which lithium is found occupying the octahedral sites in the MoS<sub>2</sub> interlaminar spaces are thus used as precursors of the other more complex intercalation compounds to increase the conductivity, such as molybdenum disulfide dialkylamine, Li<sub>0.1</sub>MoS<sub>2</sub>(HNR<sub>2</sub>)<sub>y</sub> (Sánchez et al., 1999). Also, the lithium intercalation method can be used to develop the lithium ion batteries. When molybdenum disulfide nanosheets are changed from 2H to 1T phase, effectivity of hydrogen evolution reaction is enhanced. This phase change can be achieved by electrochemical lithium intercalation method.



**(This page intentionally left blank)**

## CHAPTER 3

### EXPERIMENTAL SECTION

#### 3.1 Synthesis

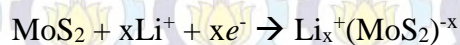
##### 3.1.1 Materials

The Molybdenum disulfide ( $\text{MoS}_2$ ) bulk powder used in these experiments was purchased from Alfa Aesar (99%) and 2.5 M n-butyl lithium in hexane was purchased from Chemetall.

##### 3.1.2 Preparation of $\text{MoS}_2$ nanosheets

To make the single-layer  $\text{MoS}_2$  suspension, molybdenum disulfide bulk powder (300mg) was placed in a 100 mL schlenk flask, to which a 2 mL of 2.5 M n-butyl lithium in hexane and 18 mL of hexane anhydrous were added under  $\text{N}_2$  atmosphere. Then, the solution was stirred for 5 days at room temperature.

Lithium intercalation occurs according to the chemical reaction:



The resulting suspension was gravity-filtered under  $\text{N}_2$ , and the solid washed with ~100 mL of anhydrous hexanes to remove any excess butyl lithium.

The  $\text{Li}_x\text{MoS}_2$  was gravity-filtered under  $\text{N}_2$  and the solution was removed using vacuum. The  $\text{MoS}_2$  paste was transferred to a 100 mL round-bottom flask and sealed with a septum. Then, ~60 mL of distilled-water was added into round-bottom flask quickly to quench the sample. The  $\text{MoS}_2$  paste was then taken from the round-bottom flask after the solution was removed by rotavapor.

When exfoliation occurred, excess distilled water was added to the  $\text{MoS}_2$  paste, the lithium reacts strongly with the water, forming lithium hydroxide ( $\text{LiOH}$ ), and visible bubbling occurs with the release of  $\text{H}_2$  gas and original quintuple layers are homogeneously exfoliated due to the rapid expansion in the layers and forming suspensions of  $\text{MoS}_2$  nanosheets. The following chemical reaction describes this process:



Next, 17.5 mg of the MoS<sub>2</sub> paste was suspended in 35 mL water in a 50 mL tube. Then, the mixture was sonicated continuously for 38 hours using a ½" (12.7 mm) diameter worn tip on replaceable tip (QSonica, 700W and 30% amplitude). The probe tip was adjusted to 2.5 cm from the liquid surface and bubble was formed. Bubbling by aeration at the middle of liquid and the morphology of worn tip can be helpful in the dispersion of nanosheets because the bubbling can produce a greater shearing which effect on the nanosheets in suspension. The system was kept at 5<sup>0</sup>C. The probe was pulsed on for 10 s and off for 5 s reduce solvent heating. After sonication, the solution was taken and then analyzed using UV-vis, dynamic light scattering (DLS), scanning electron microscopy (SEM), powder X-ray diffraction (P-XRD), transmission electron microscopy (TEM), and Raman Spectroscopy.

### 3.2.3 Preparation of few-layers MoS<sub>2</sub> with specific flakes dimension.

In our experiment, to achieve a certain size of few-layer MoS<sub>2</sub>. We used four procedures to reduce sheet sizes to desired dimension. The first method is via centrifugation of the sample at 2000 rpm for 60 minutes (Method A). The second method involves filtration, through polyvinylidene difluoride (PVDF) membrane with pore size 450 nm, 47 mm diameter (Method B). The third one is via centrifugation at 2000 rpm for 60 minutes, followed by filtration (Method C). The fourth method involves filtration (PVDF membrane, pore size 450 nm, 47 mm diameter) followed by centrifugation at 2000 rpm for 30 minutes (Method D). In our experiments, after sonicated, 13 mL of solutions was placed in a vial. In Method A, 4.6 mL of 12 mL solutions in vials was taken and centrifuged at 2000 rpm for 60 minutes. The top 1/2<sup>nd</sup> part of the dispersion was collected by pipette. In Method B, 2.4 mL of remaining solution was dispersed in 12 mL Di-water. After that, the solution was filtered using PVDF membrane and the filtrate was collected. In Method C, 6 mL of remaining solution in vials was centrifuged at 2000 rpm for 60 minutes, then the top 1/2<sup>nd</sup> part of the dispersion was collected by pipette and was then filtered quickly. In method D, 6 ml of the filtrate from method B was taken and centrifuged at 2000 rpm for 30 minutes. Then, the top 1/2<sup>nd</sup> part of the solution was collected by pipette. Then, all of the solution (from

Method A, B, C, and D) were analyzed using UV-vis, dynamic light scattering (DLS), scanning electron microscopy (SEM), atomic force microscopy (AFM) and Raman Spectroscopy.

### 3.2 Characterization Method

The absorbance spectra of the few-layer MoS<sub>2</sub> were recorded using a varian Cary 5000 and samples were tested in quartz glass cuvettes having 10 mm path length. The morphology of the samples was examined using scanning electron microscopy (SEM) model ZEISS-GEMINI Ultra Plus, with an Oxford Instruments EDS apparatus operated at 5 kV. For the EDS measurements, the EDS-SEM was operated at 10 kV. The sample was dropped on Silicon wafer (Si substrate) and washed three times using Di-water and evaporated at room temperature. The measurements were performed in standard carbon tip. The TEM images were examined using transmission electron microscopy instrument (Model JEOL-2010) operated at an accelerating voltage of 200 kV. The lattice and corresponding SAED pattern were characterized in a JEOL JEM-2100F TEM operated at an accelerating voltage of 200 kV. In preparation of TEM measurement, 1.5 mL of the sample was taken and centrifuged to collect the sample. Then, 1.5 ml ethanol solution was added into each of samples to disperse the exfoliated MoS<sub>2</sub>. 100  $\mu$ L of the solution was taken and diluted in 400  $\mu$ L ethanol, then dropped on copper grids, then washed three times using Di-water to remove the impurities which are probably attach on the Cu grids and let samples evaporated at room temperature. The X-ray diffraction (XRD) patterns were measured with a diffractometer (BRUKER, GADDS) using Cu K $\alpha$  ( $\lambda = 1.5418 \text{ \AA}$ ) radiation over the range of  $10^\circ \leq 2\theta \leq 80^\circ$  under a voltage of 40 kV and a current of 40 mA. In the preparation of XRD measurements, for the MoS<sub>2</sub> nanosheets, 3 ml of main solution (after sonication) was taken and centrifuged to collect the sample paste, and then dropped on Glass-deck and dried at room temperature. The number of lithium before and after exfoliation were calculated using VARIAN ICP-OES. In the ICP-OES preparations, each of 8.6 mg of Li<sub>x</sub>MoS<sub>2</sub> and 8.6 mg of MoS<sub>2</sub> nanosheets powder were dissolved in 20 ml aqua regia and allowed in the hood for overnight. Raman spectra were measured with in Via Confocal Raman

Spectroscopy (NTEGRA Spectra, NT-MDT) at excitation laser line 488 nm in air ambient environment. The power of the excitation laser line was kept well below 1 mW to avoid heating effect and the spot size of 50  $\mu\text{m}$  with exposure time at 10 s and grating line at 1800/500 with range of  $\lambda = 500$  nm. In preparation of Raman measurements, 1.5 mL of the sample was taken and centrifuged to collect the solid. Then, 1.5 ml ethanol was added into each of samples to disperse the exfoliated  $\text{MoS}_2$ , and finally the dispersions were collected using pipette and dropped on Silicon wafer (Si substrate), then washed three times using Di-water and let samples evaporated at room temperature. Atomic force microscopy images was recorded on Veeco MultiMode VIII microscope in tapping mode. In AFM measurements, 1.5 mL of sample A, B, C and D were taken and centrifuged to collect the sample. Then, 1.5 ml ethanol was added into each of samples to disperse the exfoliated  $\text{MoS}_2$ , and finally the dispersions were collected using pipette and dropped on freshly silicon wafer (Si substrate), dried, and then soaked in distilled water to remove any impurities which are attach on Si substrate and dried under vacuum at 50 $^{\circ}\text{C}$  for minimum 3 hours. The zeta potential and size distribution of the as-prepared  $\text{MoS}_2$  nanosheets were measured by using dynamic light scattering (DLS). DLS measurements were performed using a Malvern Zetasizer Nano ZS with a 633 nm He-Ne laser. Samples were tested in low volume disposable sizing cuvettes. Malvern Zetasizer Nano ZS was operated in backscatter mode at an angle of 173 $^{\circ}$  and analyzed three times for each samples. Samples were equilibrated to 25 $^{\circ}\text{C}$  for 120 s prior to measurement. Viscosity and Refractive index of solvent (water) at 25 $^{\circ}\text{C}$  are 0.8872 cP and 1.330, respectively. An automatic measurement positioning and automatic attenuation. The samples were analyzed as prepared without further dilution. In this measurements, the dispersions (for sample A, B, C, and D) were taken 600  $\mu\text{L}$  and sonicated for two minutes to avoid aggregation before measurements.

## CHAPTER 4

### RESULTS AND DISCUSSIONS

In recent years, MoS<sub>2</sub> based catalysts have been considered as promising material to replace platinum because of their high abundance and low cost. Promising catalytic activity of MoS<sub>2</sub> in the hydrogen evolution reaction (HER) is attributed to the active sites located along the edges of its two-dimensional layered crystals. If the MoS<sub>2</sub> based catalysts are to realize their potential, there is an urgent need to design MoS<sub>2</sub> nanosheets with more edge sites. The ability to control the nanosheets size during exfoliation process, achieved here by control of centrifugation and filtration, will be important for the number of applications. One of the most important applications is as catalyst for the evolution of hydrogen from proton-rich electrolytes (Jaramillo and Horch, 2007). Because the catalytically active sites reside on edge of nanosheets, Hydrogen evolution catalyst is strongly dependent on nanosheets length with small flakes performing much better than larger ones (Varrla et al., 2015). And the change of phase MoS<sub>2</sub> from semiconducting to metallic which happened during intercalation process is to be an important factor in evolution of hydrogen because in the previous research shown that the metallic phase has catalytic activity is better than semiconducting phase (Voiry et al., 2013). For another application, lithium ion batteries are still exist and high efficient energy in industrial battery. So, in here we reported the preparation MoS<sub>2</sub> nanosheets with specific flake dimensions using lithium intercalation method to provide material which can be applied in those applications.

#### 4.1 Intercalation of Lithium

The intercalation of lithium into transition metal dichalcogenides is especially relevant both to technical applications and to fundamental knowledge of layered materials. This is notably valid for MoS<sub>2</sub>, as a great part of its intercalation chemistry based on processes. Even though some research about synthesis of MoS<sub>2</sub> nanosheets using another alkali metal as intercalating agents and another method, such as mechanical exfoliation, chemical vapor deposition,



and liquid-phase exfoliation have been reported, much attention has been focused on intercalation of lithium, among others because of the potential of such materials as a high power component in batteries and a good component for hydrogen production.

Chemical exfoliation of layered materials is generally achieved by reacting the 2D nanomaterials with *n*-butyl lithium. The electrons from *n*-butyl lithium (as a guest) are transferred to the lowest-lying-unoccupied energy levels of MoS<sub>2</sub> (as a host), which are fundamentally transition metal d bands (as shown in Figure 4.1) (Knirsch et al., 2015). And also the charge transfer from *n*-BuLi to MoS<sub>2</sub> actually may induce structural changes in the host. Structural and electronic changes in the host of MoS<sub>2</sub> produced by lithium intercalation method often induce dramatic changes in the transport properties of MoS<sub>2</sub> from semiconducting to metallic (Benavente et al., 2002). The important thing is that when the bulk materials become nanosheets, the properties change, such as mechanical, electronic and thermodynamic properties (O'Neill et al., 2012).

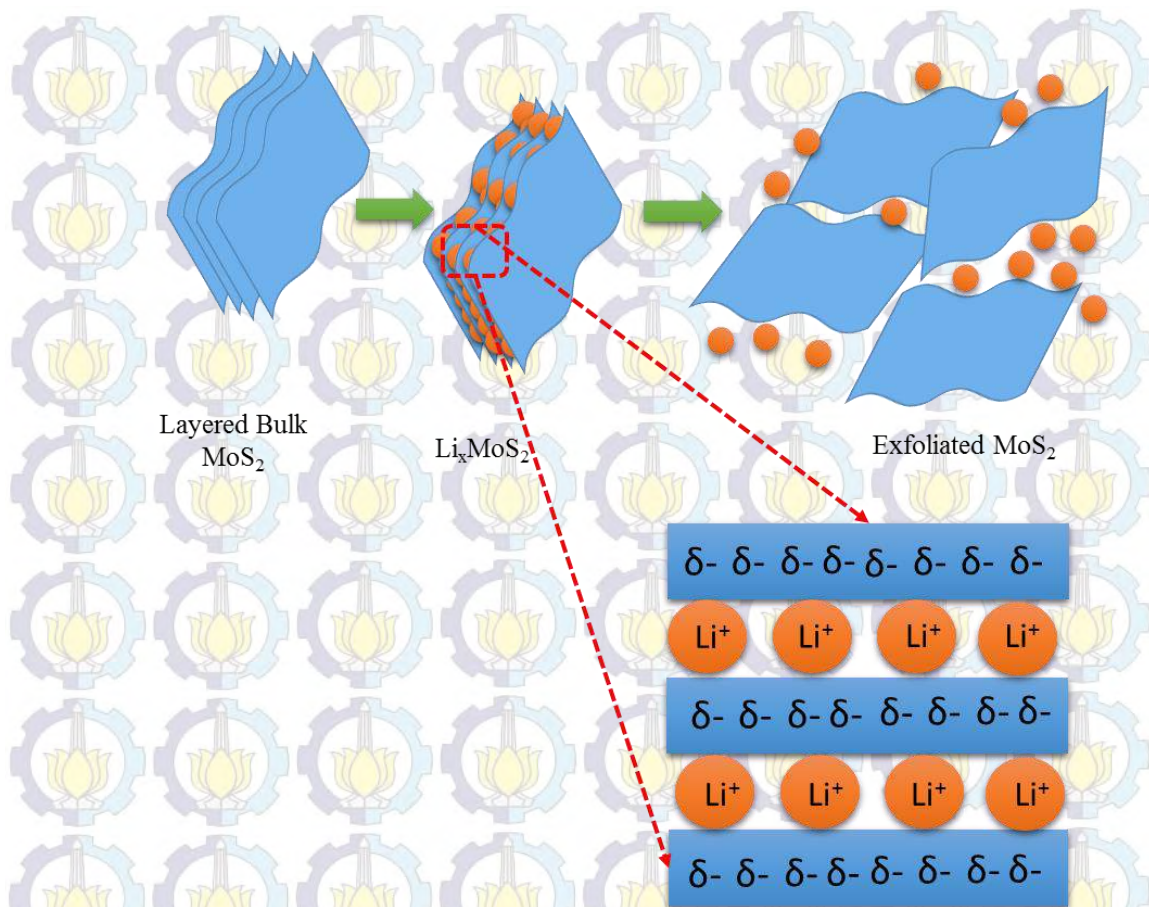
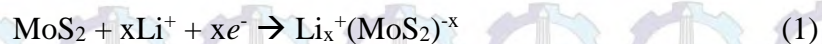
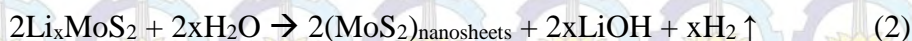


**Figure 4.1.** Schematic illustration of intercalation of lithium into MoS<sub>2</sub> layers.

Figure 4.1 illustrates the formation of MoS<sub>2</sub> nanosheets via lithium intercalation method from bulk material. The structure of molybdenum disulfide can be considered as layers coupling together by weak Van Der Waals forces, which make lithium ion being intercalated between layers under appropriate condition. During the stirring process, anhydrous hexane can serve as solvent, resulting in the lithium cations dispersed in the solvent being readily insert into MoS<sub>2</sub> layers with the formation of lithium intercalated MoS<sub>2</sub> (Li<sub>x</sub>MoS<sub>2</sub>) units according to the following chemical reaction,



Then when the Li<sub>x</sub>MoS<sub>2</sub> units are exposed to water, the lithium in the unit become rapidly solvated and produces exfoliated MoS<sub>2</sub> layers, lithium hydroxide (LiOH), and hydrogen gas (H<sub>2</sub>) based on another following chemical reaction,

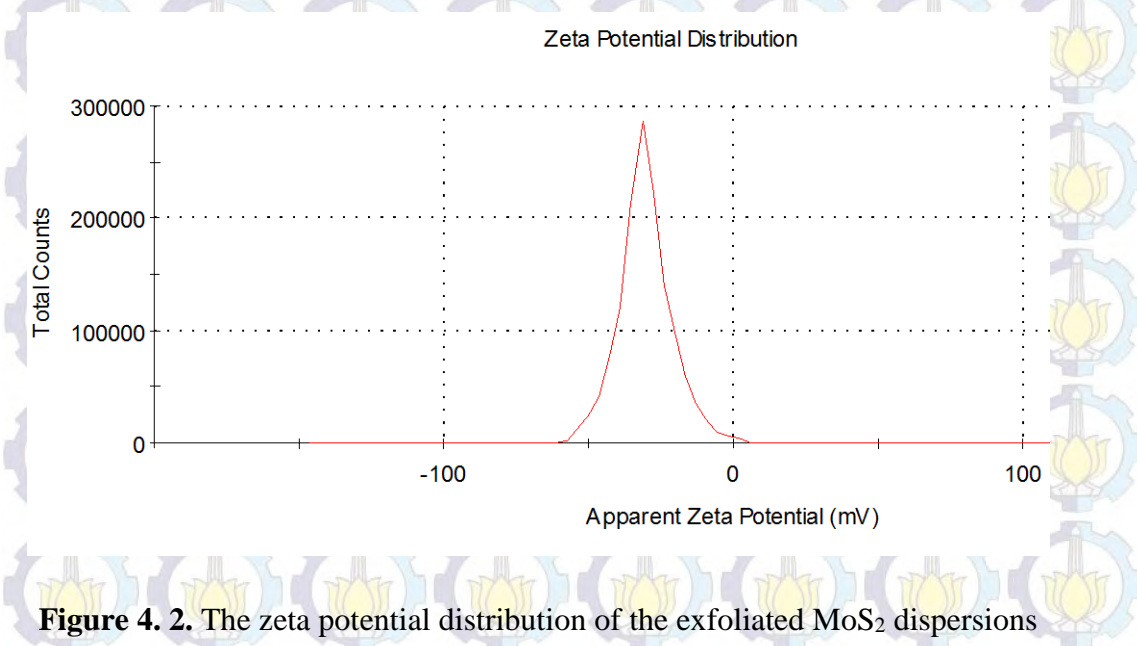


During the reaction process, original quintuple layers are homogeneously exfoliated due to the rapid expansion in the layers and forming suspensions of MoS<sub>2</sub> nanosheets.

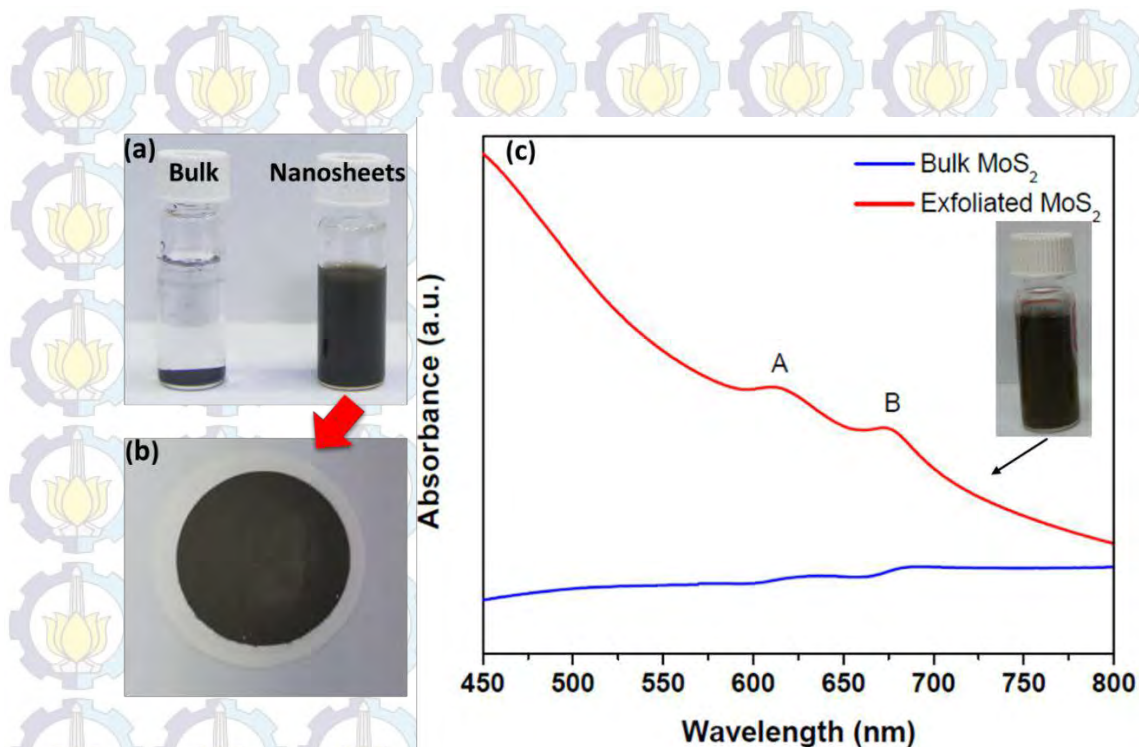
#### 4.2 Exfoliation of Molybdenum disulfide

To promote exfoliation of MoS<sub>2</sub>, here we used sonication. The MoS<sub>2</sub> exfoliated sheets were exposed to ultrasonication at room temperature for 38 h, followed by centrifugation to reduce sheet size to desired dimension. The reaction of the resulting lithiated phase of MoS<sub>2</sub> with water through the redox reaction (reaction 2) and can form few- or single-layer MoS<sub>2</sub> dispersion with partial negative charge (see Figure 4.1) (Joensen, 1986). In this work, after we got MoS<sub>2</sub> nanosheets, Zeta (ζ) potential measurements is used to prove it.

The zeta potential is an important factor for characterizing the stability of colloidal dispersions and provides a measure of the magnitude and sign of the effective surface charge. In this measurements the average value of zeta potential is about -29.18 mV (Figure 4. 2), which indicates that the MoS<sub>2</sub> nanosheets become negative charge after exfoliation due to the electron transfers from *n*-BuLi (guest) to MoS<sub>2</sub> surface (host).



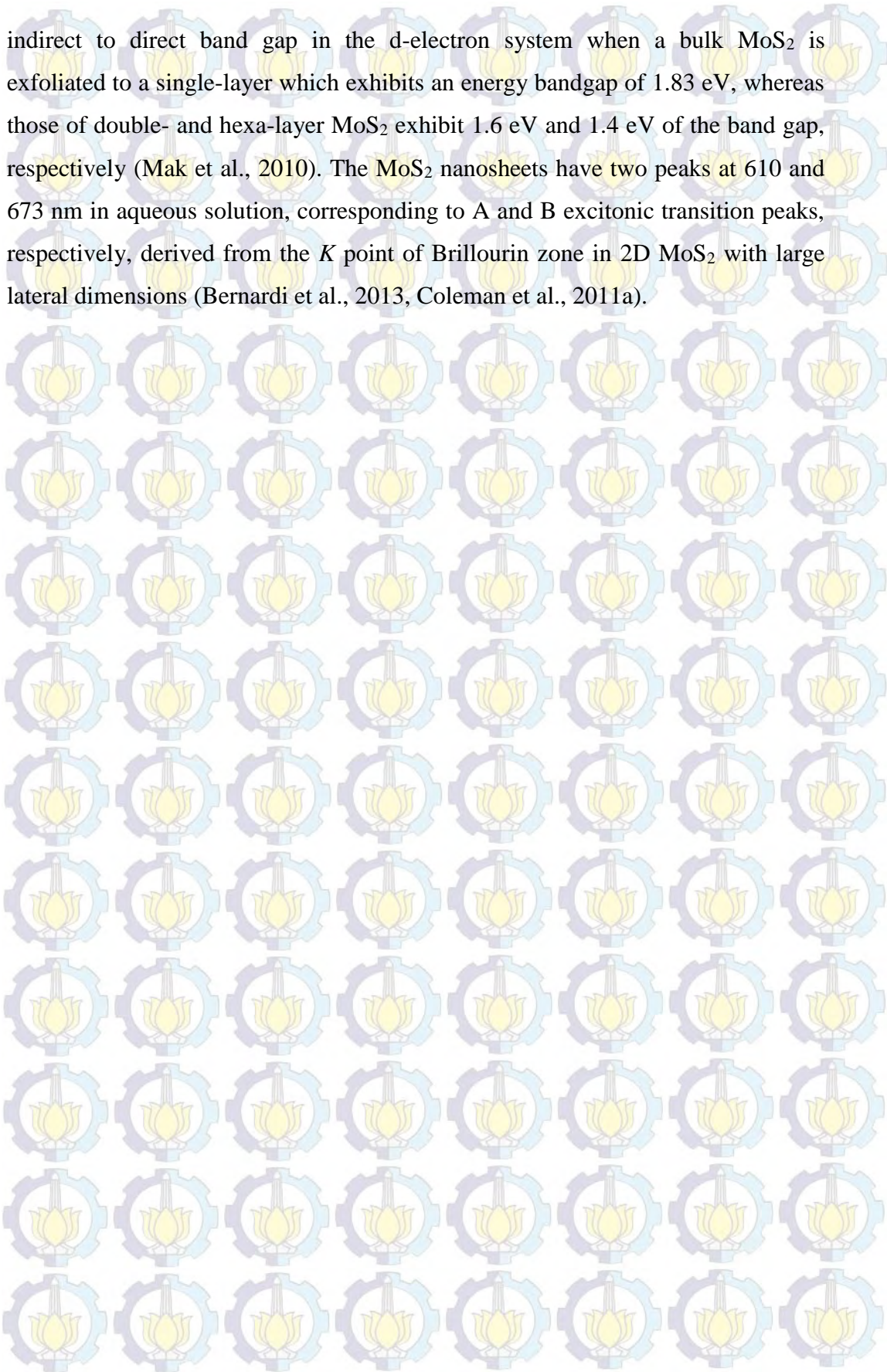
**Figure 4. 2.** The zeta potential distribution of the exfoliated MoS<sub>2</sub> dispersions



**Figure 4.3.** (a) Digital images of the change in the solution containing bulk MoS<sub>2</sub> before (left) and after (right) reaction; (b) Digital image of the MoS<sub>2</sub> nanosheets by filtration using PVDF membrane with 450 nm pore size; (c) UV-vis absorption spectra of bulk MoS<sub>2</sub> and exfoliated MoS<sub>2</sub> nanosheets (after sonication for 38 h) dispersed in water. The inset photo is the dilute solution of MoS<sub>2</sub> nanosheets.

Figure 4.3a illustrates the observable changes between the dispersion of MoS<sub>2</sub> bulk and nanosheets in water. In contrast to the former limpid solution containing a large number of MoS<sub>2</sub> bulk in the bottom, the aqueous dispersion of MoS<sub>2</sub> nanosheets presents a muddy and uniform dispersion state, implying the thin sheets of MoS<sub>2</sub> contained therein. The MoS<sub>2</sub> nanosheets can be obtained by filtration using porous polyvinylidene fluoride (PVDF) membrane (as shown in Figure 4.3b). Figure 4.3c shows typical UV-vis spectra of MoS<sub>2</sub> nanosheets and bulk suspended in water. The absorption spectrum of MoS<sub>2</sub> nanosheets suspension displays much higher peak absorption in visible region compared to that of the bulk suspension. Optical absorption is a characteristic related to band structure of a semiconductor. Bulk MoS<sub>2</sub> is a semiconducting material with an indirect band gap of about 1.3 eV. However, from the previous researches have shown an

indirect to direct band gap in the d-electron system when a bulk MoS<sub>2</sub> is exfoliated to a single-layer which exhibits an energy bandgap of 1.83 eV, whereas those of double- and hexa-layer MoS<sub>2</sub> exhibit 1.6 eV and 1.4 eV of the band gap, respectively (Mak et al., 2010). The MoS<sub>2</sub> nanosheets have two peaks at 610 and 673 nm in aqueous solution, corresponding to A and B excitonic transition peaks, respectively, derived from the *K* point of Brillouin zone in 2D MoS<sub>2</sub> with large lateral dimensions (Bernardi et al., 2013, Coleman et al., 2011a).



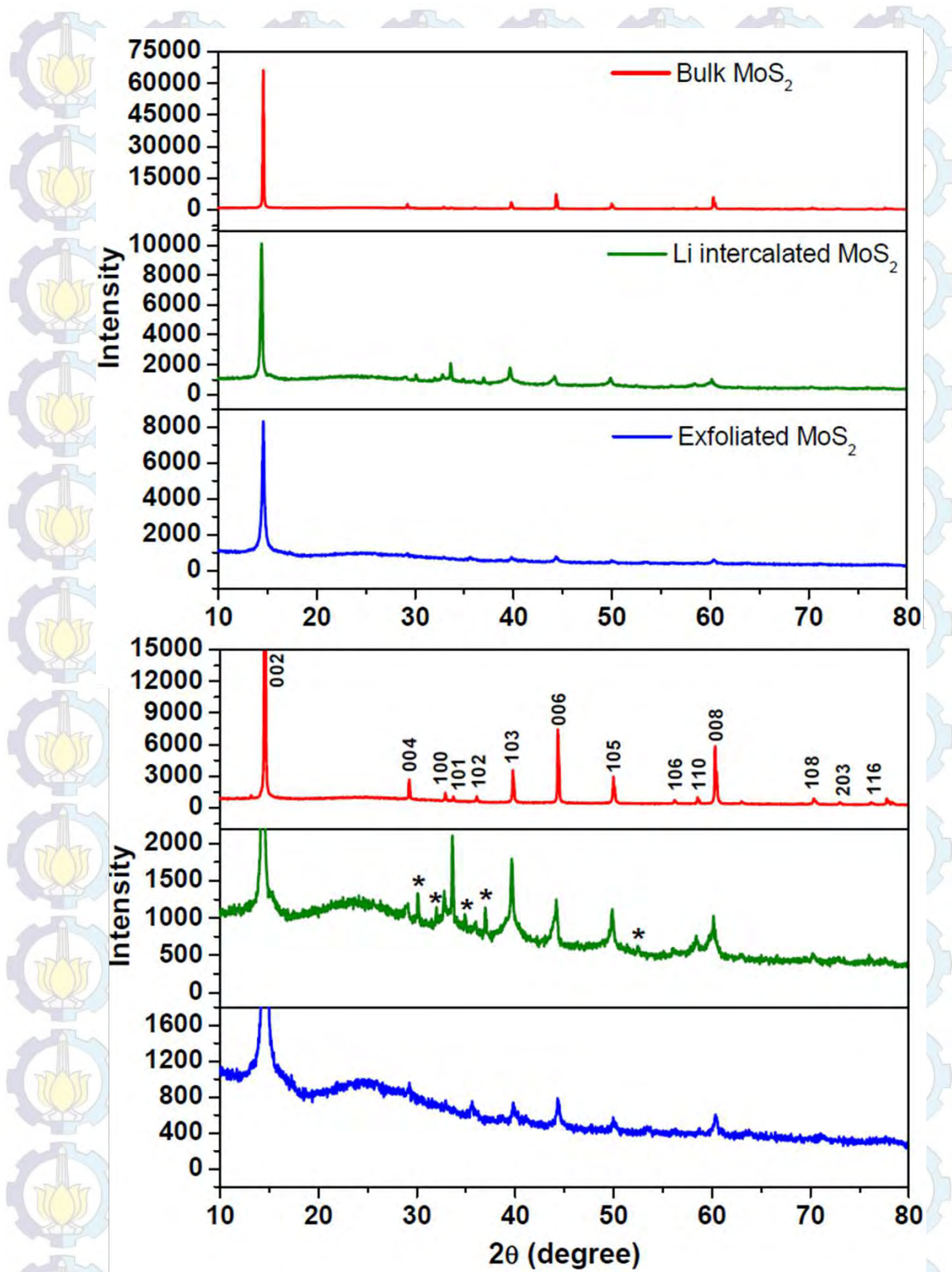


**Figure 4.4.** The XRD pattern of bulk MoS<sub>2</sub>, Li intercalated MoS<sub>2</sub>, and exfoliated MoS<sub>2</sub> nanosheets (top) with magnification of intensity of 5x (bottom).

Figure 4.4 shows the XRD results of raw bulk material, lithium intercalated MoS<sub>2</sub> and exfoliated MoS<sub>2</sub> nanosheets. All diffraction peaks of the sample were in good agreement with a hexagonal structure of MoS<sub>2</sub> (JCPDS No. 37-1492). As shown in Figure 4.4, the peak positions of MoS<sub>2</sub> bulk and nanosheets are in the same places, with different intensity, which indicates that the exfoliated MoS<sub>2</sub> has a hexagonal lattice structure and preserve well the crystalline phase of bulk MoS<sub>2</sub>. Compared with those of bulk MoS<sub>2</sub> and exfoliated MoS<sub>2</sub> nanosheets, lithium intercalated MoS<sub>2</sub> has additional diffraction peaks at 30°, 32°, 35°, 37° and 52°. These XRD peaks are originated from MoS<sub>2</sub> being intercalated by Li to form Li<sub>x</sub>MoS<sub>2</sub>, which is consistent with previous results reported by Liu et al (Liu et al., 2013b). From XRD results, these additional peaks disappear after exfoliation, indicating that intercalated Li is removed when MoS<sub>2</sub> nanosheets are formed. To confirm that the lithium become disappear after exfoliation, we performed the Inductively Coupled Plasma - Optical Emission Spectrometry (ICP-OES) (see appendix A). The result shows that before and after exfoliation of Li intercalated MoS<sub>2</sub>, 95% of lithium can be removed. Therefore, in the XRD pattern of MoS<sub>2</sub> nanosheets we cannot see the lithium intercalated peaks. In XRD results of bulk material, the very sharp peaks with high intensity and a strong [002] peak indicate good crystallization and well-stacked layered structure. Furthermore, the XRD result of MoS<sub>2</sub> nanosheets shows broadened peaks and shortened [002] peak, which is consistent with previous results (Eda et al., 2011). And the results indicate a much smaller crystallite size of MoS<sub>2</sub> nanosheets compared to bulk material.

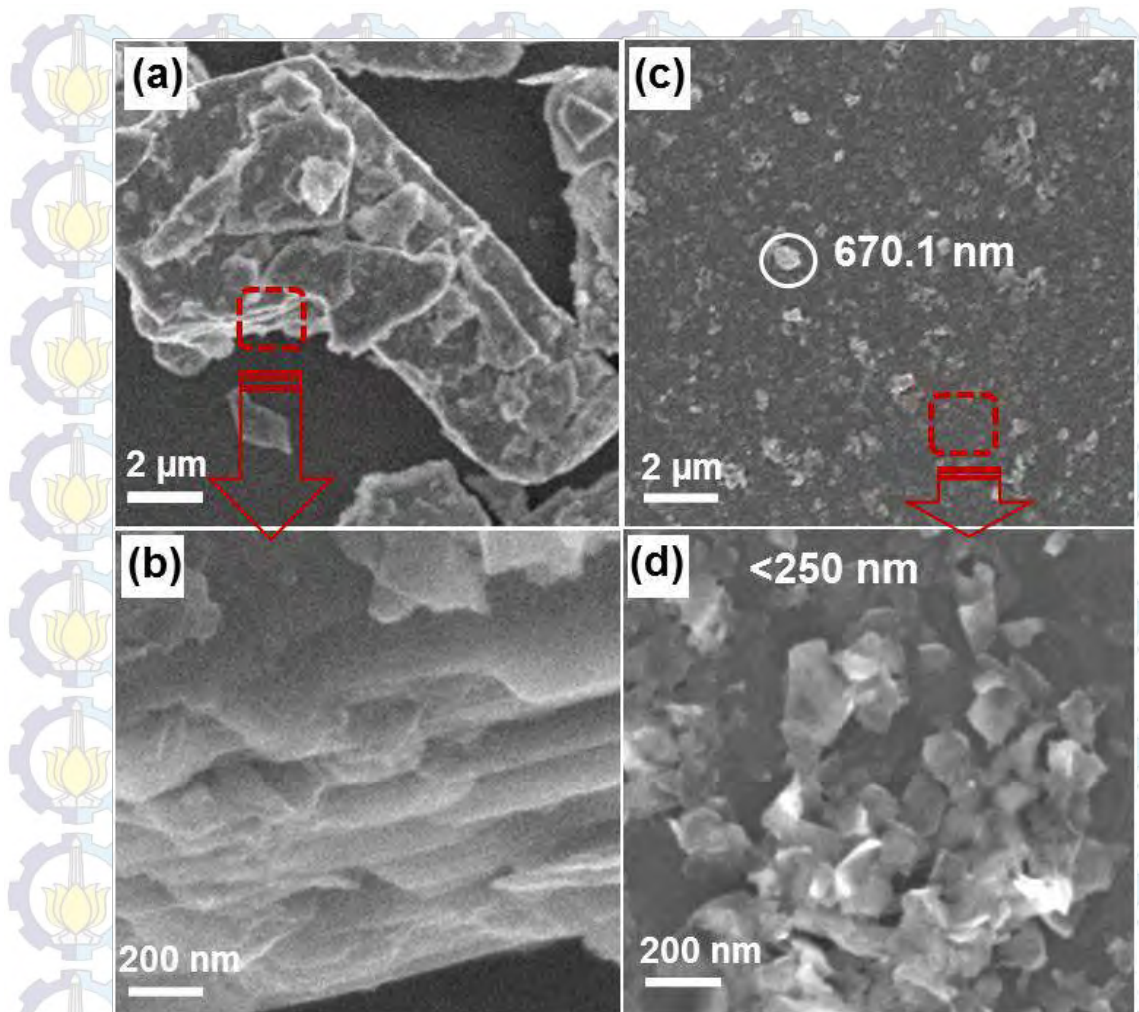


**Figure 4.5.** The typical SEM images: (a) and (b) Bulk MoS<sub>2</sub> powder with different resolution; (c) MoS<sub>2</sub> nanosheets with different lateral sizes; (d) MoS<sub>2</sub> nanosheets with lateral size <250 nm.

The morphology of the as-prepared MoS<sub>2</sub> samples was identified by SEM and high-resolution TEM (HRTEM). The SEM images of the MoS<sub>2</sub> both bulk material and exfoliated MoS<sub>2</sub> are shown in Figure 4.5. The original quintuple layers with several irregular lateral size of sheets can be observed clearly in Figure 4.5a. Figure 4.5b displays the stacked-layered structures and sharp edges of the MoS<sub>2</sub> flakes. The SEM image of the MoS<sub>2</sub> nanosheets is shown in Figure 4.5c. Many irregular MoS<sub>2</sub> nanosheets with different lateral sizes can be clearly observed. A bigger exfoliated MoS<sub>2</sub> with a size of 670.1 nm is observed in the



SEM image, and much smaller sheets are contained therein (as shown in Figure 4.5d with higher resolution).

This variation of size is mainly associated with the ultrasonic cavitation effect because in this preparation we used probe sonication to promote exfoliation.

When the resonance frequency of bubbles corresponds with that sound waves, the maximum energy coupling of acoustic field and bubbles will be generated, accompanying an obvious cavitation effect and finally, the flake MoS<sub>2</sub> nanosheets with different lateral sizes are produced.

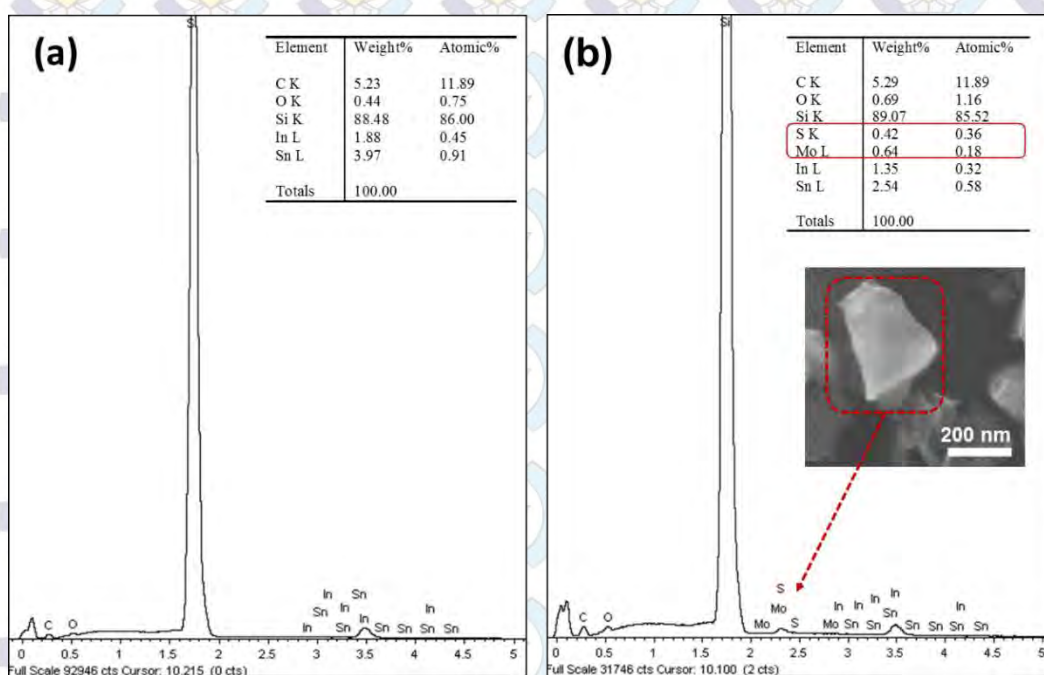


**Figure 4.6.** (a) EDS-SEM of silicon wafer; (b) A representative EDS-SEM spectrum collected from an individual MoS<sub>2</sub> nanosheets in silicon wafer. The inset image is the SEM image of MoS<sub>2</sub> nanosheets in EDS-SEM analysis.

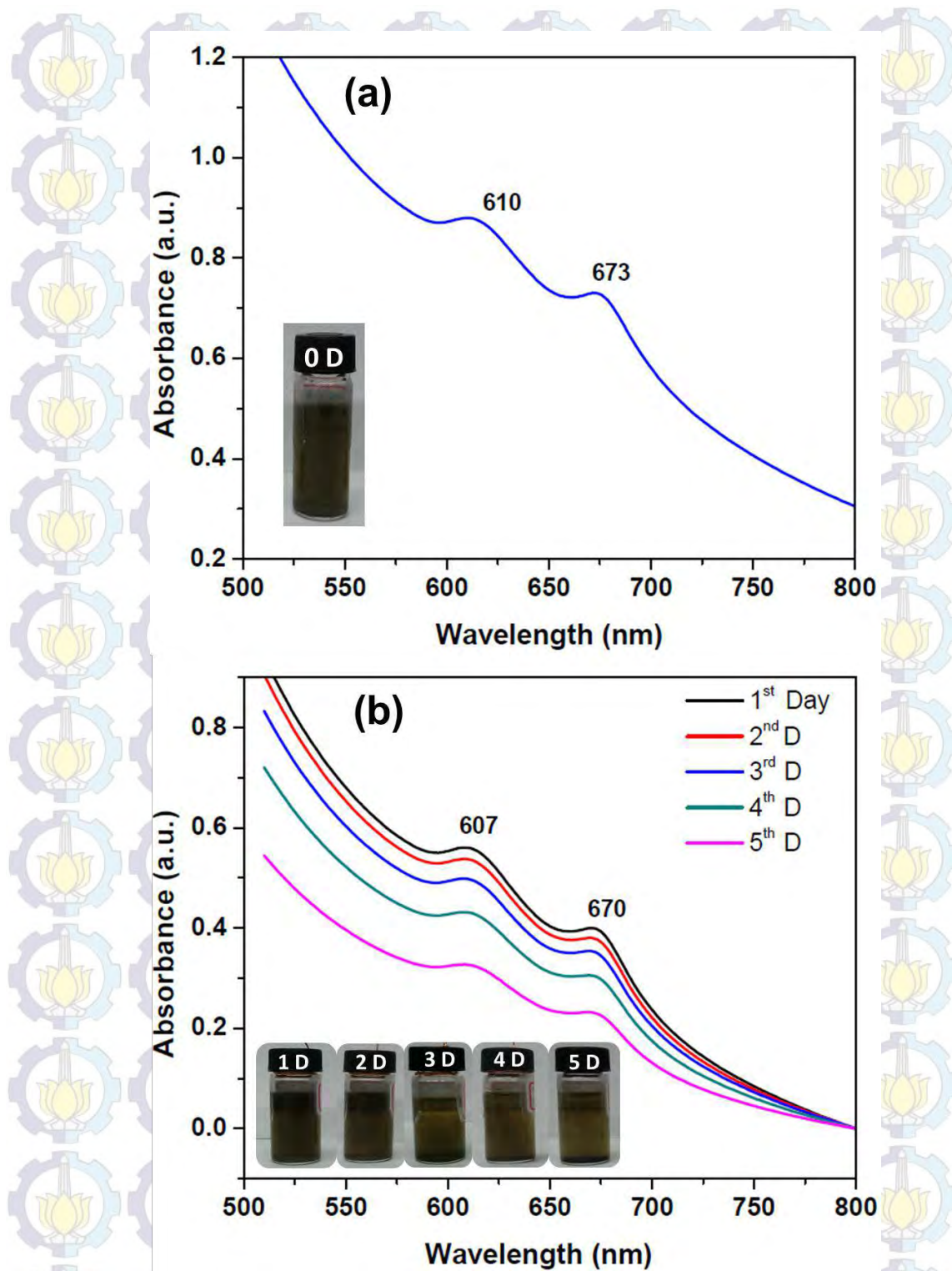


**Figure 4.7.** (a) Absorption spectrum of MoS<sub>2</sub> nanosheets after sonication (not further dilution). (b) Absorption spectra of MoS<sub>2</sub> nanosheets from (a) after 1 – 5 days. All of UV-Vis results in the same concentration: 0.6 ml of sample after sonication / 3 ml of Di-water.

The important thing in this process is the sonication with stronger cavitation and longer time produces the smaller flake sizes of MoS<sub>2</sub> nanosheets with narrow lateral size distribution. This effect is analogous to the previous results, which states that the flakes could be cut by the scission of low energy ball milling and sonication (Yao et al., 2012). Figure 4.6 illustrates the composition of elements of silicon wafer (left) and MoS<sub>2</sub> nanosheets (right) and the presence of C and O element actually comes from SEM machine. As shown in Figure 4.6b, in EDS spectrum, the atomic ratio of an individual MoS<sub>2</sub> nanosheet is 1:2, which indicates that MoS<sub>2</sub> nanosheets preserve well-qualified atomic structure of bulk MoS<sub>2</sub>. We also provided UV-vis spectra to show the different lateral sizes of MoS<sub>2</sub> nanosheets in my sample as shown in Figure 4.7. The UV-vis spectrum of MoS<sub>2</sub> nanosheets after sonication (no further treatment) exhibits two peaks at 610 nm and 673 nm which are ascribed to the *K* point of the Brillouin zone in 2D MoS<sub>2</sub> with larger lateral dimensions (Bernardi et al., 2013). In contrast to Figure 4.7a, the excitonic peaks in Figure 4.7b at 607 nm and 670 nm are in accordance with the characteristic peaks of exfoliated MoS<sub>2</sub> with smaller lateral dimensions (Wang et al., 2014). In Figure 4.7b shows that after the sample is left up to 5 days, the bigger MoS<sub>2</sub> nanosheets precipitate in the bottom and the color of solution changed to be brighter. To confirm that the bulk MoS<sub>2</sub> has been successfully exfoliated into nanosheets with various sizes, we performed dynamic light scattering (DLS) on exfoliated MoS<sub>2</sub>, as shown in Figure 4.8. The simplest way to do this is to measure the particle diffusion coefficient which can be used to infer its size via Stokes-Einstein relation. In this measurement a commercially available Malvern Zetasizer Nano ZS was used. By operating in backscatter mode (173° scattering angle) it was possible to use the machine's automatic beam positioning system. The focal position and attenuation of the incident beam were optimized by that system before data acquisition. These setting was used to probe the sample close to the cuvette wall, thus minimizing multiple scattering of the light by highly concentrated samples. So, in this measurements, the samples did not need to be diluted in order to record size data, even zeta potential data.

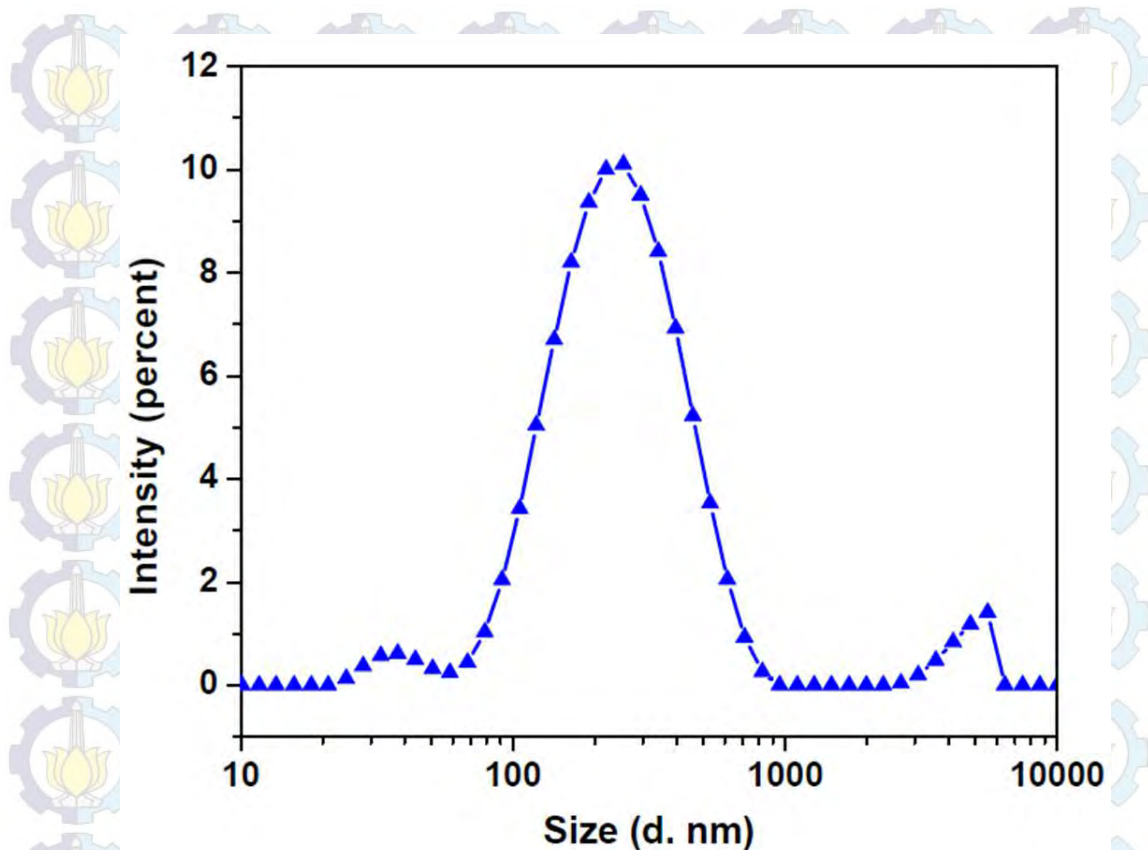


**Figure 4.8.** Size distribution of MoS<sub>2</sub> nanosheets by intensity

However, this measurements considerably work well for spherical objects, it is less reliable for non-spherical geometries, such as rods or platelets. At least here we can present the size distribution of MoS<sub>2</sub> nanosheets according to DLS measurements. The DLS software also computes an averaged particle size value known as the “Z-average diameter”. This value is derived from the entire intensity particle size distribution (PSD) and so is also strongly influenced by the presence of any spurious peaks.

In DLS results, a small peak around 38 nm is observed; this could be attributed to the presence of very small MoS<sub>2</sub> nanosheets. However, the primary peak of the distribution is centered at 220 nm which agrees well with the size distribution from SEM analysis shown in Figure 4.5d. A third small peak is observed at around 5.8 μm, this feature appeared in few samples. The origin of this peak is unclear as large objects around 5.8 μm in size were not observed in

SEM analysis. This feature may be due to small dust particles or air bubbles in this dispersions.

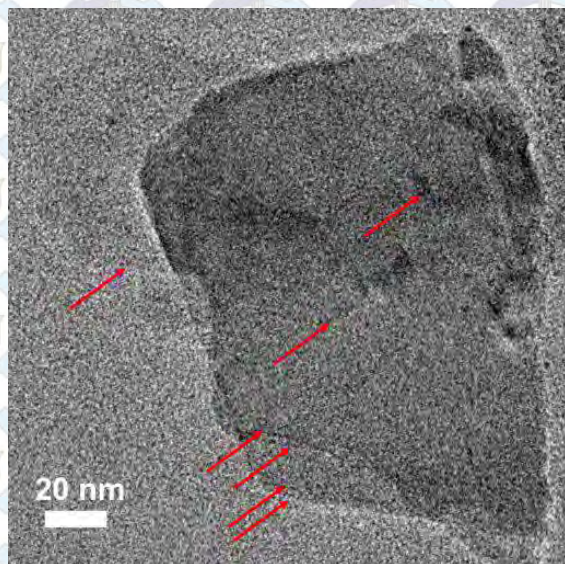


**Figure 4.9.** TEM image of MoS<sub>2</sub> nanosheets

The as-prepared MoS<sub>2</sub> nanosheets were also analyzed by TEM. The Figure 4.9 displays the typical TEM image of an individual MoS<sub>2</sub> nanosheet. It is clearly shown that the exfoliated MoS<sub>2</sub> was a thin layer with a smooth surface. The TEM image also shows the presence of 7 layers of sheets. To confirm that the MoS<sub>2</sub> bulk has been successfully exfoliated into a few-layer structure, we performed Raman spectroscopy on exfoliated MoS<sub>2</sub> and bulk MoS<sub>2</sub>, as shown in Figure 4.10. The characteristic peaks of the bulk MoS<sub>2</sub> at 377 and 402.9 cm<sup>-1</sup> are assigned to the  $E_{2g}^1$  and  $A_{1g}$  modes, respectively, while that of the exfoliated MoS<sub>2</sub> features these peaks at 383.9 and 407.8 cm<sup>-1</sup>, respectively.

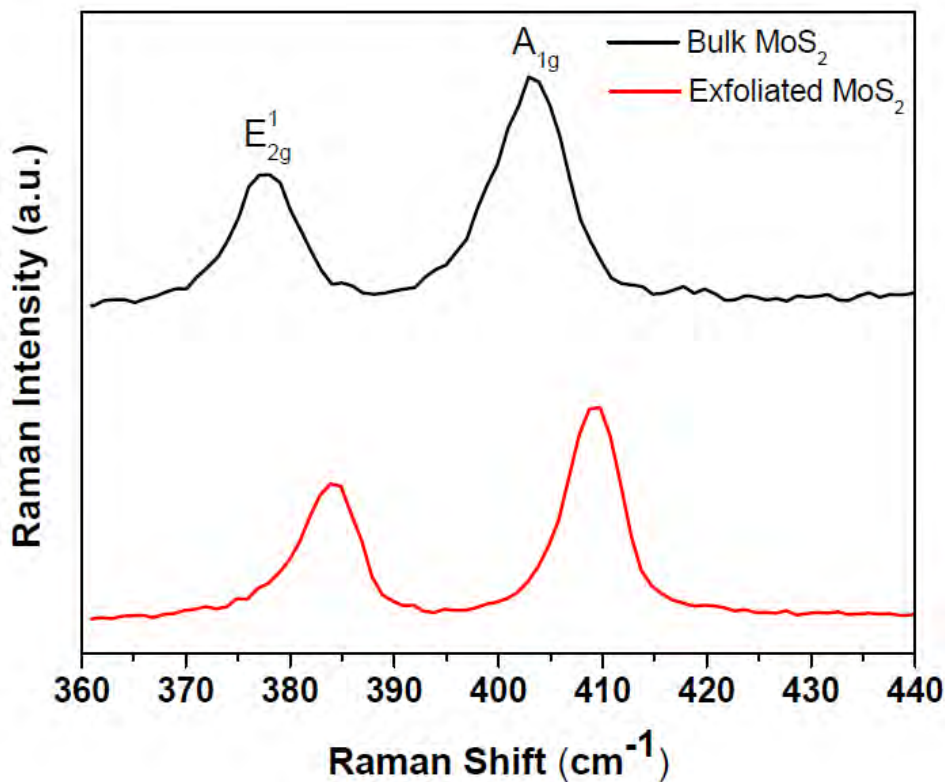


**Figure 4.10.** Raman spectra of bulk MoS<sub>2</sub> and exfoliated MoS<sub>2</sub> from lithium intercalation process.

The  $E_{2g}^1$  mode is correlated with an in plane opposite vibration of Mo and S atoms, while the  $A_{1g}$  mode is caused by an out-of-plane vibration of sulfur atoms in opposite directions (Yu et al., 2013b). Particularly, the  $E_{2g}^1$  mode is the shear mode, which is attributed to the relative vibration between the adjacent single-layers. The frequency difference ( $\Delta k$ ) between the  $E_{2g}^1$  and  $A_{1g}$  modes in the exfoliated MoS<sub>2</sub>,  $\Delta k = 23.9 - 24.9 \text{ cm}^{-1}$  is smaller than that in the bulk MoS<sub>2</sub>,  $\Delta k = 25.9 \text{ cm}^{-1}$ , consistent with the Raman signatures of MoS<sub>2</sub> nanosheets comprising over than three layers (see **Error! Reference source not found.** in appendix A) (Lee et al., 2010).

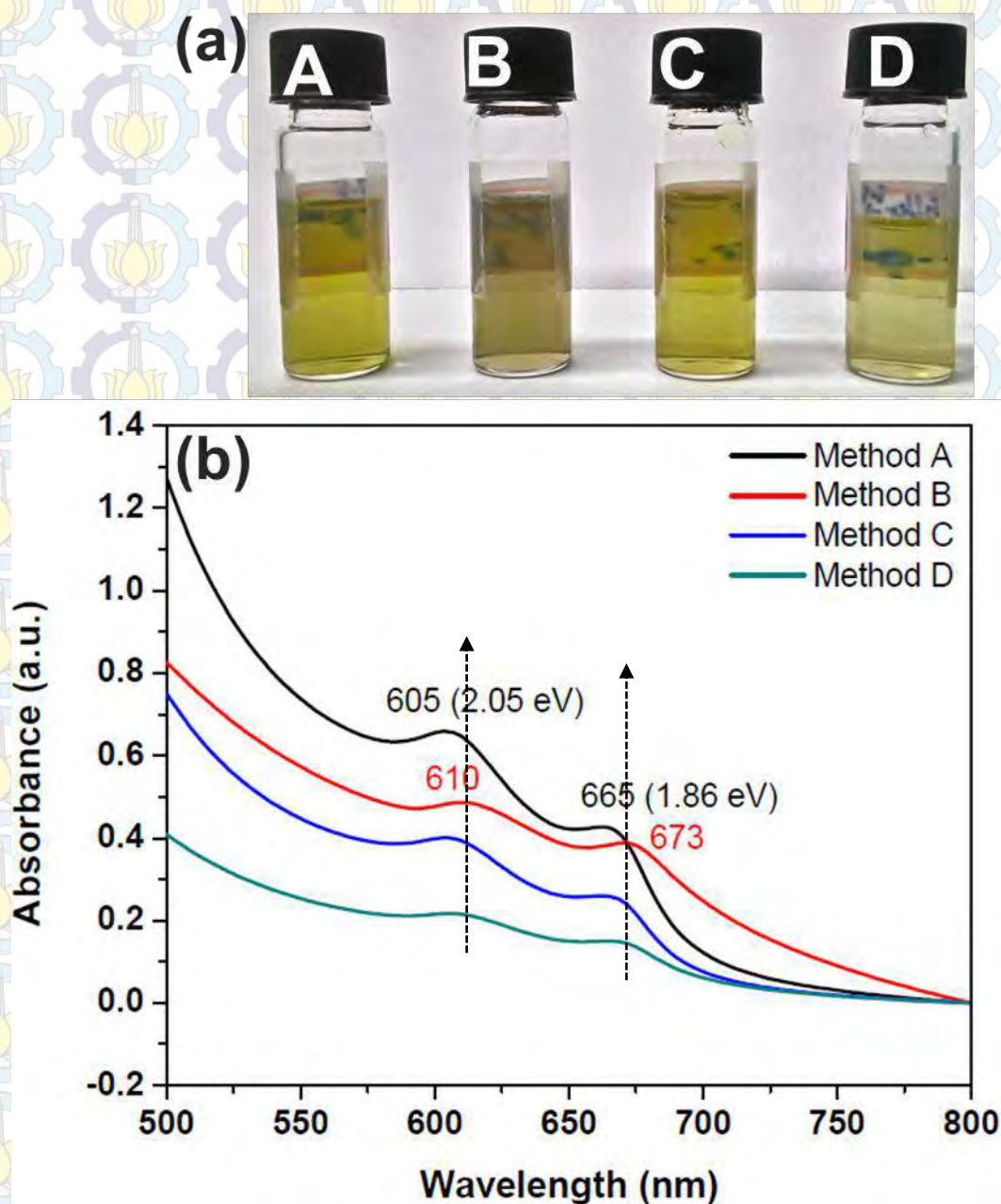
#### 4.3 Few-layer Molybdenum disulfide with Specific Flake Dimensions.

Recent research has indicated that graphene flakes can be selected by sizes by controlled centrifugation coupled with sediment recycling (Khan et al., 2012, May et al., 2012). Here we used centrifugation based on time and filtering to

control the size of few-layer MoS<sub>2</sub> nanosheets. While liquid exfoliation generally results in flakes which are small on average, the flake size distribution can be quite broad. In this work we developed methods to control sizes of MoS<sub>2</sub> nanosheets to predominately select flakes in the upper solution. To achieve this we used four methods as shown in experimental section, we combined centrifugation and filtration to reduce the bigger size of few-layer MoS<sub>2</sub> nanosheets. In method A, we used centrifugation at 2000 rpm for 60 minutes and then the top 1/2<sup>nd</sup> part of the supernatant was collected by pipette. When taking the supernatant we must be careful because sometimes the bigger size will be mixed into it. In method B, after the solution was filtered through PVDF membrane, the solution was taken while the solid sample was removed. In method C, the solution was centrifuged at 2000 rpm for 60 minutes and the followed by filtration. In the first step, the top 1/2<sup>nd</sup> part of the supernatant was collected by pipette and entered to vials and the next step the solution was filtered using PVDF membrane. Then the solution was taken while the solid sample was removed. In method D, we used the solution from method B after filtering, then the solution was centrifuged at 2000 rpm for 30 minutes, after that the top 1/2<sup>nd</sup> part of the supernatant was collected by pipette and entered to vials. After each centrifugation and filtration step, we performed spectroscopic measurements. The color of the resultant dispersions varied in different procedures (method A, B, C, and D) indicating that the nature of the nanosheets is indeed changed. As shown in Figure 4.11a, the color in the method B is the darkest than others, and after centrifuged, the color changes slowly to be brighter. According to the previous research (Wang et al., 2014), the peaks position at 673 and 610 nm are assigned to the *K* point of the Brillouin zone in 2D MoS<sub>2</sub> with relatively larger lateral dimensions (Method B). We also found large shift for the method A, C, and D in the optical absorption in comparison to those of MoS<sub>2</sub> nanosheets with relatively smaller lateral dimensions, arising from the quantum size effect of MoS<sub>2</sub> nanosheets (Figure 4.11b).

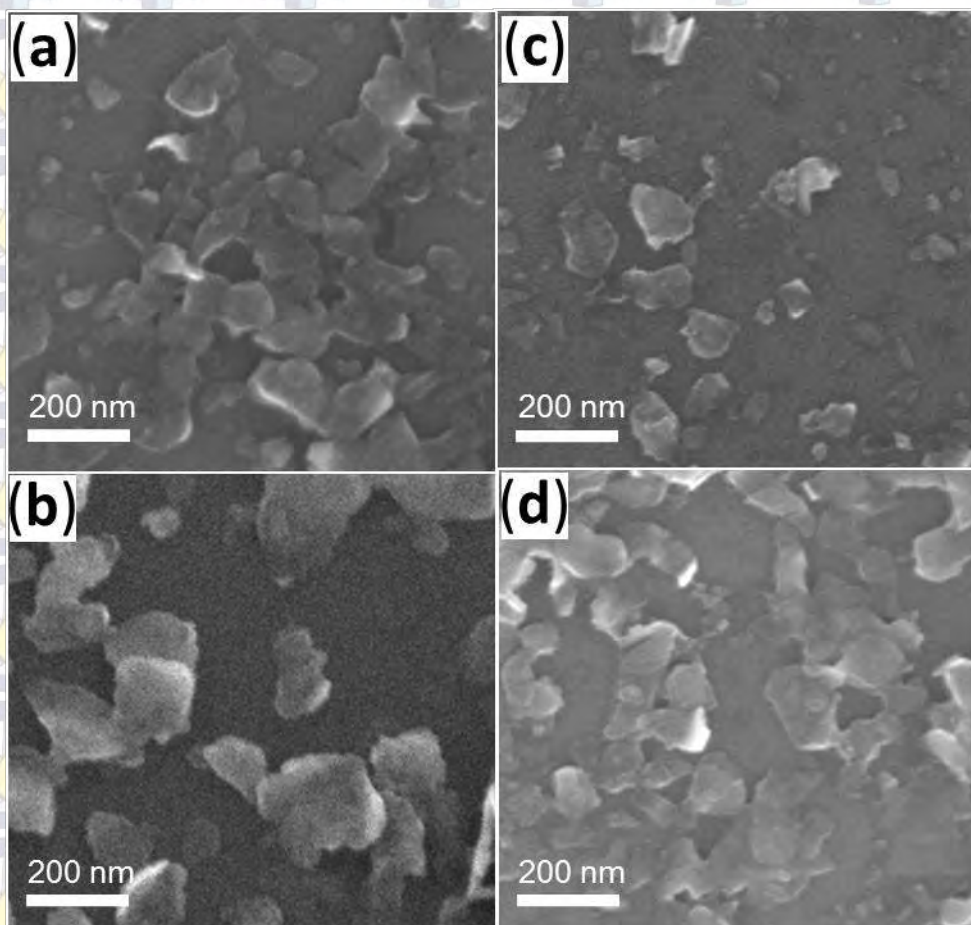
We also performed SEM, TEM and HRTEM to determine the quality and dimension of the flakes during controlled centrifugation and filtering regime. The

SEM images (Figure 4.12) illustrated that the MoS<sub>2</sub> was well exfoliated for all of methods. In addition, we noticed that size-selected few layer flakes tended to have smaller flakes adsorbed in many cases. As shown in Figure 4.12, the sample B had the largest lateral dimension, which agrees well with the UV-vis spectra (Figure 4.11).



**Figure 4.11.** (a) Digital images of the dispersions after size selection; (b) Absorption spectra of few-layer MoS<sub>2</sub> nanosheets from different methods.





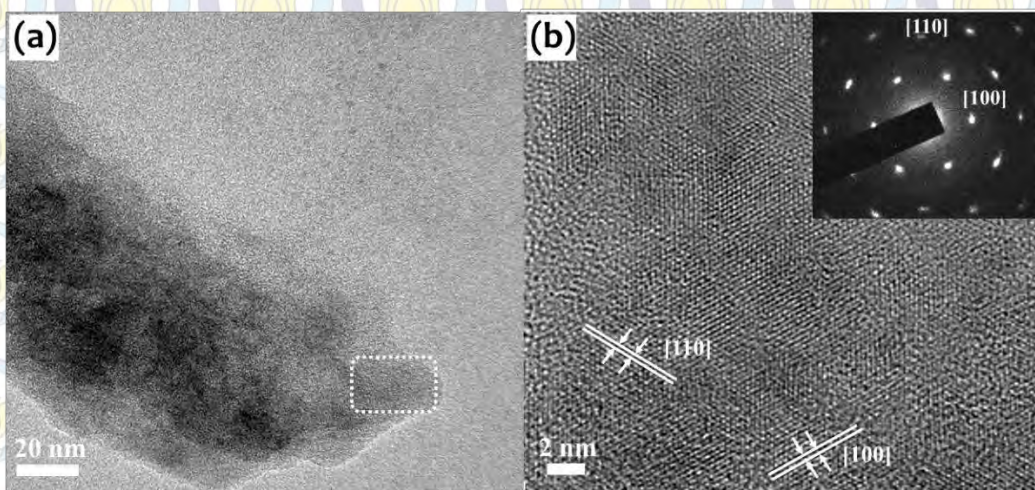
**Figure 4.12.** SEM images of size selected dispersions produced by (a) Method A, (b) Method B, (c) Method C, (d) Method D.

Table 4.1 shows that the molar ratio of every few-layer MoS<sub>2</sub> sample from different methods is close to 1:2, which is consistent with the formula. The completely EDS-SEM results can be found in appendix B (**Error! Reference source not found.**).

The lateral sizes of the few-layer flakes are also observed by SEM micrographs. The SEM micrographs illustrated that the MoS<sub>2</sub> bulk has been successfully exfoliated into few-layer MoS<sub>2</sub> nanosheets with different lateral size. Sample D displays a smaller lateral size than sample B, but it is bigger than sample A and B (see Figure 4.12).

**Table 4.1.** Summary of EDS-SEM analysis from different method

Method	Molar ratio (S/Mo)
A	2.27
B	1.97
C	1.93
D	2.13



**Figure 4.13.** (a) TEM image of an individual few-layer MoS<sub>2</sub> nanosheet; (b) High resolution TEM image of an individual few-layer MoS<sub>2</sub> nanosheet, with an inset showing the SAED pattern. All images from sample A.

Figure 4.13 shows the transmission electron microscopy image for the few-layer MoS<sub>2</sub> from sample A. From Figure 4.13a shows that the layer-structure few-layer MoS<sub>2</sub> overlap each other. The high resolution TEM image (Figure 4.13b) and the corresponding selected area electron diffraction (SAED) pattern (inset of Figure 4.13b) reveal the hexagonal lattice structure, which had good agreement with XRD pattern. And in the SAED pattern, the lattice spacing of 0.27 nm and 0.16 nm assigned to the [100] and [110] planes have been observed. Moreover, as expected, the HRTEM illustrates that the MoS<sub>2</sub> nanosheets have 2D

hexagonal symmetry crystalline structure with lattice spacing of 0.30 nm (see **Error! Reference source not found.** in appendix B), consistent with bulk MoS<sub>2</sub> materials. We also performed DLS results to confirm that the MoS<sub>2</sub> has been exfoliated into few-layer MoS<sub>2</sub> nanosheets with different lateral dimensions.

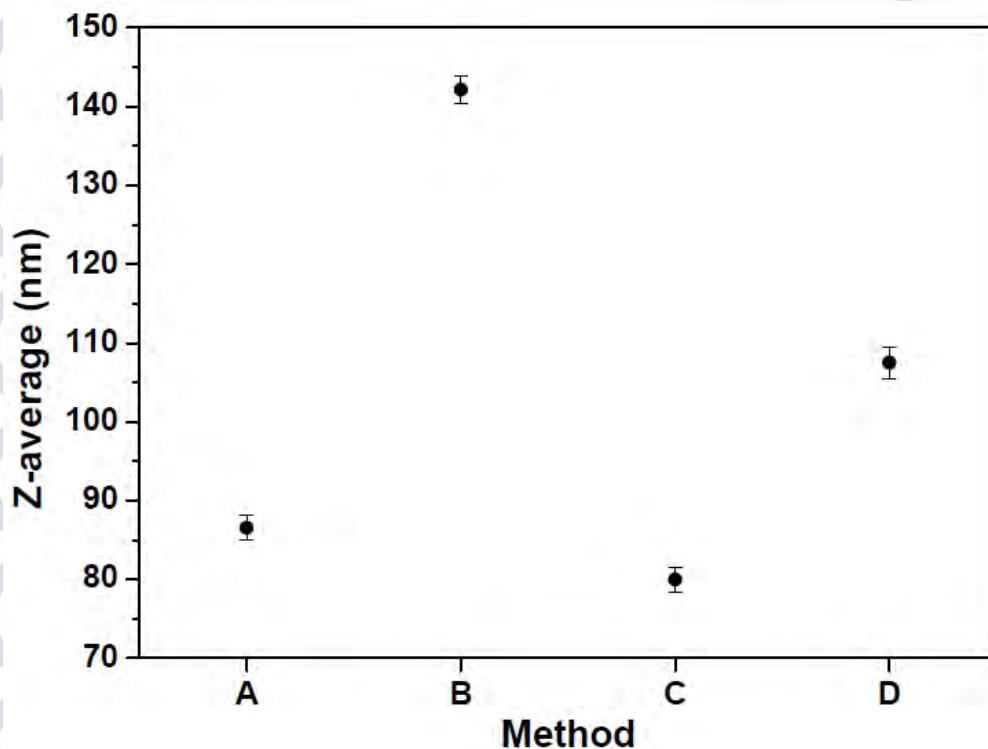


**Figure 4.14.** Various flake sizes according to DLS analysis.

Figure 4.14 shows that the few-layer MoS<sub>2</sub> nanosheets with different lateral sizes can be prepared using centrifugation and filtration. Dispersed few-layer MoS<sub>2</sub> nanosheets have Z-average particle size ranging 85-145 nm.

Sample A has a Z-average particle size of  $87.5 \pm 2.5$  nm; sample B  $142.5 \pm 2.5$  nm; sample C  $80.5 \pm 2.5$  nm; and sample D  $107.5 \pm 2.5$  nm. These results are consistent with the SEM results, which suggests that the sample B has the biggest size.

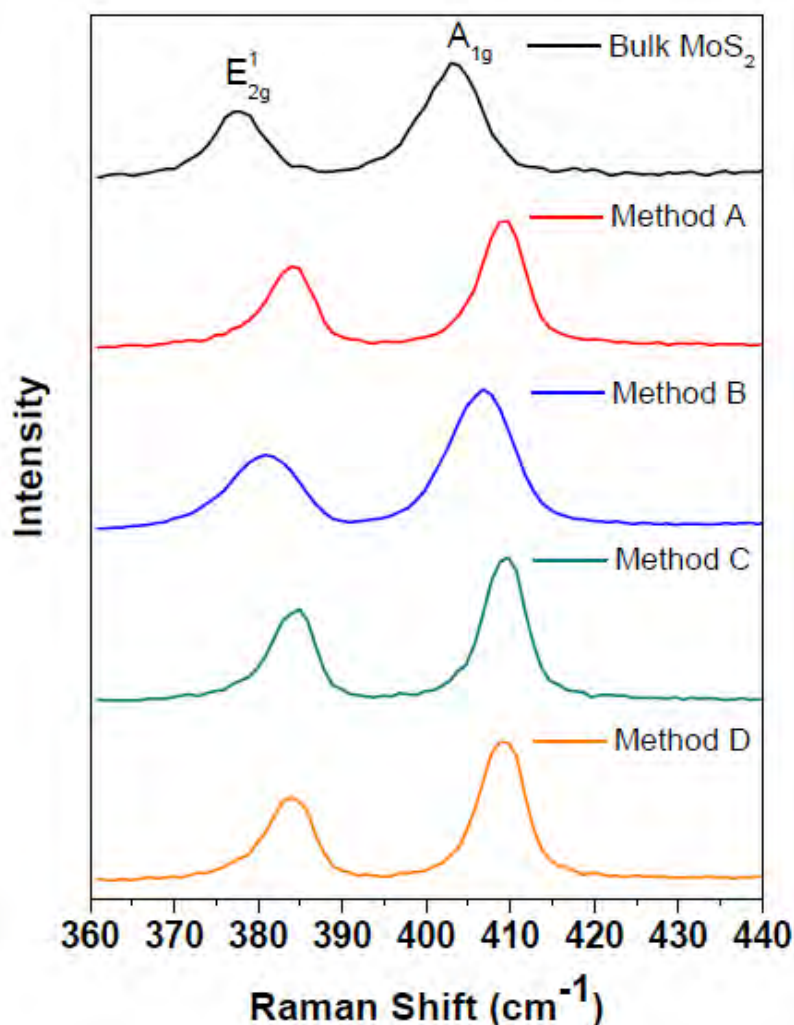


**Figure 4.15.** Typical Raman spectra of sample A, B, C, D and bulk MoS<sub>2</sub>

Raman spectroscopy was usually used to study the crystalline structures and quantitatively identify the layer numbers of graphene and MoS<sub>2</sub>. Figure 4.15 shows the two characteristic Raman modes ( $E_{2g}^1$  and  $A_{1g}$ ) of sample A, B, C, and D, which possess the similar Raman spectra like that of the sample after sonication. Sample A exhibits a smallest  $\Delta k$  (23.89 cm<sup>-1</sup>), which is consistent with the reported value for 3-5 layers (Yu et al., 2013b). Actually, the frequency differences between  $E_{2g}^1$  and  $A_{1g}$  peaks, instead of the intensities and widths of the peaks, were used as the reliable features to identify the layer of MoS<sub>2</sub>. For instance, the frequency difference ( $\Delta k$ ) 20-21.2 cm<sup>-1</sup> corresponds to a single layer MoS<sub>2</sub> (Yu et al., 2013b). A MoS<sub>2</sub> flake with  $\Delta k$  of ~23.6 cm<sup>-1</sup> has

been expected to possess three layers (Li et al., 2012) and a MoS<sub>2</sub> flake with  $\Delta k$  of  $\sim 24.3 \text{ cm}^{-1}$  has been proposed contain four layers (Ye et al., 2014) and  $\Delta k$  of  $\sim 24.9 \text{ cm}^{-1}$  to possess 6 layers (Lee et al., 2010). Thus, sample A are composed of three layers. Based on the reported data, sample B, C, and D with  $\Delta k$  of  $\sim 24.89 \text{ cm}^{-1}$  are identified as MoS<sub>2</sub> nanosheets with six layers. Atomic Force Microscopy (AFM) are also used to confirm numbers of layers in nanosheets. Tapping mode of AFM is used to assess the thickness of 2D MoS<sub>2</sub> nanosheets. From AFM images, some aggregation or overlapping between individual sheets are found. The resulting dispersion on the Si substrate was nonhomogeneous due to partial aggregation. Some individual MoS<sub>2</sub> nanosheets can be identified to have average thickness of ca. 3 nm from sample A and ca. 4 nm from sample C, indicating that one sheet consists of ca. 4 and 6 layers, respectively (as shown in Figure 4.16) (Knirsch et al., 2015).

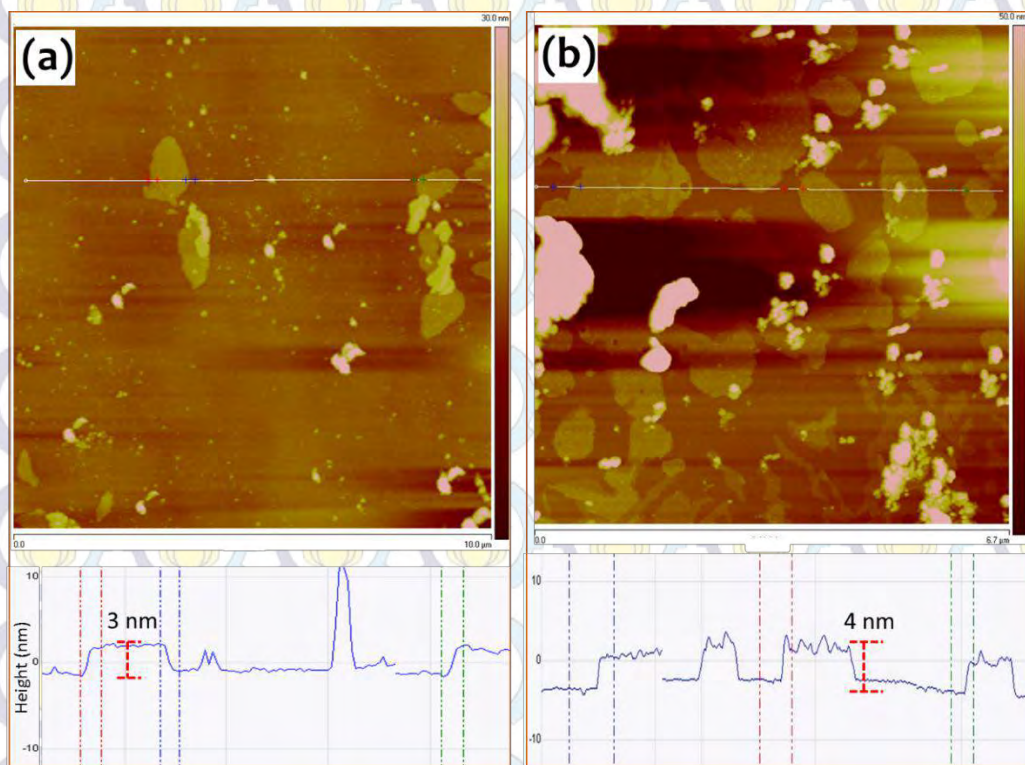
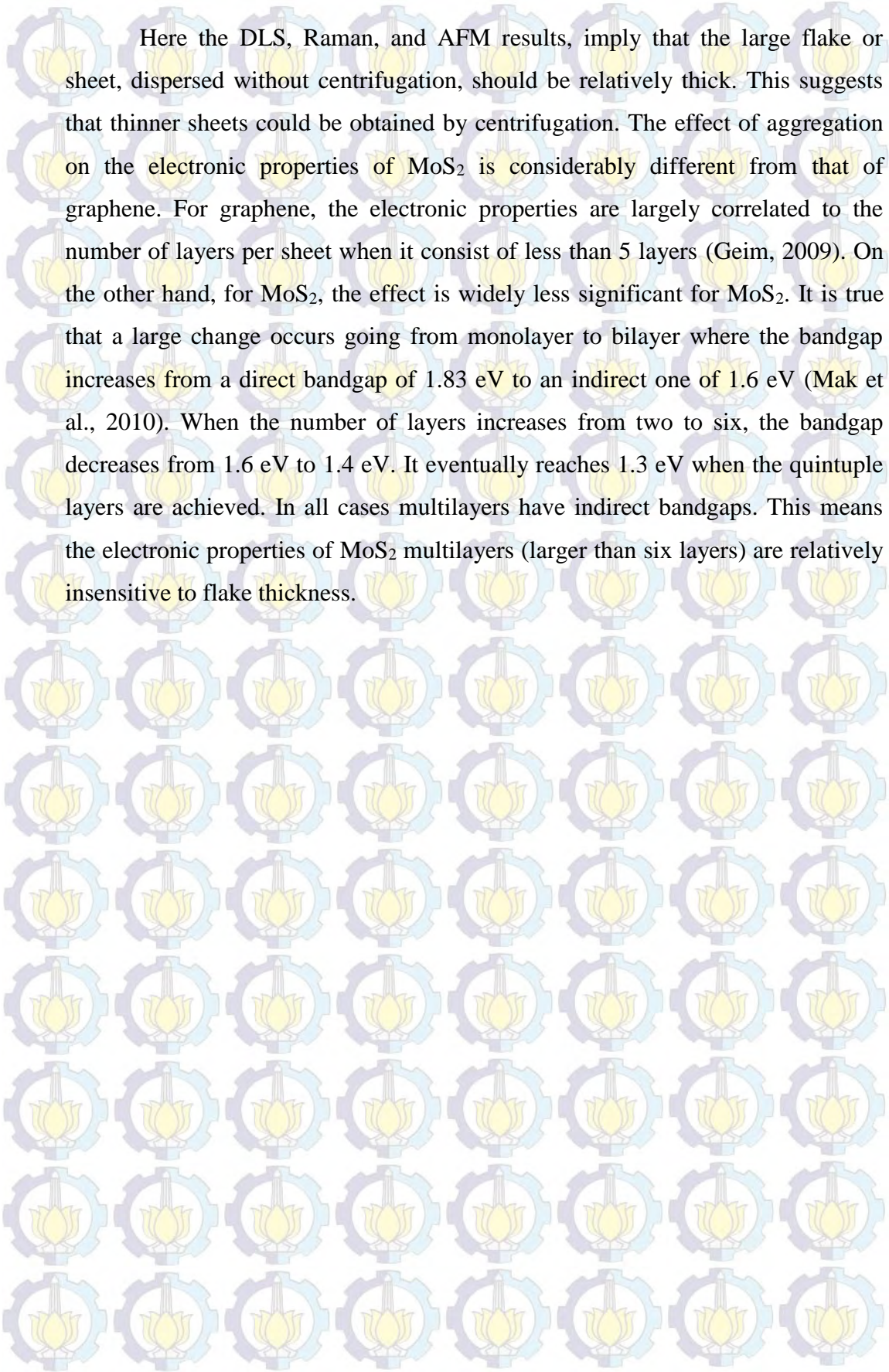
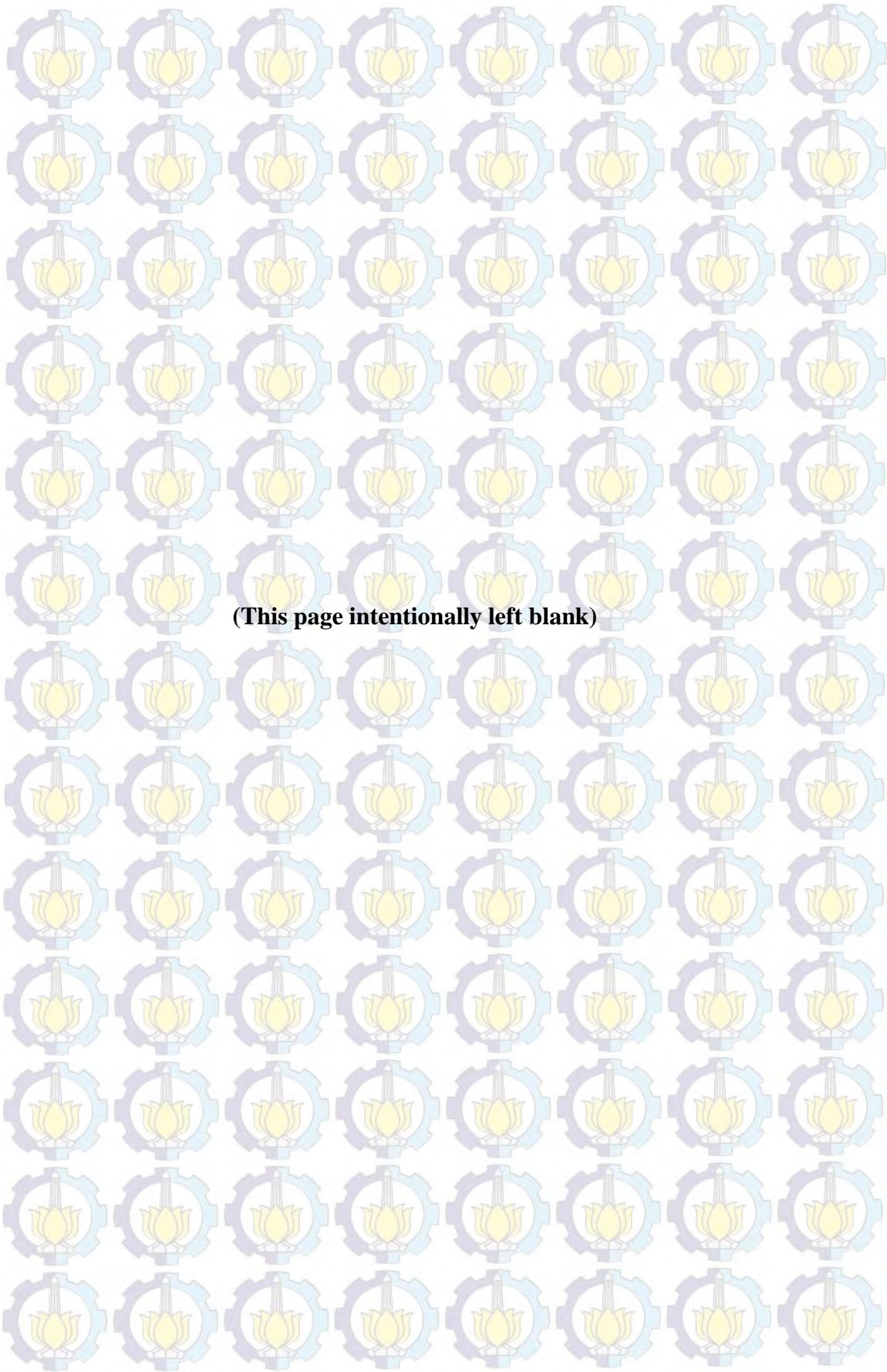


**Figure 4.16.** Atomic force microscopy (AFM) image of individual exfoliated MoS<sub>2</sub> sheets: (a) sample A; (b) sample C.



Here the DLS, Raman, and AFM results, imply that the large flake or sheet, dispersed without centrifugation, should be relatively thick. This suggests that thinner sheets could be obtained by centrifugation. The effect of aggregation on the electronic properties of MoS<sub>2</sub> is considerably different from that of graphene. For graphene, the electronic properties are largely correlated to the number of layers per sheet when it consists of less than 5 layers (Geim, 2009). On the other hand, for MoS<sub>2</sub>, the effect is widely less significant for MoS<sub>2</sub>. It is true that a large change occurs going from monolayer to bilayer where the bandgap increases from a direct bandgap of 1.83 eV to an indirect one of 1.6 eV (Mak et al., 2010). When the number of layers increases from two to six, the bandgap decreases from 1.6 eV to 1.4 eV. It eventually reaches 1.3 eV when the quintuple layers are achieved. In all cases multilayers have indirect bandgaps. This means the electronic properties of MoS<sub>2</sub> multilayers (larger than six layers) are relatively insensitive to flake thickness.



**(This page intentionally left blank)**

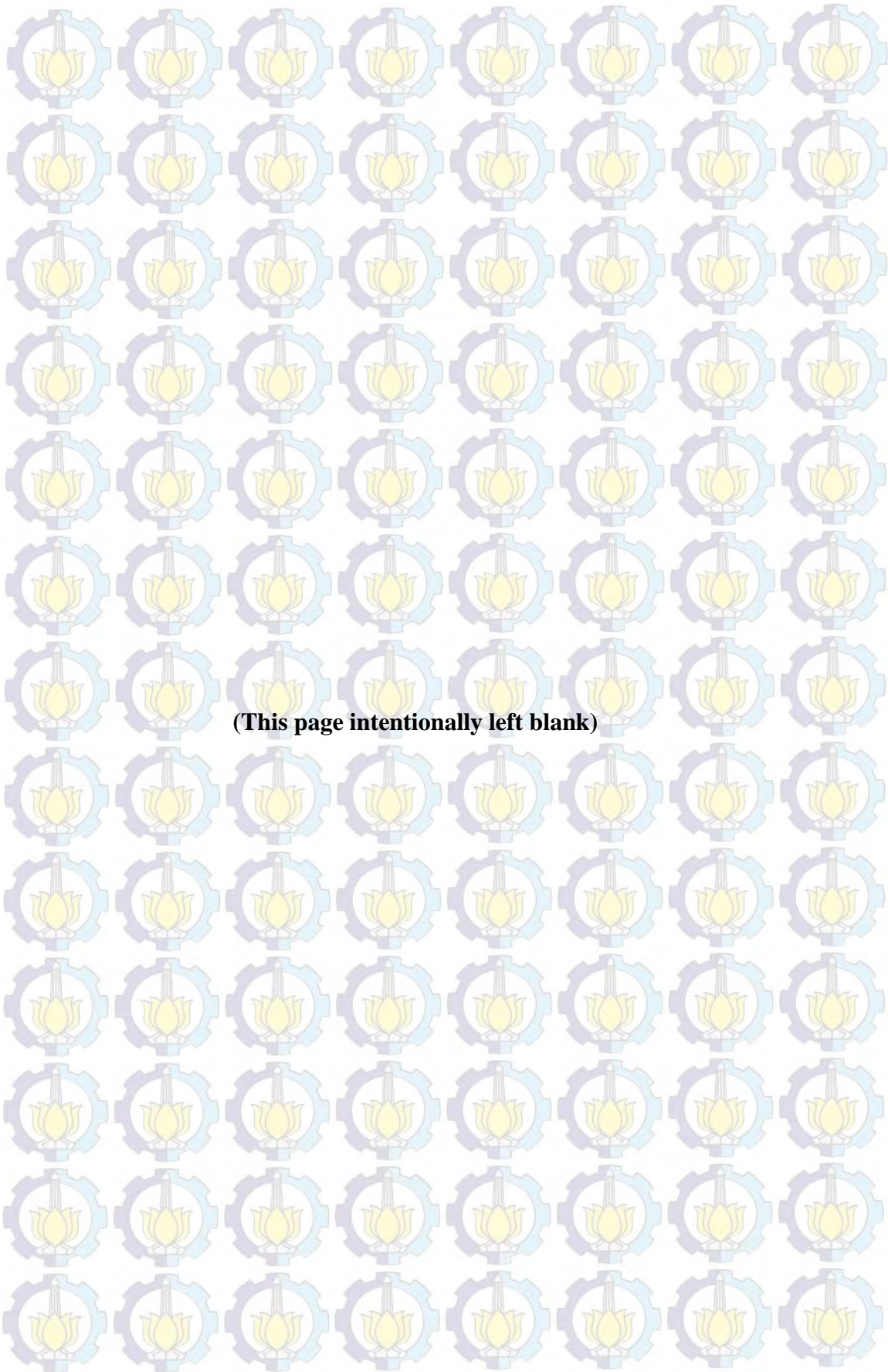


## CHAPTER 5

### CONCLUSION

Solution-based exfoliation of layered 2D materials is a promising route for producing 2D crystals in large scale. In this work, few-layer MoS<sub>2</sub> nanosheets have been prepared successfully by lithium intercalation method from bulk MoS<sub>2</sub> powder. The as-prepared MoS<sub>2</sub> nanosheets have a flat and smooth surface. We also have demonstrated that controlled centrifugation and filtration can be used to separate few-layer MoS<sub>2</sub> flakes by sizes. According to DLS analysis, MoS<sub>2</sub> nanosheets with different mean flake lengths ranging 85 – 145 nm are obtained. The as-obtained few-layer MoS<sub>2</sub> nanosheets possess 3-6 layers according to Raman and AFM results. The MoS<sub>2</sub> nanosheets are able to be used for the potential application in hydrogen production.





**(This page intentionally left blank)**

## REFERENCES

- Ambrosi, A., Sofer, Z. & Pumera, M. 2015. Lithium intercalation compound dramatically influences the electrochemical properties of exfoliated MoS<sub>2</sub>. *Small*, 11, 605-12.
- Aruchamy, A. 1992. Photoelectrochemistry and photovoltaics of layered semiconductors. *Springer*, 14.
- B. C. Windom, W. G. S., And D. W. Hahn 2011. A Raman Spectroscopic Study of MoS<sub>2</sub> and MoO<sub>3</sub>: Applications to Tribological Systems. *Tribology Letters*, 42, 301-310.
- Bang, G. S., Nam, K. W., Kim, J. Y., Shin, J., Choi, J. W. & Choi, S. Y. 2014. Effective liquid-phase exfoliation and sodium ion battery application of MoS<sub>2</sub> nanosheets. *ACS Applied Mater Interfaces*, 6, 7084-9.
- Benavente, E., Santa Ana, M. A., Mendizábal, F. & González, G. 2002. Intercalation chemistry of molybdenum disulfide. *Coordination Chemistry Reviews*, 224, 87-109.
- Bernardi, M., Palummo, M. & Grossman, J. C. 2013. Extraordinary Sunlight Absorption and One Nanometer Thick Photovoltaics Using Two-Dimensional Monolayer Materials. *Nano Letters*, 13, 3664-3670.
- Bertolazzi, S., Brivio, J. & Kis, A. 2011. Stretching and Breaking of Ultrathin MoS<sub>2</sub>. *ACS Nano*, 5, 9703-9709.
- Cao, L., Yang, S., Gao, W., Liu, Z., Gong, Y., Ma, L., Shi, G., Lei, S., Zhang, Y., Zhang, S., Vajtai, R. & Ajayan, P. M. 2013. Direct laser-patterned micro-supercapacitors from paintable MoS<sub>2</sub> films. *Small*, 9, 2905-10.
- Castellanos-Gomez, A., Poot, M., Steele, G. A., Van Der Zant, H. S., Agrait, N. & Rubio-Bollinger, G. 2012. Elastic properties of freely suspended MoS<sub>2</sub> nanosheets. *Adv Mater*, 24, 772-5.

Choi, K., Lee, Y. T., Min, S.-W., Lee, H. S., Nam, T., Kim, H. & Im, S. 2013. Direct imprinting of MoS<sub>2</sub> flakes on a patterned gate for nanosheet transistors. *Journal of Materials Chemistry C*, 1, 7803.

Chou, S. S., Kaehr, B., Kim, J., Foley, B. M., De, M., Hopkins, P. E., Huang, J., Brinker, C. J. & Dravid, V. P. 2013. Chemically exfoliated MoS<sub>2</sub> as near-infrared photothermal agents. *Angew Chem Int Ed Engl*, 52, 4160-4.

Coleman, J. N., Lotya, M., O'Neill, A., Bergin, S. D., King, P. J., Khan, U., Young, K., Gaucher, A., De, S., Smith, R. J., Shvets, I. V., Arora, S. K., Stanton, G., Kim, H. Y., Lee, K., Kim, G. T., Duesberg, G. S., Hallam, T., Boland, J. J., Wang, J. J., Donegan, J. F., Grunlan, J. C., Moriarty, G., Shmeliov, A., Nicholls, R. J., Perkins, J. M., Grievson, E. M., Theuwissen, K., Mccomb, D. W., Nellist, P. D. & Nicolosi, V. 2011a. Two-dimensional nanosheets produced by liquid exfoliation of layered materials. *Science*, 331, 568-71.

Coleman, J. N., Lotya, M., O'Neill, A., Bergin, S. D., King, P. J., Khan, U., Young, K., Gaucher, A., De, S., Smith, R. J., Shvets, I. V., Arora, S. K., Stanton, G., Kim, H.-Y., Lee, K., Kim, G. T., Duesberg, G. S., Hallam, T., Boland, J. J., Wang, J. J., Donegan, J. F., Grunlan, J. C., Moriarty, G., Shmeliov, A., Nicholls, R. J., Perkins, J. M., Grievson, E. M., Theuwissen, K., Mccomb, D. W., Nellist, P. D. & Nicolosi, V. 2011b. Two-Dimensional Nanosheets Produced by Liquid Exfoliation of Layered Materials. *Science*, 331, 568-571.

Das, S., Kim, M., Lee, J.-W. & Choi, W. 2014. Synthesis, Properties, and Applications of 2-D Materials: A Comprehensive Review. *Critical Reviews in Solid State and Materials Sciences*, 39, 231-252.

Eda, G., Yamaguchi, H., Voiry, D., Fujita, T., Chen, M. & Chhowalla, M. 2011. Photoluminescence from Chemically Exfoliated MoS<sub>2</sub>. *Nano Letters*, 11, 5111-5116.

F. Wypych And R. Schollhorn 1992. *Journal of the Chemical Society, Chemical Communications*, 1386–1388.

Fontana, M., Deppe, T., Boyd, A. K., Rinzan, M., Liu, A. Y., Paranjape, M. & Barbara, P. 2013. Electron-hole transport and photovoltaic effect in gated MoS<sub>2</sub> Schottky junctions. *Scientific Reports*, 3.

Geim, A. K. 2009. Graphene: Status and Prospects. *Science*, 324, 1530-1534.

Geim, A. K. & Grigorieva, I. V. 2013. Van der Waals heterostructures. *Nature*, 499, 419-25.

Gupta, A., Arunachalam, V. & Vasudevan, S. 2015. Water Dispersible, Positively and Negatively Charged MoS<sub>2</sub> Nanosheets: Surface Chemistry and the Role of Surfactant Binding. *The Journal of Physical Chemistry Letters*, 6, 739-744.

Hara, M., Iwakabe, Y., Tochigi, K., Sasabe, H., Garito, A. F. & Yamada, A. 1990. Anchoring structure of smectic liquid-crystal layers on MoS<sub>2</sub> observed by scanning tunnelling microscopy. *Nature*, 344, 228-230.

Huang, X., Yin, Z., Wu, S., Qi, X., He, Q., Zhang, Q., Yan, Q., Boey, F. & Zhang, H. 2011. Graphene-Based Materials: Synthesis, Characterization, Properties, and Applications. *Small*, 7, 1876-1902.

Jaramillo, T. F. J., K. P.; Bonde, J.; Nielsen, J. H.; & Horch, S. C., I 2007. Identification of Active Edge Sites for Electrochemical H<sub>2</sub> Evolution from MoS<sub>2</sub> Nanocatalysts. *Science*, 317, 100-102.

Ji, S., Yang, Z., Zhang, C., Liu, Z., Tjiu, W. W., Phang, I. Y., Zhang, Z., Pan, J. & Liu, T. 2013. Exfoliated MoS<sub>2</sub> nanosheets as efficient catalysts for electrochemical hydrogen evolution. *Electrochimica Acta*, 109, 269-275.

Joensen, P., Frindt, R. F. & Morrison, S. R. 1986. Single-Layer MoS<sub>2</sub>. *Materials Research Bulletin*, 21, 457–461.

- Khan, U., O'Neill, A., Porwal, H., May, P., Nawaz, K. & Coleman, J. N. 2012. Size selection of dispersed, exfoliated graphene flakes by controlled centrifugation. *Carbon*, 50, 470-475.
- King, L. A., Zhao, W., Chhowalla, M., Riley, D. J. & Eda, G. 2013. Photoelectrochemical properties of chemically exfoliated MoS<sub>2</sub>. *Journal of Materials Chemistry A*, 1, 8935.
- Knirsch, K. C., Berner, N. C., Nerl, H. C., Cucinotta, C. S., Gholamvand, Z., Mcevoy, N., Wang, Z., Abramovic, I., Vecera, P., Halik, M., Sanvito, S., Duesberg, G. S., Nicolosi, V., Hauke, F., Hirsch, A., Coleman, J. N. & Backes, C. 2015. Basal-Plane Functionalization of Chemically Exfoliated Molybdenum Disulfide by Diazonium Salts. *ACS Nano*, 9, 6018-6030.
- Korn, T., Heydrich, S., Hirmer, M., Schmutzler, J. & Schüller, C. 2011. Low-temperature photocarrier dynamics in monolayer MoS<sub>2</sub>. *Applied Physics Letters*, 99, 102109.
- Lacaze, E., Barois, P. & Lacaze, R. 1997. A Model for the Structure of Crystalline Adsorbed Organic Monolayers with Application to nCB. *J. Phys. I France*, 7, 1645-1664.
- Lee, C., Yan, H., Brus, L. E., Heinz, T. F., Hone, J. & Ryu, S. 2010. Anomalous Lattice Vibrations of Single- and Few-Layer MoS<sub>2</sub>. *ACS Nano*, 4, 2695-2700.
- Lee, J. H., Jang, W. S., Han, S. W. & Baik, H. K. 2014. Efficient hydrogen evolution by mechanically strained MoS<sub>2</sub> nanosheets. *Langmuir*, 30, 9866-73.
- Li, H., Wu, J., Yin, Z. & Zhang, H. 2014. Preparation and applications of mechanically exfoliated single-layer and multilayer MoS<sub>2</sub> and WSe<sub>2</sub> nanosheets. *Accounts of Chemical Research*, 47, 1067-75.
- Li, H., Zhang, Q., Yap, C. C. R., Tay, B. K., Edwin, T. H. T., Olivier, A. & Baillargeat, D. 2012. From Bulk to Monolayer MoS<sub>2</sub>: Evolution of Raman Scattering. *Advanced Functional Materials*, 22, 1385-1390.

Li, X., Li, W., Li, M., Cui, P., Chen, D., Gengenbach, T., Chu, L., Liu, H. & Song, G. 2015. Glucose-assisted synthesis of the hierarchical TiO<sub>2</sub> nanowire@MoS<sub>2</sub> nanosheet nanocomposite and its synergistic lithium storage performance. *Journal of Materials Chemistry A*, 3, 2762-2769.

Lin, Y.-C., Dumcenco, D. O., Huang, Y.-S. & Suenaga, K. 2014. Atomic mechanism of the semiconducting-to-metallic phase transition in single-layered MoS<sub>2</sub>. *Nature Nanotechnology*, 9, 391-396.

Liu, H., Si, M., Najmaei, S., Neal, A. T., Du, Y., Ajayan, P. M., Lou, J. & Ye, P. D. 2013a. Statistical study of deep submicron dual-gated field-effect transistors on monolayer chemical vapor deposition molybdenum disulfide films. *Nano Letters*, 13, 2640-6.

Liu, Y., Ren, L., Qi, X., Yang, L., Li, J., Wang, Y. & Zhong, J. 2014. Hydrothermal exfoliated molybdenum disulfide nanosheets as anode material for lithium ion batteries. *Journal of Energy Chemistry*, 23, 207-212.

Liu, Y. D., Ren, L., Qi, X., Yang, L. W., Hao, G. L., Li, J., Wei, X. L. & Zhong, J. X. 2013b. Preparation, characterization and photoelectrochemical property of ultrathin MoS<sub>2</sub> nanosheets via hydrothermal intercalation and exfoliation route. *Journal of Alloys and Compounds*, 571, 37-42.

Lopez-Sanchez, O., Lembke, D., Kayci, M., Radenovic, A. & Kis, A. 2013. Ultrasensitive photodetectors based on monolayer MoS<sub>2</sub>. *Nature Nanotechnology*, 8, 497-501.

Lukowski, M. A., Daniel, A. S., Meng, F., Forticaux, A., Li, L. & Jin, S. 2013. Enhanced hydrogen evolution catalysis from chemically exfoliated metallic MoS<sub>2</sub> nanosheets. *Journal of the American Society*, 135, 10274-7.

Ma, L., Chen, W.-X., Xu, L.-M., Zhou, X.-P. & Jin, B. 2012. One-pot hydrothermal synthesis of MoS<sub>2</sub> nanosheets/C hybrid microspheres. *Ceramics International*, 38, 229-234.

- Mak, K. F., He, K., Shan, J. & Heinz, T. F. 2012. Control of valley polarization in monolayer MoS<sub>2</sub> by optical helicity. *Nature Nanotechnology*, 7, 494-8.
- Mak, K. F., Lee, C., Hone, J., Shan, J. & Heinz, T. F. 2010. Atomically Thin MoS<sub>2</sub>: A New Direct-Gap Semiconductor. *Physical Review Letters*, 105, 136805.
- May, P., Khan, U., O'Neill, A. & Coleman, J. N. 2012. Approaching the theoretical limit for reinforcing polymers with graphene. *Journal of Materials Chemistry*, 22, 1278-1282.
- Novoselov, K. S., Jiang, D., Schedin, F., Booth, T. J., Khotkevich, V. V., Morozov, S. V. & Geim, A. K. 2005. Two-dimensional atomic crystals. *Proceedings of the National Academy of Sciences of the United States of America*, 102, 10451-10453.
- O'Neill, A., Khan, U. & Coleman, J. N. 2012. Preparation of High Concentration Dispersions of Exfoliated MoS<sub>2</sub> with Increased Flake Size. *Chemistry of Materials*, 24, 2414-2421.
- Park, S. K., Yu, S. H., Woo, S., Quan, B., Lee, D. C., Kim, M. K., Sung, Y. E. & Piao, Y. 2013. A simple L-cysteine-assisted method for the growth of MoS<sub>2</sub> nanosheets on carbon nanotubes for high-performance lithium ion batteries. *Dalton Trans*, 42, 2399-405.
- Py, M. A. & Haering, R. R. 1983. Structural destabilization induced by lithium intercalation in MoS<sub>2</sub> and related compounds. *Canadian Journal of Physics*, 61, 76-84.
- Sánchez, V., Benavente, E., Santa Ana, M. A. & González, G. 1999. High Electronic Conductivity Molybdenum Disulfide-Dialkylamine Nanocomposites. *Chemistry of Materials*, 11, 2296-2298.
- Singh, A. K., Mathew, K., Zhuang, H. L. & Hennig, R. G. 2015. Computational Screening of 2D Materials for Photocatalysis. *The Journal of Physical Chemistry Letters*, 6, 1087-1098.

Somoano, R. & Woollam, J. 1979. Intercalation Compounds of Molybdenum Disulfide. *In: LÉVY, F. (ed.) Intercalated Layered Materials*. Springer Netherlands.

Somoano, R. B., Hadek, V. & Rembaum, A. 1973. Alkali metal intercalates of molybdenum disulfide. *The Journal of Chemical Physics*, 58, 697-701.

Splendiani, A., Sun, L., Zhang, Y., Li, T., Kim, J., Chim, C. Y., Galli, G. & Wang, F. 2010. Emerging photoluminescence in monolayer MoS<sub>2</sub>. *Nano Letters*, 10, 1271-5.

Su, D., Dou, S. & Wang, G. 2015. Ultrathin MoS<sub>2</sub> Nanosheets as Anode Materials for Sodium-Ion Batteries with Superior Performance. *Advanced Energy Materials*, 5, n/a-n/a.

Van Thanh, D., Pan, C.-C., Chu, C.-W. & Wei, K.-H. 2014. Production of few-layer MoS<sub>2</sub> nanosheets through exfoliation of liquid N<sub>2</sub>-quenched bulk MoS<sub>2</sub>. *RSC Advances*, 4, 15586.

Varrla, E., Backes, C., Paton, K. R., Harvey, A., Gholamvand, Z., McCauley, J. & Coleman, J. N. 2015. Large-Scale Production of Size-Controlled MoS<sub>2</sub> Nanosheets by Shear Exfoliation. *Chemistry of Materials*, 27, 1129-1139.

Voiry, D., Salehi, M., Silva, R., Fujita, T., Chen, M., Asefa, T., Shenoy, V. B., Eda, G. & Chhowalla, M. 2013. Conducting MoS<sub>2</sub> nanosheets as catalysts for hydrogen evolution reaction. *Nano Letters*, 13, 6222-7.

Wang, H., Lu, Z., Xu, S., Kong, D., Cha, J. J., Zheng, G., Hsu, P. C., Yan, K., Bradshaw, D., Prinz, F. B. & Cui, Y. 2013. Electrochemical tuning of vertically aligned MoS<sub>2</sub> nanofilms and its application in improving hydrogen evolution reaction. *Proceedings of the National Academy of Sciences of the United States of America*, 110, 19701-6.

Wang, N., Wei, F., Qi, Y., Li, H., Lu, X., Zhao, G. & Xu, Q. 2014. Synthesis of strongly fluorescent molybdenum disulfide nanosheets for cell-targeted labeling. *ACS Applied Material & Interfaces*, 6, 19888-94.



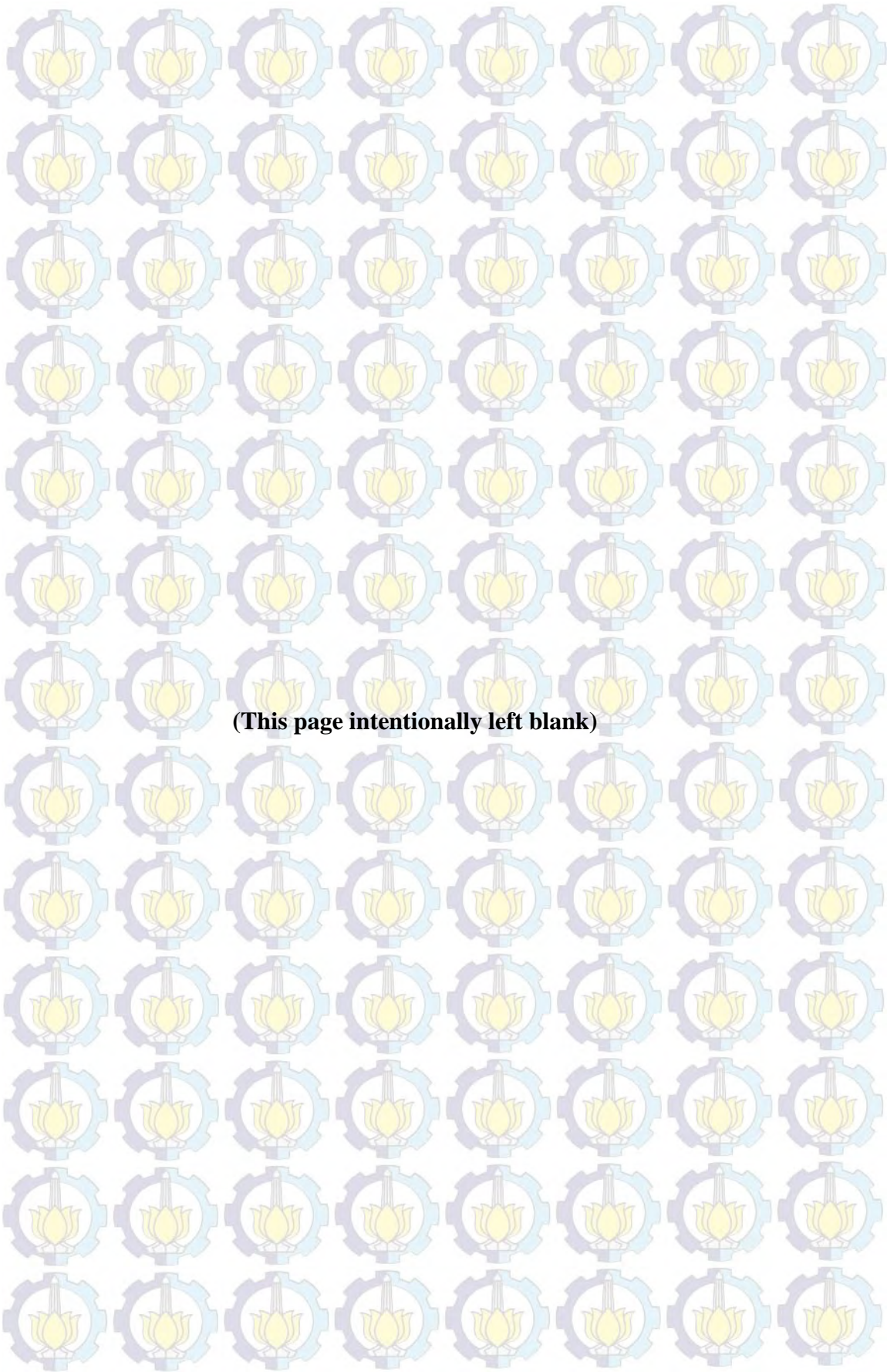
- Wang, Q. H., Kalantar-Zadeh, K., Kis, A., Coleman, J. N. & Strano, M. S. 2012a. Electronics and optoelectronics of two-dimensional transition metal dichalcogenides. *Nature Nanotechnology*, 7, 699-712.
- Wang, Q. H., Kalantar-Zadeh, K., Kis, A., Coleman, J. N. & Strano, M. S. 2012b. Electronics and optoelectronics of two-dimensional transition metal dichalcogenides. *Nature Nanotechnology*, 7, 699-712.
- Xiao, J., Choi, D., Cosimbescu, L., Koech, P., Liu, J. & Lemmon, J. P. 2010. Exfoliated MoS<sub>2</sub> Nanocomposite as an Anode Material for Lithium Ion Batteries. *Chemistry of Materials*, 22, 4522-4524.
- Yao, Y., Lin, Z., Li, Z., Song, X., Moon, K.-S. & Wong, C.-P. 2012. Large-scale production of two-dimensional nanosheets. *Journal of Materials Chemistry*, 22, 13494.
- Ye, L., Xu, H., Zhang, D. & Chen, S. 2014. Synthesis of bilayer MoS<sub>2</sub> nanosheets by a facile hydrothermal method and their methyl orange adsorption capacity. *Materials Research Bulletin*, 55, 221-228.
- Yin, Z., Chen, B., Bosman, M., Cao, X., Chen, J., Zheng, B. & Zhang, H. 2014. Au nanoparticle-modified MoS<sub>2</sub> nanosheet-based photoelectrochemical cells for water splitting. *Small*, 10, 3537-43.
- Yin, Z., Li, H., Li, H., Jiang, L., Shi, Y., Sun, Y., Lu, G., Zhang, Q., Chen, X. & Zhang, H. 2012. Single-Layer MoS<sub>2</sub> Phototransistors. *ACS Nano*, 6, 74-80.
- Yoon, Y., Ganapathi, K. & Salahuddin, S. 2011. How Good Can Monolayer MoS<sub>2</sub> Transistors Be? *Nano Letters*, 11, 3768-3773.
- You, X., Liu, N., Lee, C. J. & Pak, J. J. 2014. An electrochemical route to MoS<sub>2</sub> nanosheets for device applications. *Materials Letters*, 121, 31-35.
- Yu, Y., Li, C., Liu, Y., Su, L., Zhang, Y. & Cao, L. 2013a. Controlled Scalable Synthesis of Uniform, High-Quality Monolayer and Few-layer MoS<sub>2</sub> Films. *Scientific Reports*, 3.

Yu, Y., Li, C., Liu, Y., Su, L., Zhang, Y. & Cao, L. 2013b. Controlled scalable synthesis of uniform, high-quality monolayer and few-layer MoS<sub>2</sub> films. *Scientific Reports*, 3, 1866.

Zhang, Q., Xu, Z., Li, H., Wu, L., Cao, G. & Li, K. 2011. Synthesis of MoS<sub>2</sub> Nanosheets by Solid-State Reaction in CVD Furnace. *Integrated Ferroelectrics*, 128, 125-129.

Zhang, S.-L., Choi, H.-H., Yue, H.-Y. & Yang, W.-C. 2014. Controlled exfoliation of molybdenum disulfide for developing thin film humidity sensor. *Current Applied Physics*, 14, 264-268.

Zhou, X., Wang, Z., Chen, W., Ma, L., Chen, D. & Lee, J. Y. 2014. Facile synthesis and electrochemical properties of two dimensional layered MoS<sub>2</sub>/graphene composite for reversible lithium storage. *Journal of Power Sources*, 251, 264-268.



**(This page intentionally left blank)**

## APPENDIX A

### Few-layer MoS<sub>2</sub> without Selection of Size

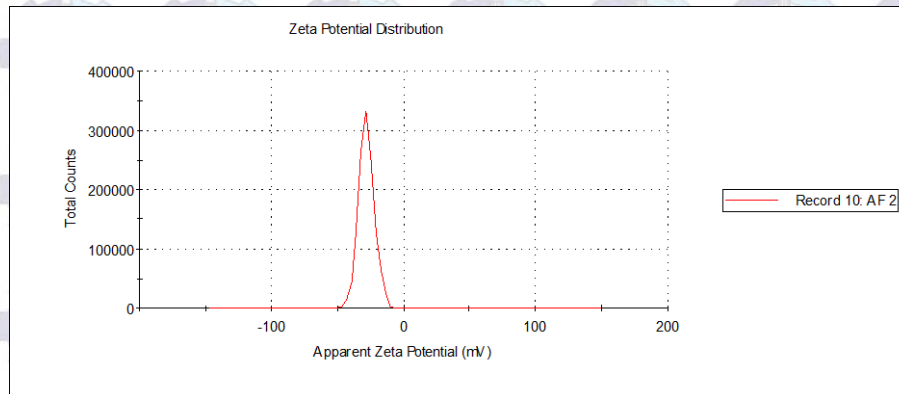
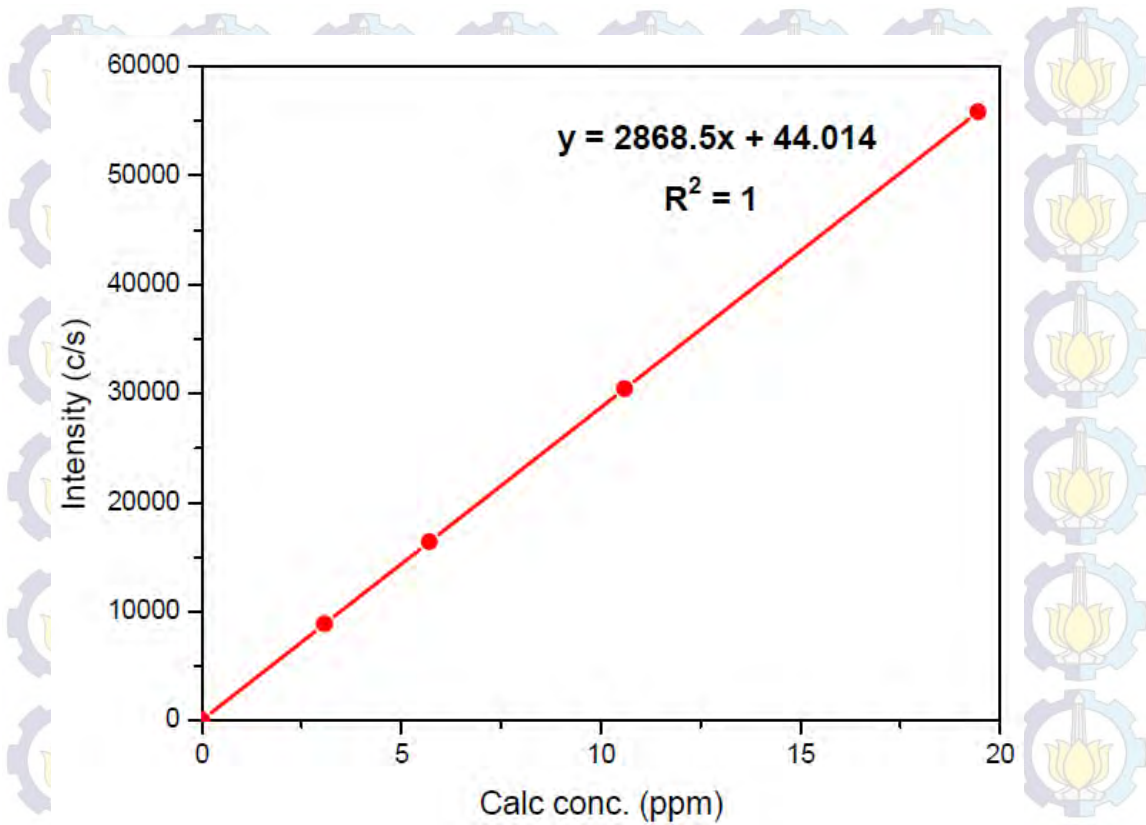


Figure A.1. Zeta potential distribution of 5<sup>th</sup> experiment

Table A.1. Summary of zeta potential in each of experiments

Experiment	1 <sup>st</sup>	2 <sup>nd</sup>	3 <sup>rd</sup>	4 <sup>th</sup>	5 <sup>th</sup>
Zeta Potential (mV)	-30	-30	-27.9	-29.9	-28.1



**Figure A.2.** The Calibration curve of lithium concentration in ICP-OES measurement

Li intercalated		MoS <sub>2</sub> nanosheets	
Intensity (c/s)	Calc conc. (ppm)	Intensity (c/s)	Calc conc. (ppm)
3363.70	<b>1.16</b>	201.33	<b>0.06</b>

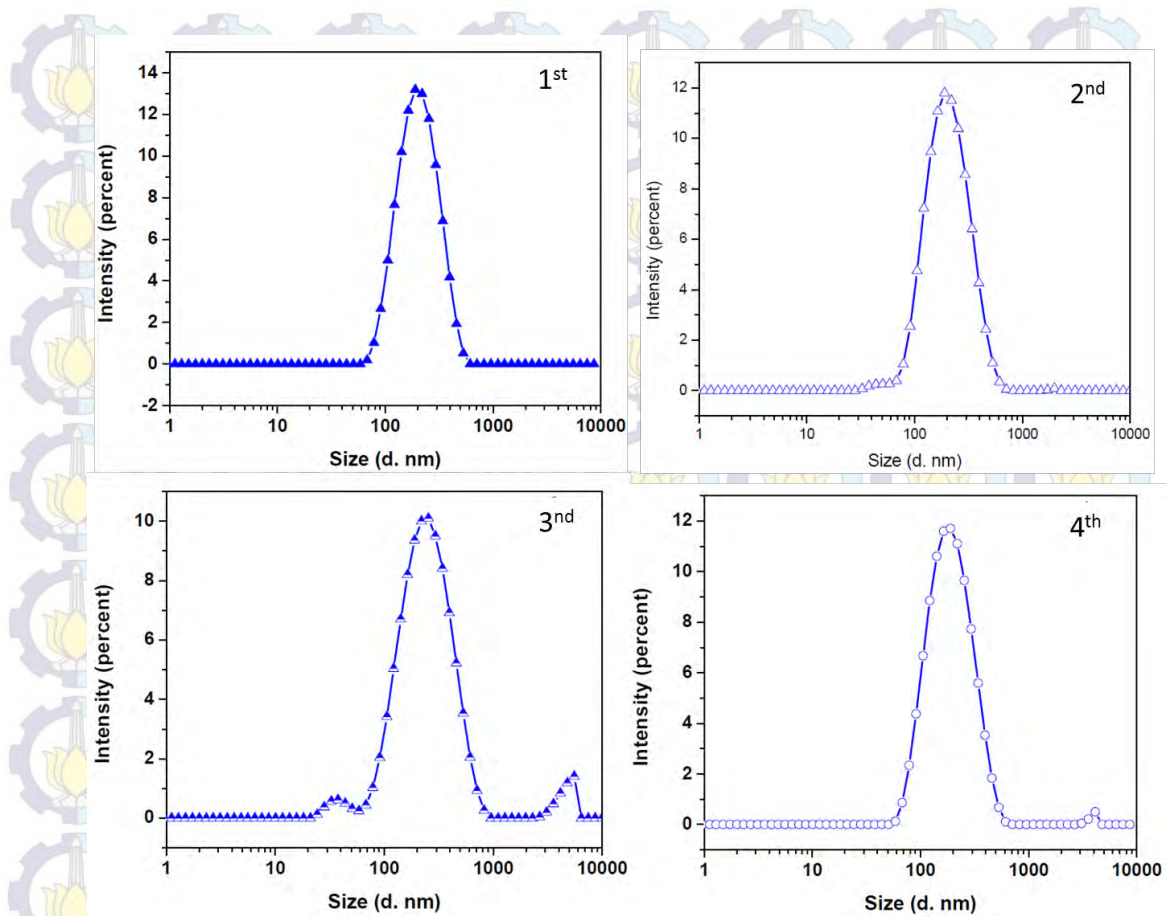


**Figure A.3.** Size distribution by intensity in repeating experiment.

Figure A.3 shows that in repeating experiment result the mean flake length of  $\sim 220$  nm, and some of nanosheets with smaller mean flake length of  $\sim 38$  and  $\sim 40$  nm. And the maximum of the mean flake length of the  $\text{MoS}_2$  nanosheets is about  $3 \mu\text{m}$  (see 4<sup>th</sup> experiment). And also in 3<sup>rd</sup> experiment, the small peak is observed at around  $5.8 \mu\text{m}$ . But during the SEM and TEM analysis, we did not see large objects around  $5.8 \mu\text{m}$ . However, this feature may be due to small dust particles or air bubbles in this dispersion.

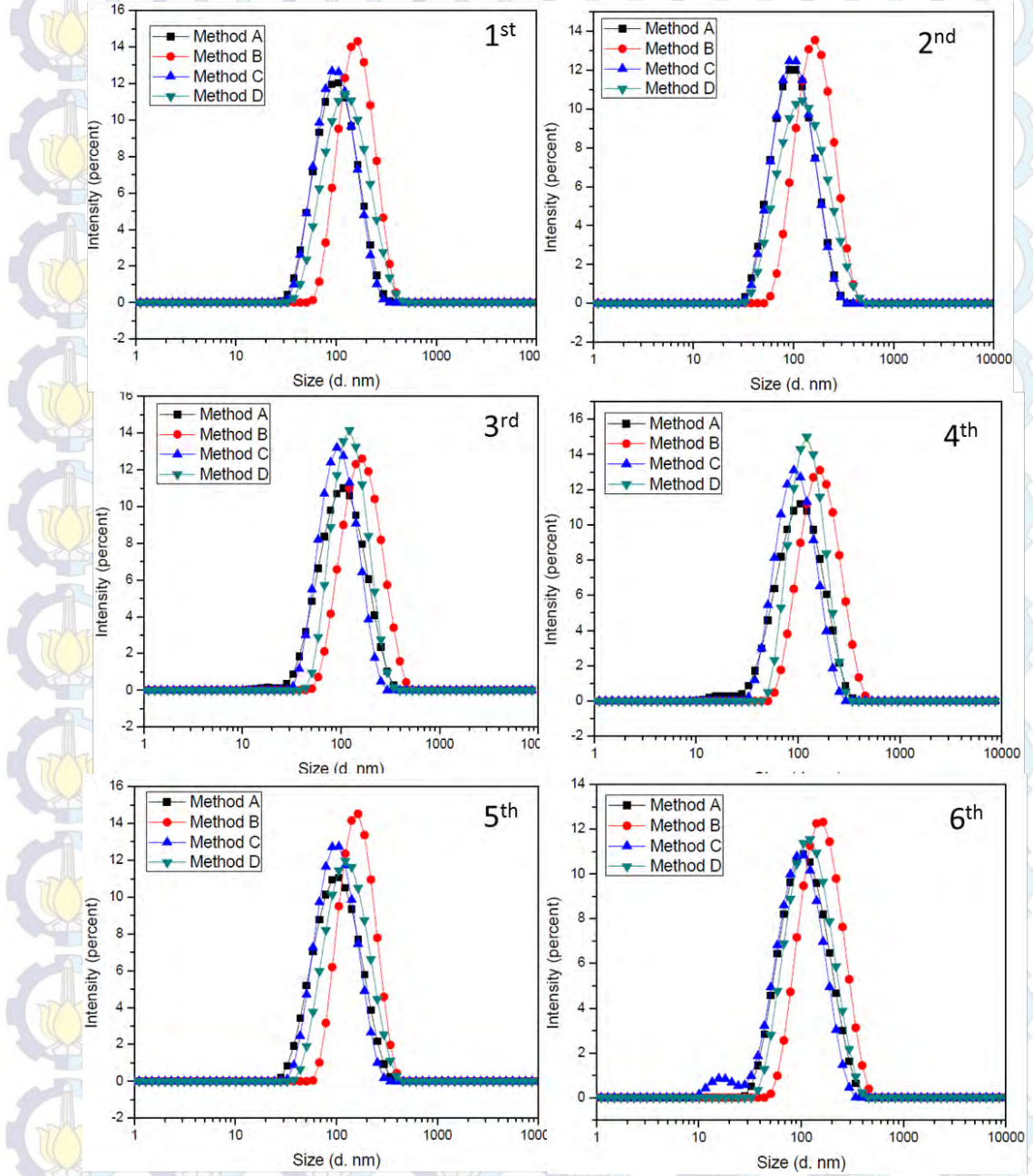
**Table A.2.** The frequency difference ( $\Delta k$ ) of MoS<sub>2</sub> nanosheets as the function of layer number.

Reported by	$\Delta k$ (A <sub>1g</sub> -E <sub>12g</sub> ) cm <sup>-1</sup>	Layer number of MoS <sub>2</sub>
Korn, T. et al <sup>73</sup>	18	1 layer
Yu, Y. et al <sup>68</sup>	20-21.2	1 layer
Van Thanh, V. et al <sup>74</sup>	21.7	2 layers
Yu, Y. et al <sup>68</sup>	22.4-23.2	2 layers
Yu, Y. et al <sup>68</sup>	23.6-23.9	3 layers
Yu, Y. et al <sup>68</sup>	24.0-24.2	4 layers
Lee, C. et al <sup>69</sup>	24.9	6 layers
Lee, C. et al <sup>69</sup>	25.6	bulk
Van Thanh, D. et al <sup>74</sup>	27.2	bulk

Note:  $k$  = wavenumber.

## APPENDIX B

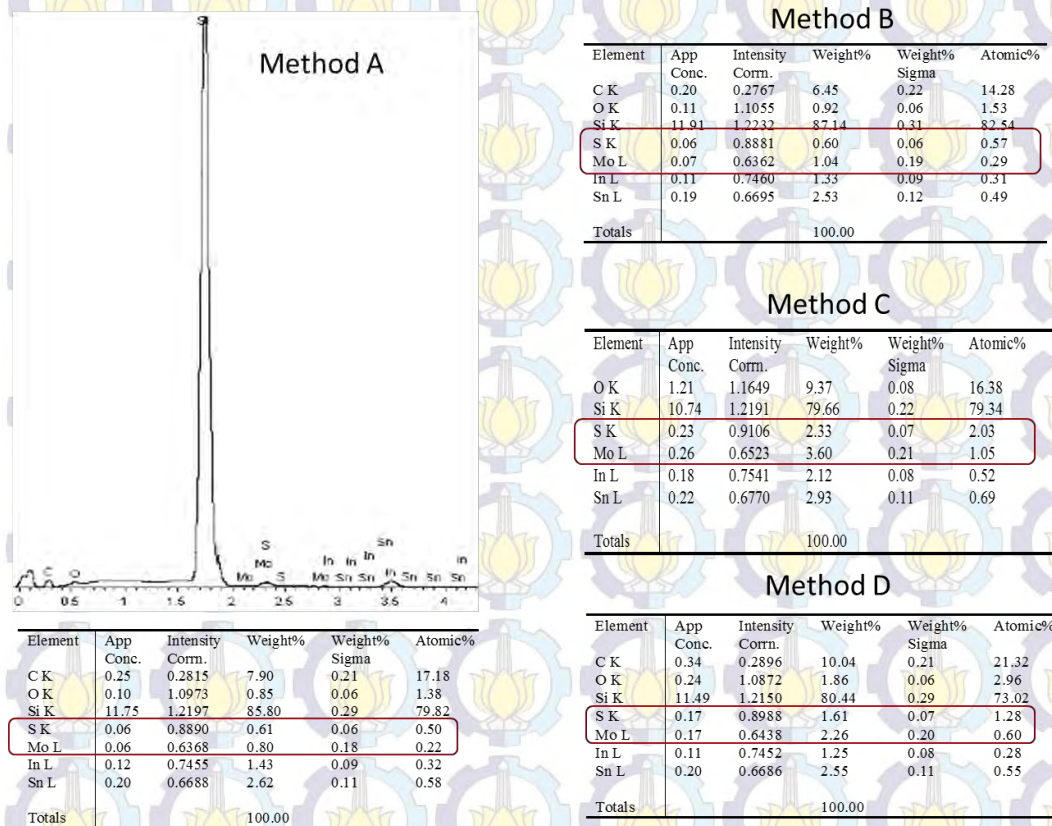
### Few-layer MoS<sub>2</sub> with Selection of Size



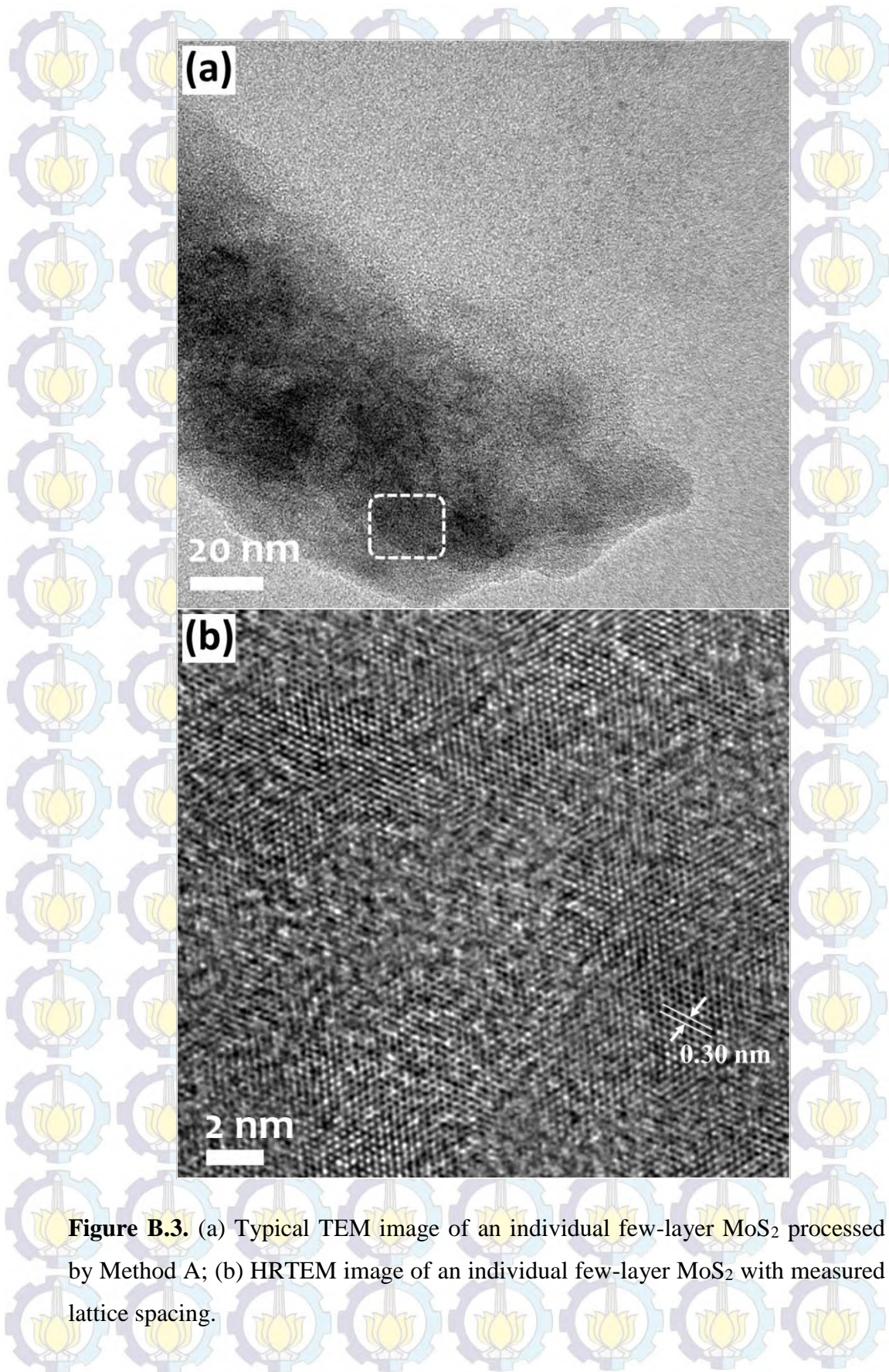
**Figure B.1.** Size distribution of Method A, B, C, and D by intensity in repeating experiment.



Figure B.1 shows that according to DLS measurements we have gotten MoS<sub>2</sub> nanosheets with different mean flake length. In the sixth experiment, the peak around 18 nm is observed, indicating the very small nanosheets contained therein. However, in others measurements we did not see this peak, may be the nanosheets were clustered by air bubbles in this dispersion.



**Figure B.2.** EDS-SEM spectra of an individual few-layer MoS<sub>2</sub> processed by Method A, B, C, and D.



**Figure B.3.** (a) Typical TEM image of an individual few-layer MoS<sub>2</sub> processed by Method A; (b) HRTEM image of an individual few-layer MoS<sub>2</sub> with measured lattice spacing.



**(This page intentionally left blank)**

## BIOGRAPHY



**Mohammad Sholeh** (born in Pati, Central Java, March 2, 1991) is a double degree student ITS-NTUST-Academia Sinica, Taiwan. The author started the education formal (kindergarten) in TK Pucakwangi 02 Pati at 1996-1997, then continued his primary school in SD Negeri Pucakwangi 02 at 1997-2003, junior high school in SMP Pucakwangi 01 Pati at 2003-2006 and for senior high school in SMAN 1 Pati at 2006-2009. He received his bachelor degree from the

Chemical Engineering, Faculty of Industrial Technology, Sepuluh Nopember Institute of Technology (Kampus ITS) Surabaya (2014), and his master degree from the Chemical Engineering, Faculty of Industrial Technology, Sepuluh Nopember Institute of Technology (Kampus ITS) and National Taiwan University of Science and Technology (NTUST)-Taiwan (2015). He also did research in Institute of Chemistry, Academia Sinica (AS) - Taiwan. He completed his master degree under the supervision of Professor Ming-Hsi Chiang (AS) and Dr. Kuswandi, DEA (ITS). His current research interests include two-dimensional nanomaterials, especially for molybdenum disulfide ( $\text{MoS}_2$ ) and its application in hydrogen production and also thermodynamic area, especially for liquid-liquid equilibria (LLE). If any question about this research, please contact me. Email: [mohammadsholeh126@gmail.com](mailto:mohammadsholeh126@gmail.com)

Thank you, 謝謝, Terima kasih ... Bye..bye...

“一切都很好”

## LIST OF FIGURES

<b>Figure 2.1.</b> Schematics illustration of the structural polytypes in TMDs, with the chalcogen atoms (X) in yellow and the metal atoms (M) in grey: 2H (hexagonal symmetry, two layers per unit cell, trigonal prismatic coordination), 3R (rhombohedral symmetry, three layers per unit cell, trigonal prismatic coordination) and 1T (tetragonal symmetry, one layer per unit cell, octahedral coordination). The lattice constants $a$ are in the range 3.1 to 3.7 Å for different materials, The stacking index $c$ indicates the number of layers in each stacking order, and the interlayer spacing is $\sim 6.5$ Å.....	8
<b>Figure 2.2.</b> (A) Bulk MoS <sub>2</sub> observed parallel to basal plane shows stacked trilayer structure. (B) Perpendicular to the basal plane the trigonal crystal structure can be observed.....	9
<b>Figure 2.3.</b> Electronic bandgap of bulk and monolayer MoS <sub>2</sub> .....	12
<b>Figure 4.1.</b> Schematic illustration of intercalation of lithium into MoS <sub>2</sub> layers. ....	21
<b>Figure 4. 2.</b> The zeta potential distribution of the exfoliated MoS <sub>2</sub> dispersions.....	22
<b>Figure 4.3.</b> (a) Digital images of the change in the solution containing bulk MoS <sub>2</sub> before (left) and after (right) reaction; (b) Digital image of the MoS <sub>2</sub> nanosheets by filtration using PVDF membrane with 450 nm pore size; (c) UV-vis absorption spectra of bulk MoS <sub>2</sub> and exfoliated MoS <sub>2</sub> nanosheets (after sonication for 38 h) dispersed in water. The inset photo is the dilute solution of MoS <sub>2</sub> nanosheets. ....	23
<b>Figure 4.4.</b> The XRD pattern of bulk MoS <sub>2</sub> , Li intercalated MoS <sub>2</sub> , and exfoliated MoS <sub>2</sub> nanosheets (top) with magnification of intensity of 5x (bottom).....	25
<b>Figure 4.5.</b> The typical SEM images: (a) and (b) Bulk MoS <sub>2</sub> powder with different resolution; (c) MoS <sub>2</sub> nanosheets with different lateral sizes; (d) MoS <sub>2</sub> nanosheets with lateral size <250 nm. ....	27
<b>Figure 4.6.</b> (a) EDS-SEM of silicon wafer; (b) A representative EDS-SEM spectrum collected from an individual MoS <sub>2</sub> nanosheets in silicon wafer. The inset image is the SEM image of MoS <sub>2</sub> nanosheets in EDS-SEM analysis.....	28
<b>Figure 4.7.</b> (a) Absorption spectrum of MoS <sub>2</sub> nanosheets after sonication (not further dilution). (b) Absorption spectra of MoS <sub>2</sub> nanosheets from (a) after 1 – 5 days. ....	29
<b>Figure 4.8.</b> Size distribution of MoS <sub>2</sub> nanosheets by intensity .....	31
<b>Figure 4.9.</b> TEM image of MoS <sub>2</sub> nanosheets .....	32

<b>Figure 4.10.</b> Raman spectra of bulk MoS <sub>2</sub> and exfoliated MoS <sub>2</sub> from lithium intercalation process. ....	33
<b>Figure 4.11.</b> (a) Digital images of the dispersions after size selection; (b) Absorption spectra of few-layer MoS <sub>2</sub> nanosheets from different methods. ....	35
<b>Figure 4.12.</b> SEM images of size selected dispersions produced by (a) Method A, (b) Method B, (c) Method C, (d) Method D. ....	36
<b>Figure 4.13.</b> (a) TEM image of an individual few-layer MoS <sub>2</sub> nanosheet; (b) High resolution TEM image of an individual few-layer MoS <sub>2</sub> nanosheet, with an inset showing the SAED pattern. All images from sample A. ....	37
<b>Figure 4.14.</b> Various flake sizes according to DLS analysis. ....	38
<b>Figure 4.15.</b> Typical Raman spectra of sample A, B, C, D and bulk MoS <sub>2</sub> ....	39
<b>Figure 4.16.</b> Atomic force microscopy (AFM) image of individual exfoliated MoS <sub>2</sub> sheets: (a) sample A; (b) sample C. ....	40
<b>Figure A.1.</b> Zeta potential distribution of 5 <sup>th</sup> experiment ....	55
<b>Figure A.2.</b> The Calibration curve of lithium concentration in ICP-OES measurement. ....	56
<b>Figure A.3.</b> Size distribution by intensity in repeating experiment. ....	57
<b>Figure B.1.</b> Size distribution of Method A, B, C, and D by intensity in repeating experiment. ....	59
<b>Figure B.2.</b> EDS-SEM spectra of an individual few-layer MoS <sub>2</sub> processed by Method A, B, C, and D. ....	60
<b>Figure B.3.</b> (a) Typical TEM image of an individual few-layer MoS <sub>2</sub> processed by Method A; (b) HRTEM image of an individual few-layer MoS <sub>2</sub> with measured lattice spacing. ....	61

# Preparation of MoS<sub>2</sub> Nanosheets for Energy Applications

**Mohammad Sholeh<sup>1,2,3</sup>, Ming-Hsi Chiang<sup>\*3</sup>**

<sup>1</sup> Department of Chemical Engineering, Institut Teknologi Sepuluh Nopember, Surabaya 60111, Indonesia

<sup>2</sup> Department of Chemical Engineering, National Taiwan University of Science and Technology, Taipei 10607, Taiwan

<sup>3</sup> Institute of Chemistry, Academia Sinica, Taipei 11529, Taiwan

\*Email: mhchiang@chem.sinica.edu.tw

**Abstract - Exfoliation of bulk MoS<sub>2</sub> via Li intercalation is an attractive route to large-scale preparation of MoS<sub>2</sub> few-layers and it can be used to realize their unique properties in practical applications. In general, solution-based exfoliation of layered materials results in flakes with lateral sizes of one micron or less on average. In this report, we performed the various preparations using a Li-intercalation method at room temperature to prepare MoS<sub>2</sub> few-layers with various flake sizes according to dynamic light scattering (DLS) analysis. MoS<sub>2</sub> few-layers with particle sizes ranging 85 to 145 nm are reported. We also characterize the few-layer MoS<sub>2</sub> nanosheets by various microscopic and spectroscopic techniques.**

**Keywords - MoS<sub>2</sub>, Nanosheets, Intercalation, Exfoliation.**

## INTRODUCTION

In recent decades, nanomaterials have attracted major attentions due to their fascinating properties and wide ranges of applications. There are two categories of nanomaterials: organic (mostly carbon allotropes) and inorganic nanomaterials, such as iron, silver, gold, boron nitride nanosheets (BNNs), molybdenum disulfide (MoS<sub>2</sub>), tungsten disulfide (WS<sub>2</sub>), etc. Inorganic nanomaterials, especially two-dimensional (2D) nanomaterials, have received tremendous attention in recent years because of unique both chemical and physical properties. The two-dimensional nanomaterials have completely different properties compared to the bulk materials (the quintuple layers). These properties includes high surface areas, mobility, conductivity, mechanical strength, transparency, electronics and optoelectronics. As one of the 2D nanomaterials, molybdenum disulfide possesses a sandwich structure which consist of covalent bonds in S-Mo-S structures that form by weak Van Der Waals forces between sheets. Therefore, it is probably easy to peel MoS<sub>2</sub> nanosheets from bulk material.<sup>1</sup> Bulk MoS<sub>2</sub> is a

semiconducting material with an indirect band gap of about 1.2 eV. When layered MoS<sub>2</sub> pristine is peeled to single-layer, it become a semiconductor with 1.8 eV direct band gap.<sup>2,3</sup> The wide band gap, which is thickness-dependent (bulk to single-layer), makes MoS<sub>2</sub> a promising candidate for many applications, such as electronic devices,<sup>4</sup> optoelectronic devices,<sup>5-8</sup> sensors,<sup>9</sup> and energy storage devices, like lithium ion batteries (LIB),<sup>10-13</sup> sodium ion batteries (SIB),<sup>14</sup> and capacitors.<sup>15</sup>

The other applications, which have become hot topics until now are utilization and optimization of exfoliated MoS<sub>2</sub> in either hydrogen evolution reaction (HER)<sup>16-18</sup> or water splitting.<sup>19,20</sup> If MoS<sub>2</sub>-based catalysts are to actualize their potential, there is an important need to increase the numbers of active sites and the catalytic activity by changing their electronic properties and conductivity via exfoliation of MoS<sub>2</sub> from bulk materials to nanosheets.<sup>17</sup> And also the size of nanosheets is an important factor in the hydrogen evolution reaction (HER).<sup>21</sup>

Recently, several methods have been reported for synthesizing single- and multi-layer MoS<sub>2</sub>. There are the mechanical exfoliation method,<sup>22,23</sup> chemical lithium intercalation and exfoliation using *n*-butyllithium,<sup>24,25</sup> electrochemical lithium intercalation and exfoliation,<sup>26</sup> liquid phase exfoliation using solvent and surfactants,<sup>27,28</sup> and synthesis of MoS<sub>2</sub> nanosheets via sear exfoliation.<sup>21</sup> Recently, many researchers made good quality MoS<sub>2</sub> monolayers using a chemical vapor deposition (CVD) or a Scotch tape-based micromechanical exfoliation method. However, a low yield is generally achieved in the Scotch tape method and a high temperature and cost of instruments are required for experiments in the CVD method.

Coleman et al. reported direct exfoliation of MoS<sub>2</sub> sheets with thickness of 3–12 nm and the lateral nanosheets size of 0.1-2 μm in organic solvents through sonication.<sup>27</sup> However this method leads to a low yield and the major issue is that specific nanosheet sizes cannot be obtained. It

is essential for various applications. For example, composite reinforcement requires large nanosheets<sup>29</sup> at least around 2  $\mu\text{m}$  in length, whereas a catalyst of hydrogen production requires small nanosheets with lateral size or length below 100 nm.<sup>30</sup> Significance of this work focuses on synthesis of few-layer MoS<sub>2</sub> nanosheets with specific lateral size via the lithium intercalation method and characterization of the materials.

## EXPERIMENTAL SECTION

**Materials.** The Molybdenum disulfide (MoS<sub>2</sub>) bulk powder used in these experiments was purchased from Alfa Aesar (99%) and 2.5 M n-butyl lithium in hexane was purchased from Chemetall.

**Preparation of MoS<sub>2</sub> nanosheets.** To make the MoS<sub>2</sub> nanosheets suspension, molybdenum disulfide bulk powder (300mg) was placed in a 100 mL flask, to which a 2 mL of 2.5 M n-butyl lithium in hexane and 18 mL of hexane anhydrous were added under N<sub>2</sub> atmosphere. Then, the solution was stirred for 5 days at room temperature. The resulting suspension was gravity-filtered under N<sub>2</sub>, and the solid washed with a few ml of anhydrous hexanes to remove any excess butyl lithium. Then, a few ml of distilled-water was added quickly to quench the sample. The MoS<sub>2</sub> paste was then taken after the solution was removed by rotavapor. To achieve the exfoliation of MoS<sub>2</sub>, 17.5 mg of the MoS<sub>2</sub> paste was suspended in 35 mL water in a 50 mL tube. Then, the mixture was sonicated continuously for 38 hours using a 1/2" (12.7 mm) diameter worn tip on replaceable tip (QSonica, 700W and 30% amplitude).

**Preparation of few-layers MoS<sub>2</sub> with specific flakes dimension.** In our experiment, to achieve a certain size of few-layer MoS<sub>2</sub>. We used four procedures to reduce sheet sizes to desired dimension. The first method is via centrifugation of the sample at 2000 rpm for 60 minutes (Method A). The second method involves filtration, through polyvinylidene difluoride (PVDF) membrane with pore size 450 nm, 47 mm diameter (Method B). The third one is via centrifugation at 2000 rpm for 60 minutes, followed by filtration (Method C). The fourth method involves filtration (PVDF membrane, pore size 450 nm, 47 mm diameter) followed by centrifugation at 2000 rpm for 30 minutes (Method D). In our experiments, after sonicated, 13 mL of solutions was placed in a vial. In Method A, 4.6 mL of 12 mL solutions in vials was taken and centrifuged at 2000 rpm for 60 minutes. The top 1/2<sup>nd</sup> part of the dispersion was collected by pipette. In Method B, 2.4 mL of remaining solution was dispersed in 12 mL Di-water. After that, the solution was filtered using PVDF membrane and the filtrate was collected. In Method C, 6 mL of remaining solution in vials was centrifuged at 2000 rpm for 60 minutes, then the top 1/2<sup>nd</sup> part of the dispersion was collected by pipette and was then filtered quickly. In

method D, 6 ml of the filtrate from method B was taken and centrifuged at 2000 rpm for 30 minutes. Then, the top 1/2<sup>nd</sup> part of the solution was collected by pipette. Then, all of the solution (from Method A, B, C, and D) were analyzed using UV-vis, dynamic light scattering (DLS), scanning electron microscopy (SEM), and Raman Spectroscopy.

**Characterization Method.** The absorbance spectra of the few-layer MoS<sub>2</sub> were recorded using a varian Cary 5000 and samples were tested in quartz glass cuvettes having 10 mm path length. The morphology of the samples was examined using scanning electron microscopy (SEM) model ZEISS-GEMINI Ultra Plus, with an Oxford Instruments EDS apparatus operated at 5 kV. For the EDS measurements, the EDS-SEM was operated at 10 kV. The TEM images were examined using transmission electron microscopy instrument (JEOL JEM-2100F) operated at an accelerating voltage of 200 kV. The X-ray diffraction (XRD) patterns were measured with a diffractometer (BRUKER, GADDS) using Cu K $\alpha$  ( $\lambda = 1.5418 \text{ \AA}$ ) radiation over the range of  $10^\circ \leq 2\theta \leq 80^\circ$  under a voltage of 40 kV and a current of 40 mA. Raman spectra were measured with in Via Confocal Raman Spectroscopy (NTEGRA Spectra, NT-MDT) at excitation laser line 488 nm in air ambient environment. The power of the excitation laser line was kept well below 1 mW to avoid heating effect and the spot size of 50  $\mu\text{m}$  with exposor time at 10 s and grating line at 1800/500 with range of  $\lambda = 500 \text{ nm}$ . Atomic force microscopy images was recorded on Veeco MultiMode VIII microscope in tapping mode. DLS measurements were performed using a Malvern Zetasizer Nano ZS with a 633 nm He-Ne laser. Samples were tested in low volume disposable sizing cuvettes. Malvern Zetasizer Nano ZS was operated in backscatter mode at an angle of  $173^\circ$  and analyzed three times for each samples. Samples were equilibrated to 25°C for 120 s prior to measurement. Viscosity and Refractive index of solvent (water) at 25°C are 0.8872 cP and 1.330, respectively. An automatic measurement positioning and automatic attenuation.

## RESULTS AND DISCUSSION

In recent years, MoS<sub>2</sub> based catalysts have been considered as promising material to replace platinum because of their high abundance and low cost. Promising catalytic activity of MoS<sub>2</sub> in the hydrogen evolution reaction (HER) is attributed to the active sites located along the edges of its two-dimensional layered crystals. If the MoS<sub>2</sub> based catalysts are to realize their potential, there is an urgent need to design MoS<sub>2</sub> nanosheets with more edge sites. The ability to control the nanosheets size during exfoliation process, achieved here by control of centrifugation and filtration, will be important for the number of applications. One of the most important applications is as catalyst for the evolution of hydrogen



from proton-rich electrolytes.<sup>30</sup> Because the catalytically active sites reside on edge of nanosheets, Hydrogen evolution catalyst is strongly dependent on nanosheets length with small flakes performing much better than larger ones.<sup>21</sup> And the change of phase MoS<sub>2</sub> from semiconducting to metallic which happened during intercalation process is to be an important factor in evolution of hydrogen because in the previous research shown that the metallic phase has catalytic activity is better than semiconducting phase.<sup>18</sup> For another application, lithium ion batteries are still exist and high efficient energy in industrial battery. So, in here we reported the preparation MoS<sub>2</sub> nanosheets with specific flake dimensions using lithium intercalation method to provide material which can be applied in those applications.

**Intercalation of Lithium** - Chemical exfoliation of layered materials is generally achieved by reacting the 2D nanomaterials with *n*-butyl lithium. The electrons from *n*-butyl lithium (as a guest) are transferred to the lowest-lying-unoccupied energy levels of MoS<sub>2</sub> (as a host), which are fundamentally transition metal d bands (as shown in Figure 1).<sup>31</sup> And also the charge transfer from *n*-BuLi to MoS<sub>2</sub> actually may induce structural changes in the host. Structural and electronic changes in the host of MoS<sub>2</sub> produced by lithium intercalation method often induce dramatic changes in the transport properties of MoS<sub>2</sub> from semiconducting to metallic.<sup>32</sup> The important thing is that when the bulk materials become nanosheets, the properties change, such as mechanical, electronic and thermodynamic properties.<sup>33</sup>

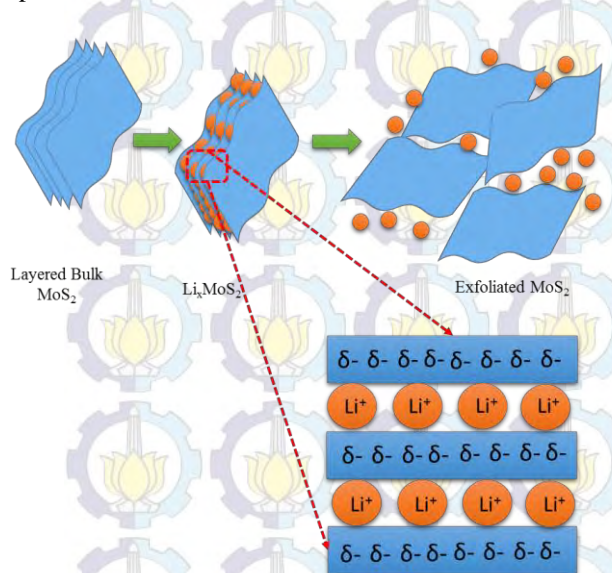
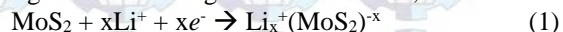


**FIGURE 1.** SCHEMATIC ILLUSTRATION OF INTERCALATION OF LITHIUM INTO MoS<sub>2</sub> LAYERS.

During the stirring process, anhydrous hexane can serve as solvent, resulting in the lithium cations dispersed

in the solvent being readily insert into MoS<sub>2</sub> layers with the formation of lithium intercalated MoS<sub>2</sub> (Li<sub>x</sub>MoS<sub>2</sub>) units according to the following chemical reaction,



Then when the Li<sub>x</sub>MoS<sub>2</sub> units are exposed to water, the lithium in the unit become rapidly solvated and produces exfoliated MoS<sub>2</sub> layers, lithium hydroxide (LiOH), and hydrogen gas (H<sub>2</sub>) based on another following chemical reaction,



During the reaction process, original quintuple layers are homogeneously exfoliated due to the rapid expansion in the layers and forming suspensions of MoS<sub>2</sub> nanosheets.

**Exfoliation of Molybdenum disulfide** - To promote exfoliation of MoS<sub>2</sub>, here we used sonication. The MoS<sub>2</sub> exfoliated sheets were exposed to ultrasonication at room temperature for 38 h, followed by centrifugation to reduce sheet size to desired dimension. The reaction of the resulting lithiated phase of MoS<sub>2</sub> with water through the redox reaction (reaction 2) and can form few- or single-layer MoS<sub>2</sub> dispersion with partial negative charge (see Figure 1).<sup>34</sup> In this work, after we got MoS<sub>2</sub> nanosheets, Zeta (ζ) potential measurements is used to prove it.

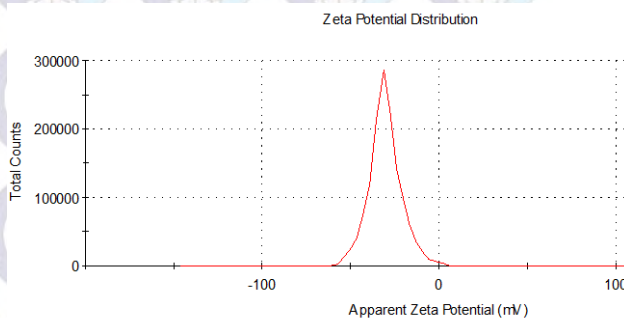


**FIGURE 2.** THE ZETA POTENTIAL DISTRIBUTION OF THE EXFOLIATED MoS<sub>2</sub> DISPERSIONS.

The zeta potential is an important factor for characterizing the stability of colloidal dispersions and provides a measure of the magnitude and sign of the effective surface charge. In this measurements the average value of zeta potential is about -29.18 mV (Figure 2), which indicates that the MoS<sub>2</sub> nanosheets become negative charge after exfoliation due to the electron transfers from *n*-BuLi (guest) to MoS<sub>2</sub> surface (host).

Figure 3 shows the XRD results of raw bulk material, lithium intercalated MoS<sub>2</sub> and exfoliated MoS<sub>2</sub> nanosheets. All diffraction peaks of the sample were in good agreement with a hexagonal structure of MoS<sub>2</sub> (JCPDS No. 37-1492). As shown in Figure 3, the peak positions of MoS<sub>2</sub> bulk and nanosheets are in the same places, with different intensity, which indicates that the exfoliated MoS<sub>2</sub> has a hexagonal lattice structure and

preserve well the crystalline phase of bulk MoS<sub>2</sub>. Compared with those of bulk MoS<sub>2</sub> and exfoliated MoS<sub>2</sub> nanosheets, lithium intercalated MoS<sub>2</sub> has additional diffraction peaks at 30°, 32°, 35°, 37° and 52°.

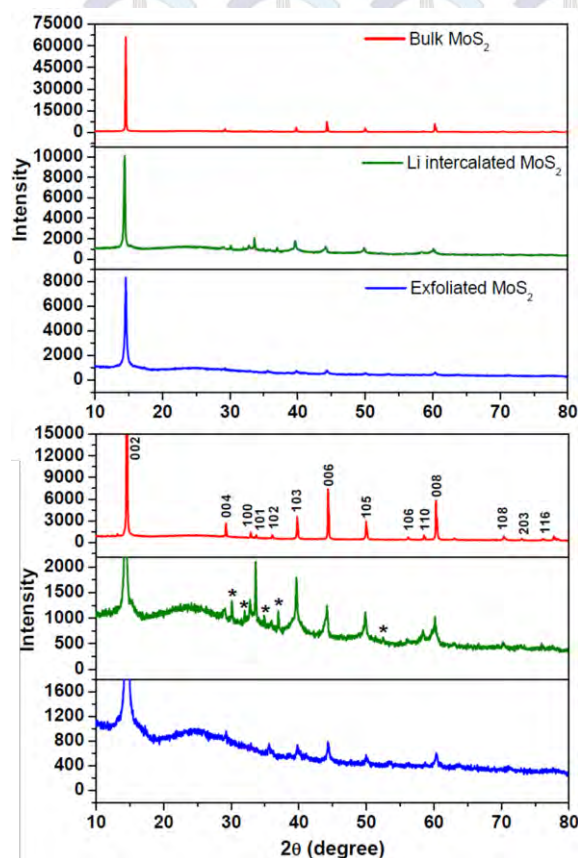


**FIGURE 3.** THE XRD PATTERN OF BULK MoS<sub>2</sub>, LI INTERCALATED MoS<sub>2</sub>, AND EXFOLIATED MoS<sub>2</sub> NANOSHEETS (TOP) WITH MAGNIFICATION OF INTENSITY OF 5X (BOTTOM).

These XRD peaks are originated from MoS<sub>2</sub> being intercalated by Li to form Li<sub>x</sub>MoS<sub>2</sub>, which is consistent with previous results reported by Liu et al.<sup>35</sup> From XRD results, these additional peaks disappear after exfoliation, indicating that intercalated Li is removed when MoS<sub>2</sub> nanosheets are formed.

**Few-layer Molybdenum disulfide with Specific Flake Dimensions** - Recent research has indicated that graphene flakes can be selected by sizes by controlled centrifugation coupled with sediment recycling.<sup>29,36</sup> Here we used centrifugation based on time and filtering to control the size of few-layer MoS<sub>2</sub> nanosheets. While liquid exfoliation generally results in flakes which are small on average, the flake size distribution can be quite broad. In this work we developed methods to control sizes of MoS<sub>2</sub> nanosheets to predominately select flakes in the upper solution. To achieve this we used four methods as shown

in experimental section, we combined centrifugation and filtration to reduce the bigger size of few-layer MoS<sub>2</sub> nanosheets.

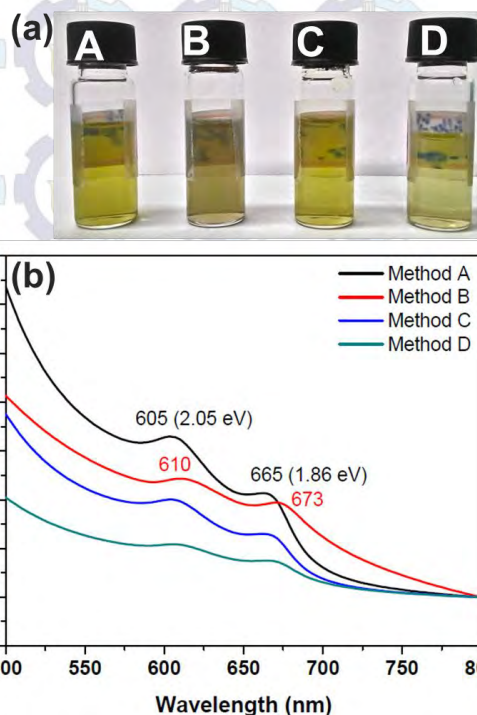


**FIGURE 4.** (A) DIGITAL IMAGES OF THE DISPERSIONS AFTER SIZE SELECTION; (B) ABSORPTION SPECTRA OF FEW-LAYER MoS<sub>2</sub> NANOSHEETS FROM DIFFERENT METHODS.

The color of the resultant dispersions varied in different procedures (method A, B, C, and D) indicating that the nature of the nanosheets is indeed changed. As shown in Figure 4a, the color in the method B is the darkest than others, and after centrifuged, the color changes slowly to be brighter. According to the previous research,<sup>37</sup> the peaks position at 673 and 610 nm are assigned to the *K* point of the Brillouin zone in 2D MoS<sub>2</sub> with relatively larger lateral dimensions (Method B). We also found large shift for the method A, C, and D in the optical absorption in comparison to those of MoS<sub>2</sub> nanosheets with relatively smaller lateral dimensions, arising from the quantum size effect of MoS<sub>2</sub> nanosheets (Figure 4b). We performed SEM, TEM and HRTEM to determine the quality and dimension of the flakes during controlled centrifugation and filtering regime. SEM images (Figure 5) illustrated that the MoS<sub>2</sub> was well exfoliated for all of methods. In addition, we noticed that size-selected few layer flakes tended to have smaller flakes adsorbed in many cases. As shown in Figure 5, the sample B had the largest lateral dimension, which agrees well with the UV-vis spectra (Figure 4b). The SEM micrographs illustrated that the MoS<sub>2</sub> bulk has been successfully exfoliated into few-layer MoS<sub>2</sub> nanosheets with different lateral size. Sample D

displays a smaller lateral size than sample B, but it is bigger than sample A and B (see Figure 5).

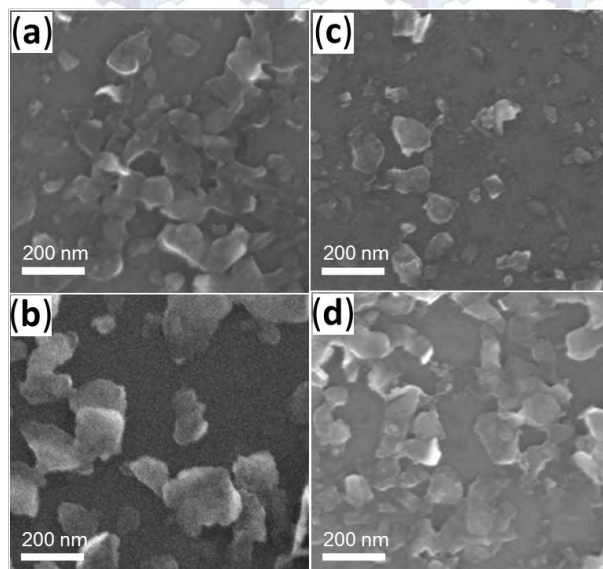


**FIGURE 5.** SEM IMAGES OF SIZE SELECTED DISPERSIONS PRODUCED BY (A) METHOD A, (B) METHOD B, (C) METHOD C, (D) METHOD D.

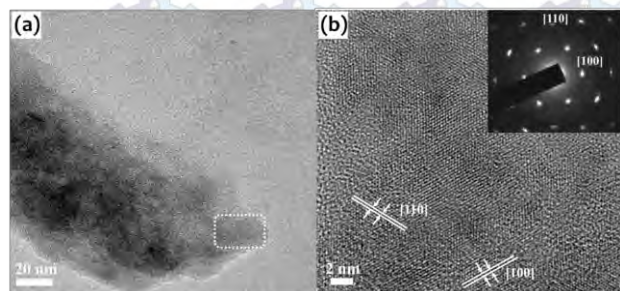


**FIGURE 6.** (A) TEM IMAGE OF AN INDIVIDUAL FEW-LAYER  $\text{MoS}_2$  NANOSHEET; (B) HIGH RESOLUTION TEM IMAGE OF AN INDIVIDUAL FEW-LAYER  $\text{MoS}_2$  NANOSHEET, WITH AN INSET SHOWING THE SAED PATTERN. ALL IMAGES FROM SAMPLE A.

The as-prepared  $\text{MoS}_2$  nanosheets was also analyzed by TEM. Figure 6 shows the transmission electron microscopy image for the few-layer  $\text{MoS}_2$  from sample A. From Figure 6a shows that the layer-structure few-layer  $\text{MoS}_2$  overlap each other. The high resolution TEM image (Figure 6b) and the corresponding selected area electron diffraction (SAED) pattern (inset of Figure 5b) reveal the hexagonal lattice structure, which had good agreement with XRD pattern. And in the SAED pattern, the lattice spacing of 0.27 nm and 0.16 nm assigned to the [100] and [110] planes have been observed.

We also performed dynamic light scattering (DLS) results to confirm that the  $\text{MoS}_2$  has been exfoliated into few-layer  $\text{MoS}_2$  nanosheets with different lateral size.

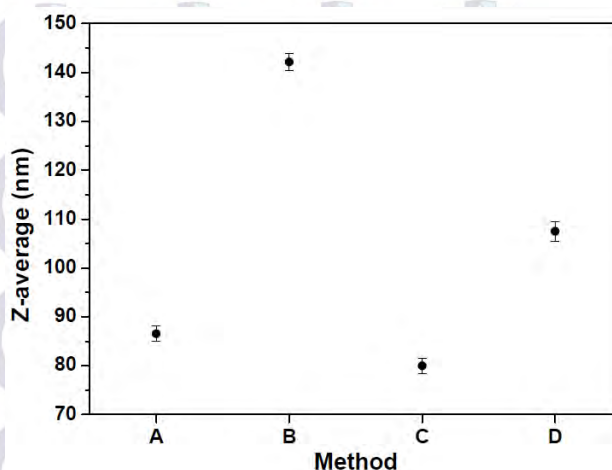


**FIGURE 7.** VARIOUS FLAKE SIZES ACCORDING TO DLS ANALYSIS.

Figure 7 shows that the few-layer  $\text{MoS}_2$  nanosheets with different lateral sizes can be prepared using centrifugation and filtration. Dispersed few-layer  $\text{MoS}_2$  nanosheets have Z-average particle size ranging 85-145 nm. Sample A has a Z-average particle size of  $87.5 \pm 2.5$  nm; sample B  $142.5 \pm 2.5$  nm; sample C  $80.5 \pm 2.5$  nm; and sample D  $107.5 \pm 2.5$  nm. These results are consistent with the SEM results, which suggests that the sample B has the biggest size. To confirm that the  $\text{MoS}_2$  bulk has been successfully exfoliated into few-layers structure, we performed Raman spectroscopy on exfoliated  $\text{MoS}_2$  and bulk  $\text{MoS}_2$ , as shown in Figure 8. Raman spectroscopy was usually used to study the crystalline structures and quantitatively identify the layer numbers of graphene and  $\text{MoS}_2$ . The  $E_{2g}^1$  mode is correlated with an in plane opposite vibration of Mo and S atoms, while the  $A_{1g}$  mode is caused by an out-of-plane vibration of sulfur atoms in opposite directions.<sup>38</sup> Particularly, the  $E_{2g}^1$  mode is the shear mode, which is attributed to the relative vibration between the adjacent single-layers. The characteristic peaks of the bulk  $\text{MoS}_2$  at 377 and 402.9  $\text{cm}^{-1}$  are assigned to the  $E_{2g}^1$  and  $A_{1g}$  modes, respectively. The frequency difference ( $\Delta k$ ) between the  $E_{2g}^1$  and  $A_{1g}$  modes in the exfoliated  $\text{MoS}_2$ ,  $\Delta k = 23.9 - 24.9 \text{ cm}^{-1}$  is smaller than that in the bulk  $\text{MoS}_2$ ,  $\Delta k = 25.9 \text{ cm}^{-1}$ . Sample A exhibits a smallest  $\Delta k$  ( $23.89 \text{ cm}^{-1}$ ), which is consistent with the reported value for 3-5 layers.<sup>38</sup> Actually, the frequency differences between  $E_{2g}^1$  and  $A_{1g}$  peaks, instead of the intensities and widths of the peaks, were used as the reliable features to identify the layer of  $\text{MoS}_2$ . For instance, the frequency difference ( $\Delta k$ ) 20-21.2  $\text{cm}^{-1}$  corresponds to a single layer  $\text{MoS}_2$ .<sup>38</sup> A  $\text{MoS}_2$  flake with  $\Delta k$  of  $\sim 23.6 \text{ cm}^{-1}$  has been expected to possess three

layers.<sup>39</sup> and A MoS<sub>2</sub> flake with  $\Delta k$  of  $\sim 24.3 \text{ cm}^{-1}$  has been proposed contain four layers<sup>40</sup> and  $\Delta k$  of  $\sim 24.9 \text{ cm}^{-1}$  to possess 6 layers.<sup>41</sup>

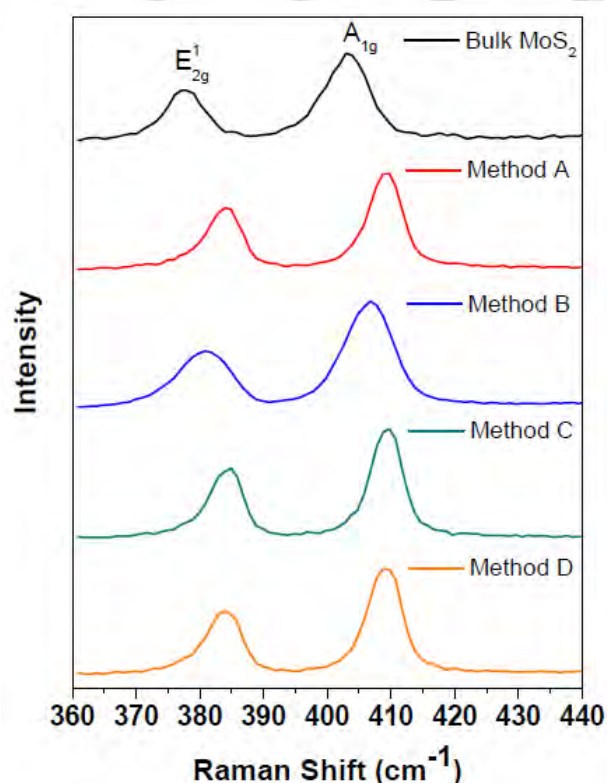


**FIGURE 8.** SEM IMAGES OF SIZE SELECTED DISPERSIONS PRODUCED BY (A) METHOD A, (B) METHOD B, (C) METHOD C, (D) METHOD D.

Thus, sample A are composed of three layers. Based on the reported data, sample B, C, and D with  $\Delta k$  of  $\sim 24.89 \text{ cm}^{-1}$  are identified as MoS<sub>2</sub> nanosheets with six layers.

Atomic Force Microscopy (AFM) are also used to confirm numbers of layers in nanosheets. Tapping mode of AFM is used to assess the thickness of 2D MoS<sub>2</sub> nanosheets. From AFM images, some aggregation or overlapping between individual sheets are found. The resulting dispersion on the Si substrate was nonhomogeneous due to partial aggregation. Some individual MoS<sub>2</sub> nanosheets can be identified to have average thickness of ca. 3 nm from sample A and ca. 4 nm from sample C, indicating that one sheet consists of ca. 4 and 6 layers, respectively (as shown in Figure 9).<sup>31</sup>

Here the DLS, Raman, and AFM results, imply that the large flake or sheet, dispersed without centrifugation, should be relatively thick. This suggests that thinner sheets could be obtained by centrifugation. The effect of aggregation on the electronic properties of MoS<sub>2</sub> is considerably different from that of graphene. For graphene, the electronic properties are largely correlated to the

number of layers per sheet when it consist of less than 5 layers.<sup>42</sup>

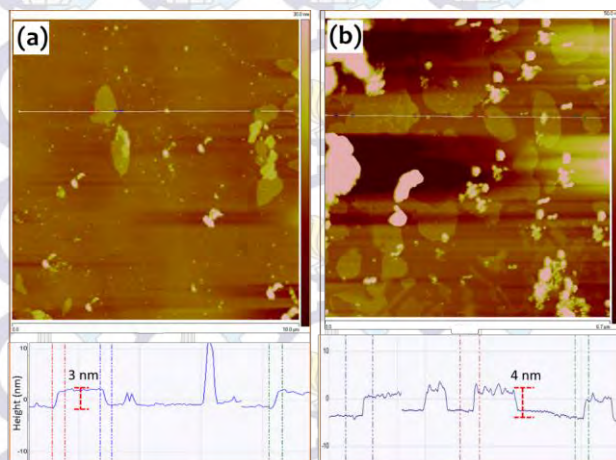


**FIGURE 9.** ATOMIC FORCE MICROSCOPY (AFM) IMAGE OF INDIVIDUAL EXFOLIATED MoS<sub>2</sub> SHEETS: (A) SAMPLE A; (B) SAMPLE C.

On the other hand, for MoS<sub>2</sub>, the effect is widely less significant for MoS<sub>2</sub>. It is true that a large change occurs going from monolayer to bilayer where the bandgap increases from a direct bandgap of 1.83 eV to an indirect one of 1.6 eV.<sup>43</sup> When the number of layers increases from two to six, the bandgap decreases from 1.6 eV to 1.4 eV. It eventually reaches 1.3 eV when the quintuple layers are achieved. In all cases multilayers have indirect bandgaps. This means the electronic properties of MoS<sub>2</sub> multilayers (larger than six layers) are relatively insensitive to flake thickness.

## CONCLUSION

Solution-based exfoliation of layered 2D materials is a promising route for producing 2D crystals in large scale. In this work, few-layer MoS<sub>2</sub> nanosheets have been prepared successfully by lithium intercalation method from bulk MoS<sub>2</sub> powder. The as-prepared MoS<sub>2</sub> nanosheets have a flat and smooth surface. We also have demonstrated that controlled centrifugation and filtration can be used to separate few-layer MoS<sub>2</sub> flakes by sizes. According to DLS analysis, MoS<sub>2</sub> nanosheets with different mean flake lengths ranging 85 – 145 nm are obtained. The as-obtained few-layer MoS<sub>2</sub> nanosheets possess 3-6 layers according to Raman and AFM results. The MoS<sub>2</sub> nanosheets are able to be used for the potential application in hydrogen production.

## ACKNOWLEDGEMENTS

The author would like to thank to Institute of Chemistry, Institute of Atomic and Molecular Science and Institute of Biological Chemistry Academia Sinica.

## REFERENCES

- (1) Novoselov, K. S.; Jiang, D.; Schedin, F.; Booth, T. J.; Khotkevich, V. V.; Morozov, S. V.; Geim, A. K. *Proc. Natl. Acad. Sci. U.S.A* **2005**, *102*, 10451.
- (2) Wang, Q. H.; Kalantar-Zadeh, K.; Kis, A.; Coleman, J. N.; Strano, M. S. *Nat. Nanotechnol.* **2012**, *7*, 699.
- (3) Yoon, Y.; Ganapathi, K.; Salahuddin, S. *Nano Lett.* **2011**, *11*, 3768.
- (4) Choi, K.; Lee, Y. T.; Min, S.-W.; Lee, H. S.; Nam, T.; Kim, H.; Im, S. *J. Mater. Chem. C* **2013**, *1*, 7803.
- (5) Yin, Z.; Li, H.; Li, H.; Jiang, L.; Shi, Y.; Sun, Y.; Lu, G.; Zhang, Q.; Chen, X.; Zhang, H. *ACS Nano* **2012**, *6*, 74.
- (6) Lopez-Sanchez, O.; Lembke, D.; Kayci, M.; Radenovic, A.; Kis, A. *Nat. Nanotechnol.* **2013**, *8*, 497.
- (7) Fontana, M.; Deppe, T.; Boyd, A. K.; Rinzan, M.; Liu, A. Y.; Paranjape, M.; Barbara, P. *Sci. Rep.* **2013**, *3*.
- (8) Yu, Y.; Li, C.; Liu, Y.; Su, L.; Zhang, Y.; Cao, L. *Sci. Rep.* **2013**, *3*.
- (9) Zhang, S.-L.; Choi, H.-H.; Yue, H.-Y.; Yang, W.-C. *Curr. Appl. Phys.* **2014**, *14*, 264.
- (10) Park, S. K.; Yu, S. H.; Woo, S.; Quan, B.; Lee, D. C.; Kim, M. K.; Sung, Y. E.; Piao, Y. *Dalton Trans.* **2013**, *42*, 2399.
- (11) Zhou, X.; Wang, Z.; Chen, W.; Ma, L.; Chen, D.; Lee, J. Y. *J. Power Sources* **2014**, *251*, 264.
- (12) Li, X.; Li, W.; Li, M.; Cui, P.; Chen, D.; Gengenbach, T.; Chu, L.; Liu, H.; Song, G. *J. Mater. Chem. A* **2015**, *3*, 2762.
- (13) Su, D.; Dou, S.; Wang, G. *Adv. Energy Mater.* **2015**, *5*, 1570067.
- (14) Bang, G. S.; Nam, K. W.; Kim, J. Y.; Shin, J.; Choi, J. W.; Choi, S. Y. *ACS Appl. Mater. Interfaces* **2014**, *6*, 7084.
- (15) Cao, L.; Yang, S.; Gao, W.; Liu, Z.; Gong, Y.; Ma, L.; Shi, G.; Lei, S.; Zhang, Y.; Zhang, S.; Vajtai, R.; Ajayan, P. M. *Small* **2013**, *9*, 2905.
- (16) Ji, S.; Yang, Z.; Zhang, C.; Liu, Z.; Tjiu, W. W.; Phang, I. Y.; Zhang, Z.; Pan, J.; Liu, T. *Electrochim. Acta* **2013**, *109*, 269.
- (17) Lukowski, M. A.; Daniel, A. S.; Meng, F.; Forticaux, A.; Li, L.; Jin, S. *J. Am. Chem. Soc.* **2013**, *135*, 10274.
- (18) Voiry, D.; Salehi, M.; Silva, R.; Fujita, T.; Chen, M.; Asefa, T.; Shenoy, V. B.; Eda, G.; Chhowalla, M. *Nano Lett.* **2013**, *13*, 6222.
- (19) Yin, Z.; Chen, B.; Bosman, M.; Cao, X.; Chen, J.; Zheng, B.; Zhang, H. *Small* **2014**, *10*, 3537.
- (20) Singh, A. K.; Mathew, K.; Zhuang, H. L.; Hennig, R. G. *J. Phys. Chem. Lett.* **2015**, *6*, 1087.
- (21) Varrla, E.; Backes, C.; Paton, K. R.; Harvey, A.; Gholamvand, Z.; McCauley, J.; Coleman, J. N. *Chem. Mater.* **2015**, *27*, 1129.
- (22) Lee, J. H.; Jang, W. S.; Han, S. W.; Baik, H. K. *Langmuir* **2014**, *30*, 9866.
- (23) Li, H.; Wu, J.; Yin, Z.; Zhang, H. *Acc. Chem. Res.* **2014**, *47*, 1067.
- (24) Chou, S. S.; Kaehr, B.; Kim, J.; Foley, B. M.; De, M.; Hopkins, P. E.; Huang, J.; Brinker, C. J.; Dravid, V. P. *Angew. Chem. Int. Ed.* **2013**, *52*, 4160.
- (25) Xiao, J.; Choi, D.; Cosimbescu, L.; Koech, P.; Liu, J.; Lemmon, J. P. *Chem. Mater.* **2010**, *22*, 4522.
- (26) You, X.; Liu, N.; Lee, C. J.; Pak, J. J. *Mater. Lett.* **2014**, *121*, 31.
- (27) Coleman, J. N.; Lotya, M.; O'Neill, A.; Bergin, S. D.; King, P. J.; Khan, U.; Young, K.; Gaucher, A.; De, S.; Smith, R. J.; Shvets, I. V.; Arora, S. K.; Stanton, G.; Kim, H.-Y.; Lee, K.; Kim, G. T.; Duesberg, G. S.; Hallam, T.; Boland, J. J.; Wang, J. J.; Donegan, J. F.; Grunlan, J. C.; Moriarty, G.; Shmeliov, A.; Nicholls, R. J.; Perkins, J. M.; Grievson, E. M.; Theuwissen, K.; McComb, D. W.; Nellist, P. D.; Nicolosi, V. *Science* **2011**, *331*, 568.
- (28) Gupta, A.; Arunachalam, V.; Vasudevan, S. *J. Phys. Chem. Lett.* **2015**, *6*, 739.
- (29) May, P.; Khan, U.; O'Neill, A.; Coleman, J. N. *J. Mater. Chem.* **2012**, *22*, 1278.
- (30) Jaramillo, T. F. J., K. P.; Bonde, J.; Nielsen, J. H.; Horch, S. C., I In *Science* 2007; Vol. 317, p 100.
- (31) Knirsch, K. C.; Berner, N. C.; Nerl, H. C.; Cucinotta, C. S.; Gholamvand, Z.; McEvoy, N.; Wang, Z.; Abramovic, I.; Vecera, P.; Halik, M.; Sanvito, S.; Duesberg, G. S.; Nicolosi, V.; Hauke, F.; Hirsch, A.; Coleman, J. N.; Backes, C. *ACS Nano* **2015**, *9*, 6018.
- (32) Benavente, E.; Santa Ana, M. A.; Mendizábal, F.; González, G. *coord. chem. rev.* **2002**, *224*, 87.
- (33) O'Neill, A.; Khan, U.; Coleman, J. N. *Chem. Mater.* **2012**, *24*, 2414.
- (34) Joensen, P., Frindt, R. F. & Morrison, S. R. *Mater. Res. Bull.* **1986**, *21*, 457.
- (35) Liu, Y. D.; Ren, L.; Qi, X.; Yang, L. W.; Hao, G. L.; Li, J.; Wei, X. L.; Zhong, J. X. *J. Alloys Compd.* **2013**, *571*, 37.
- (36) Khan, U.; O'Neill, A.; Porwal, H.; May, P.; Nawaz, K.; Coleman, J. N. *Carbon* **2012**, *50*, 470.
- (37) Wang, N.; Wei, F.; Qi, Y.; Li, H.; Lu, X.; Zhao, G.; Xu, Q. *ACS Appl. Mater. Interfaces* **2014**, *6*, 19888.
- (38) Yu, Y.; Li, C.; Liu, Y.; Su, L.; Zhang, Y.; Cao, L. *Sci Rep* **2013**, *3*, 1866.
- (39) Li, H.; Zhang, Q.; Yap, C. C. R.; Tay, B. K.; Edwin, T. H. T.; Olivier, A.; Baillargeat, D. *Adv. Funct. Mater.* **2012**, *22*, 1385.
- (40) Ye, L.; Xu, H.; Zhang, D.; Chen, S. *Mater. Res. Bull.* **2014**, *55*, 221.
- (41) Lee, C.; Yan, H.; Brus, L. E.; Heinz, T. F.; Hone, J.; Ryu, S. *ACS Nano* **2010**, *4*, 2695.
- (42) Geim, A. K. *Science* **2009**, *324*, 1530.
- (43) Mak, K. F.; Lee, C.; Hone, J.; Shan, J.; Heinz, T. F. *Phys. Rev. Lett.* **2010**, *105*, 136805.

# Preparation and Characterization of Few-layer MoS<sub>2</sub> Nanosheets



## 薄層二硫化鉬奈米層片的合成與鑑定

Speaker :

Mohammad Sholeh

M10306821

Advisor :

Prof. Ming-Hsi Chiang

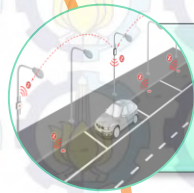
Prof. Shawn D. Lin



# Outline



Introduction



Experimental



Results and Discussion



Conclusion



Acknowledgement

# Introduction



Nanoscience: Small things can be surprisingly cool



Below 100 nm, properties change, often improving

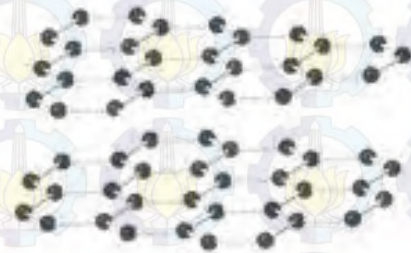
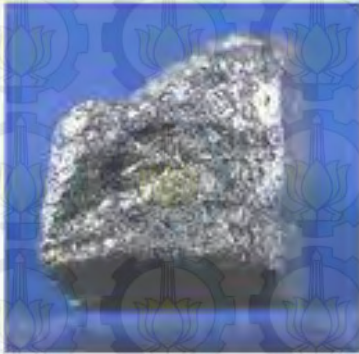




# Introduction

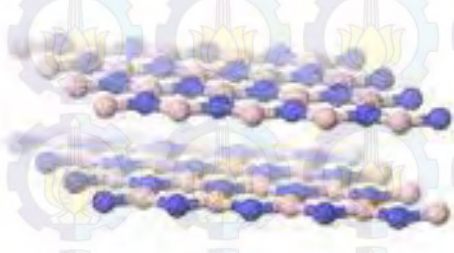
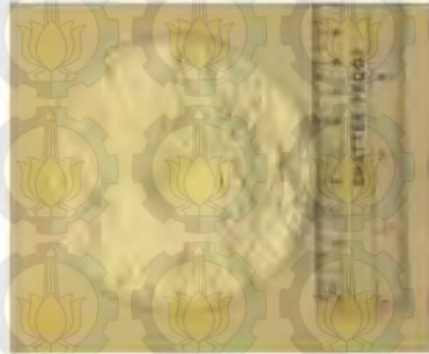


Graphite (C)



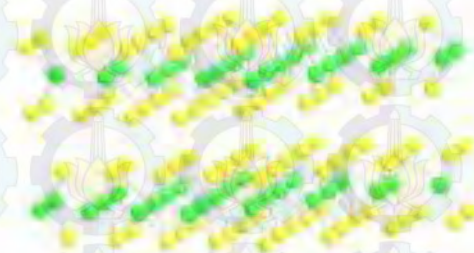
Electrical conductor

Boron Nitride (BN)



Electrical insulator

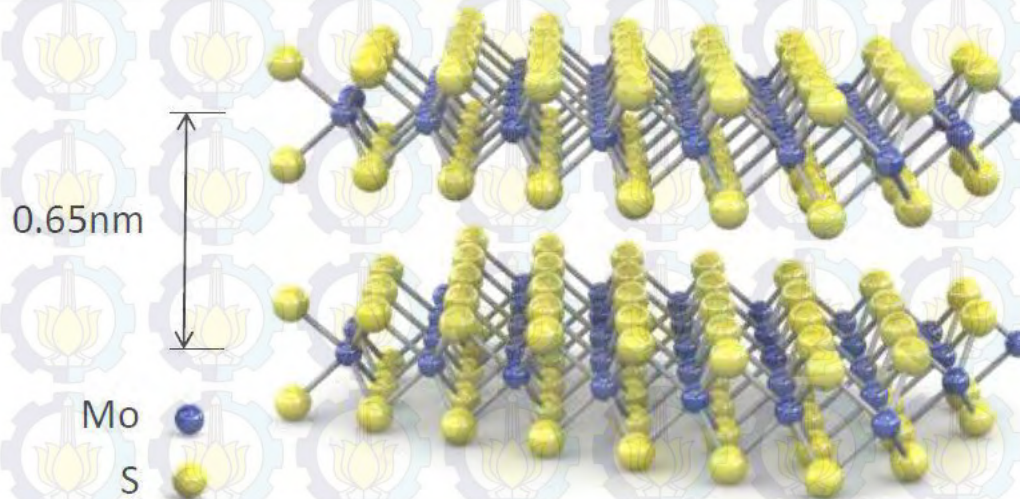
Moly disulphide ( $\text{MoS}_2$ )



Semiconductor



# Introduction



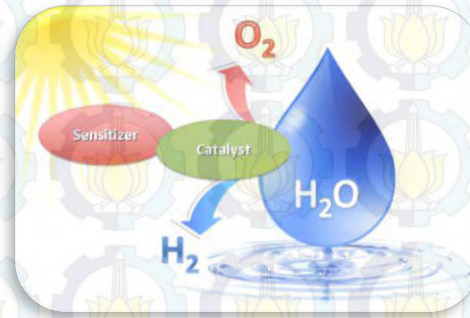
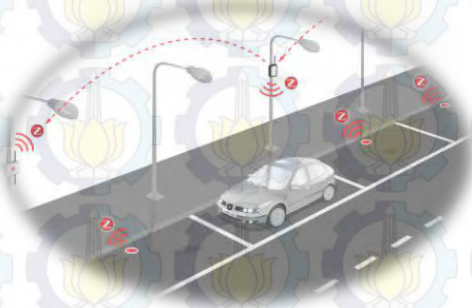
**Band gap:** 1.29 eV band gap (bulk); 1.83 eV direct gap (single layer)

**Mobility:** 200 (monolayer, RT) - 500  $\text{cm}^2/\text{Vs}$  (bulk, 70 K)

**Stability:**  $> 1000$  °C in inert atmosphere no dangling bonds

**Availability:** naturally occurring mineral, abundance similar to Ge

# Introduction



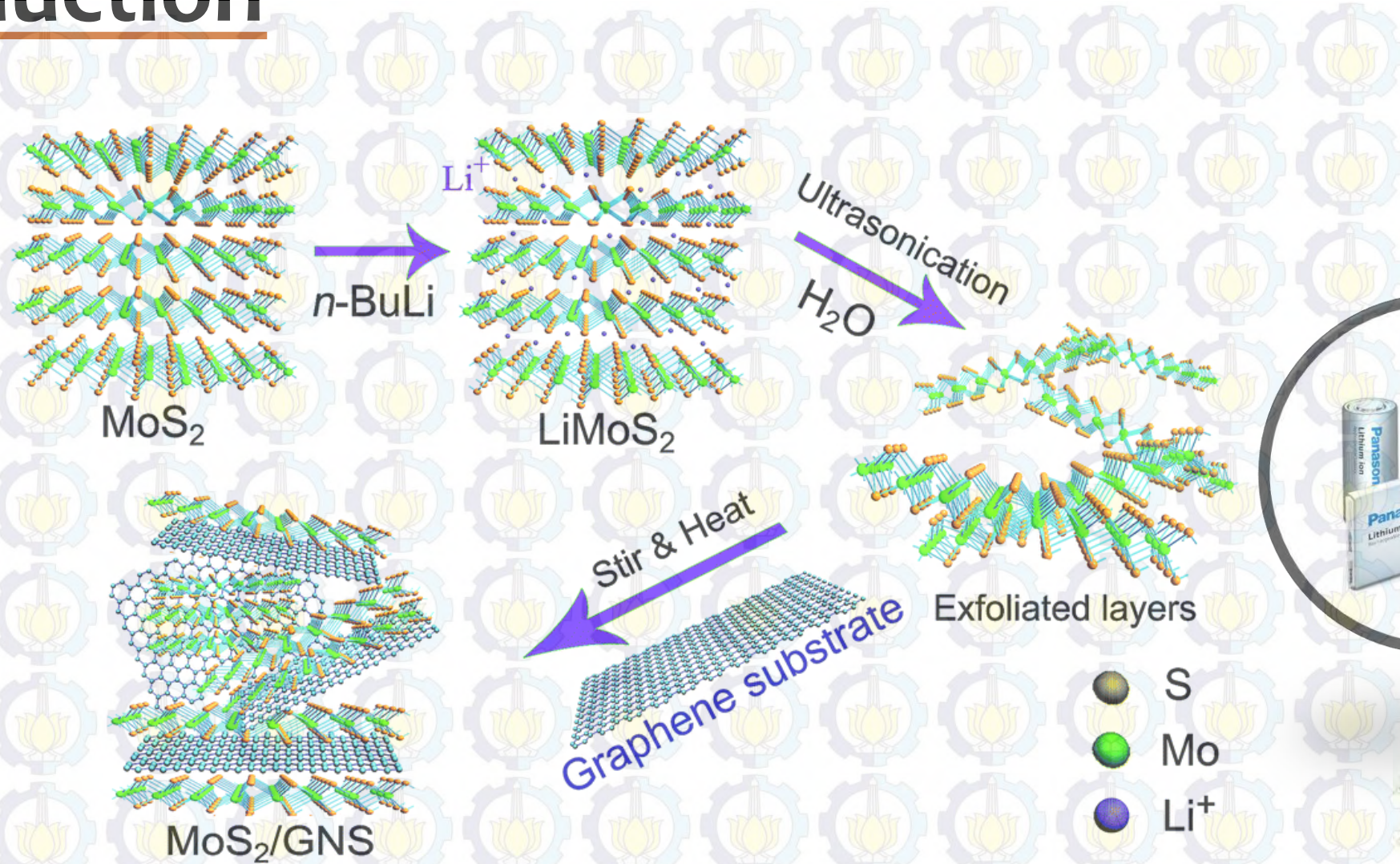
Yin, Z. Y. et al., *ACS Nano* **2012**, *6*, 74-80

Voiry, D. et al., *Nano lett.* **2013**, *13*, 6222-6227

Ma, G. et al., *Journal of power sources* **2013**, *229*, 72-78

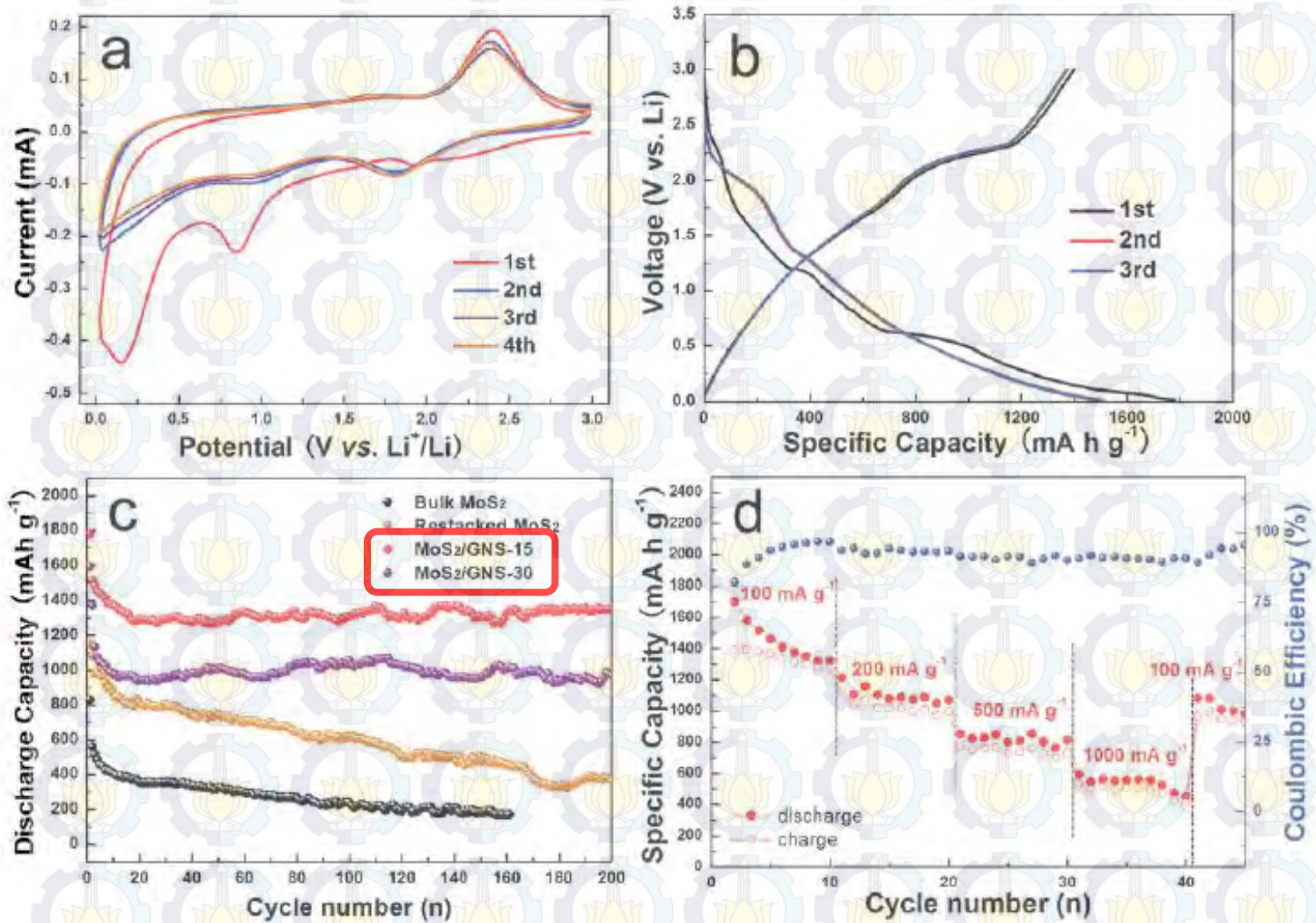
Zhang, S.-L. et al., *Current Applied Physics* **2014**, *14*, 264-268

# Introduction



Liu, Y. D. et al., *Journal of Materials Chemistry A* **2014**, 2, 13109.

# Introduction

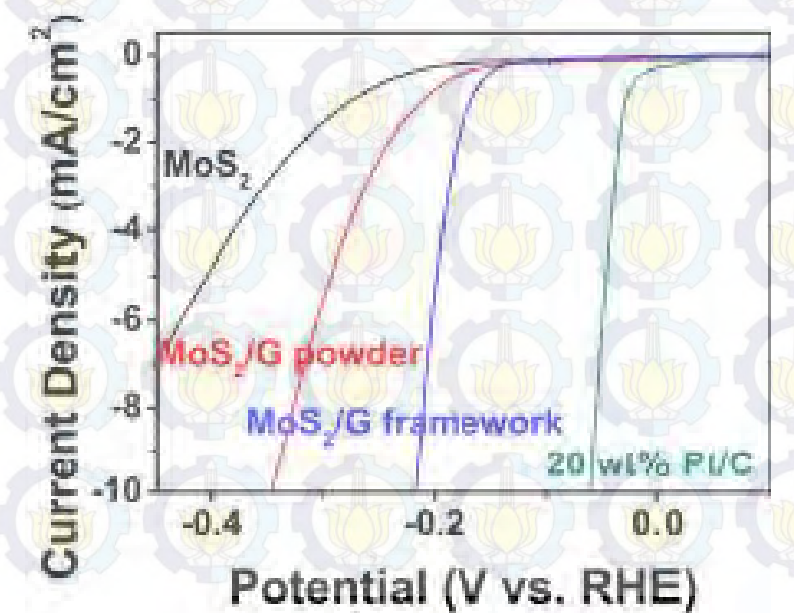
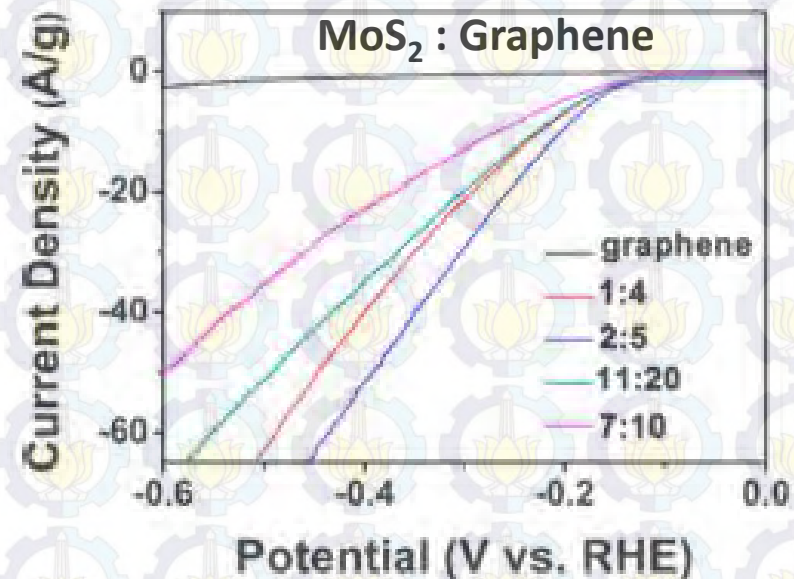


Liu, Y. D. et al., *Journal of Materials Chemistry A* **2014**, 2, 13109.

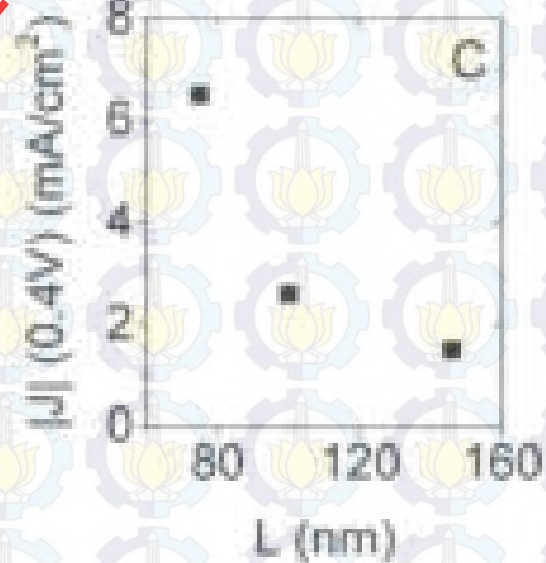
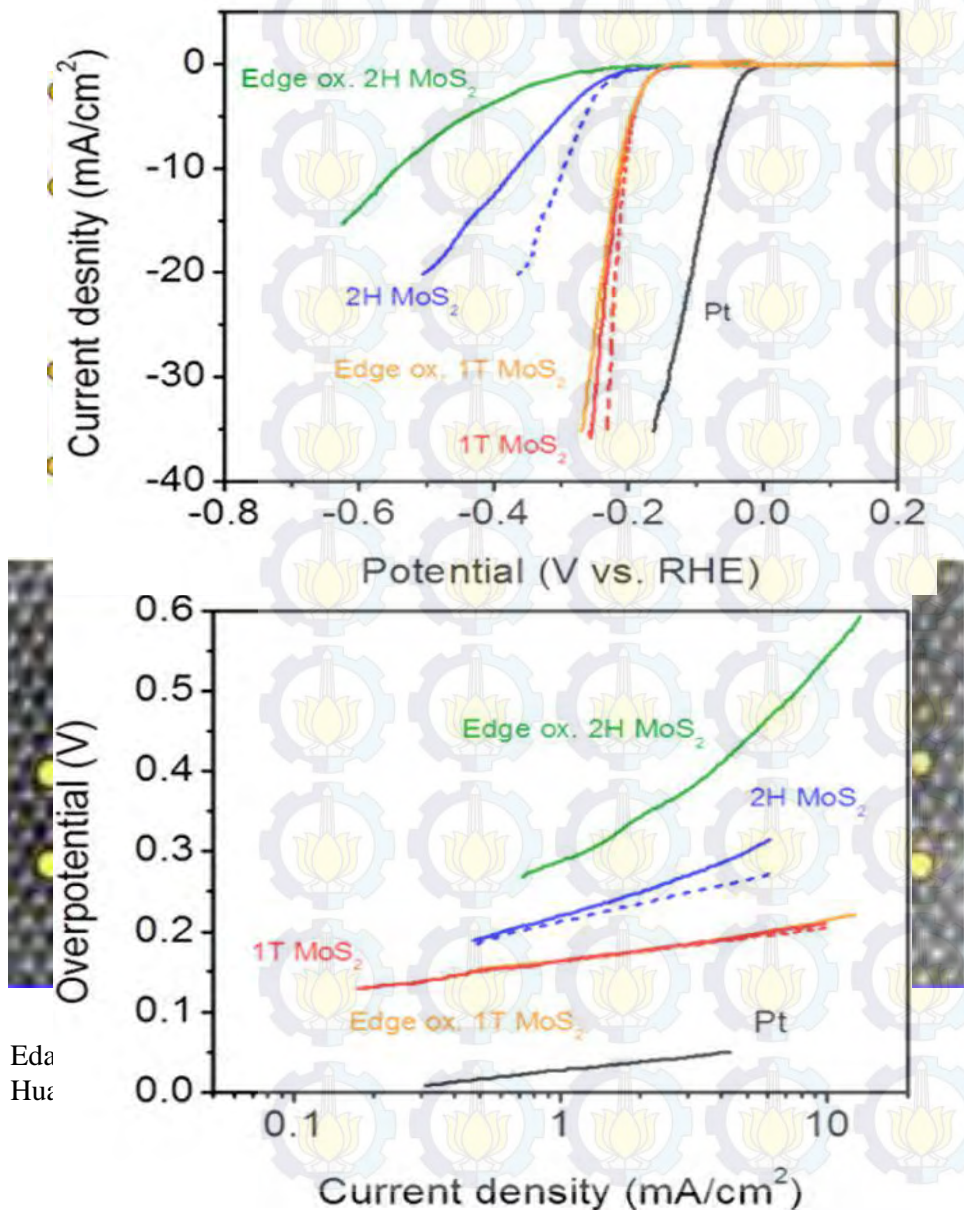
# Introduction



Zhou, W. et al., *ACS Appl. Mater. Interfaces* 2014, 6, 21534.



# Introduction



Current density produced at 0.4 V plotted versus nanosheet size.

Varrla, E. et al., *Chemistry of Materials* 2015, 27, 1129.



Eda  
Huz

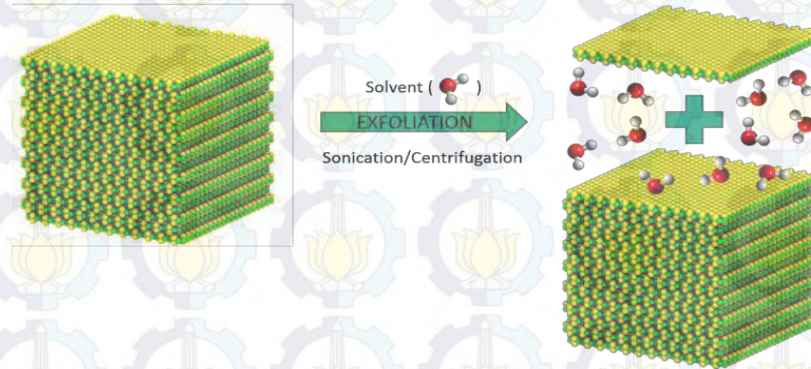
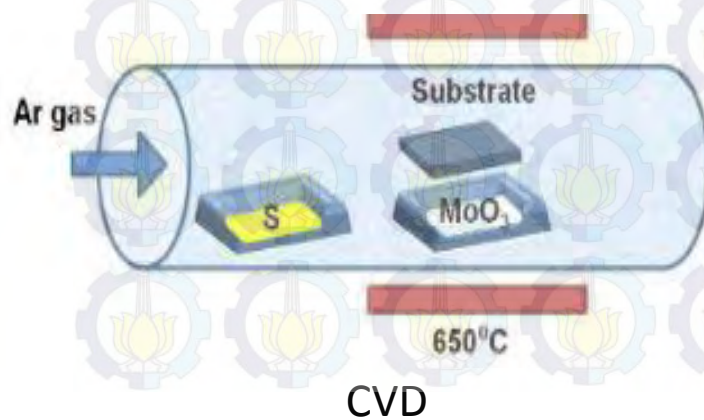
# Introduction



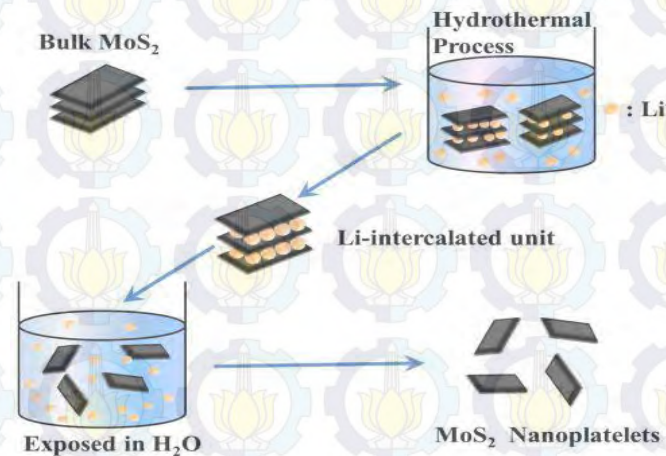
## Preparation of MoS<sub>2</sub> nanosheets



Scotch-taped



Liquid-Exfoliation



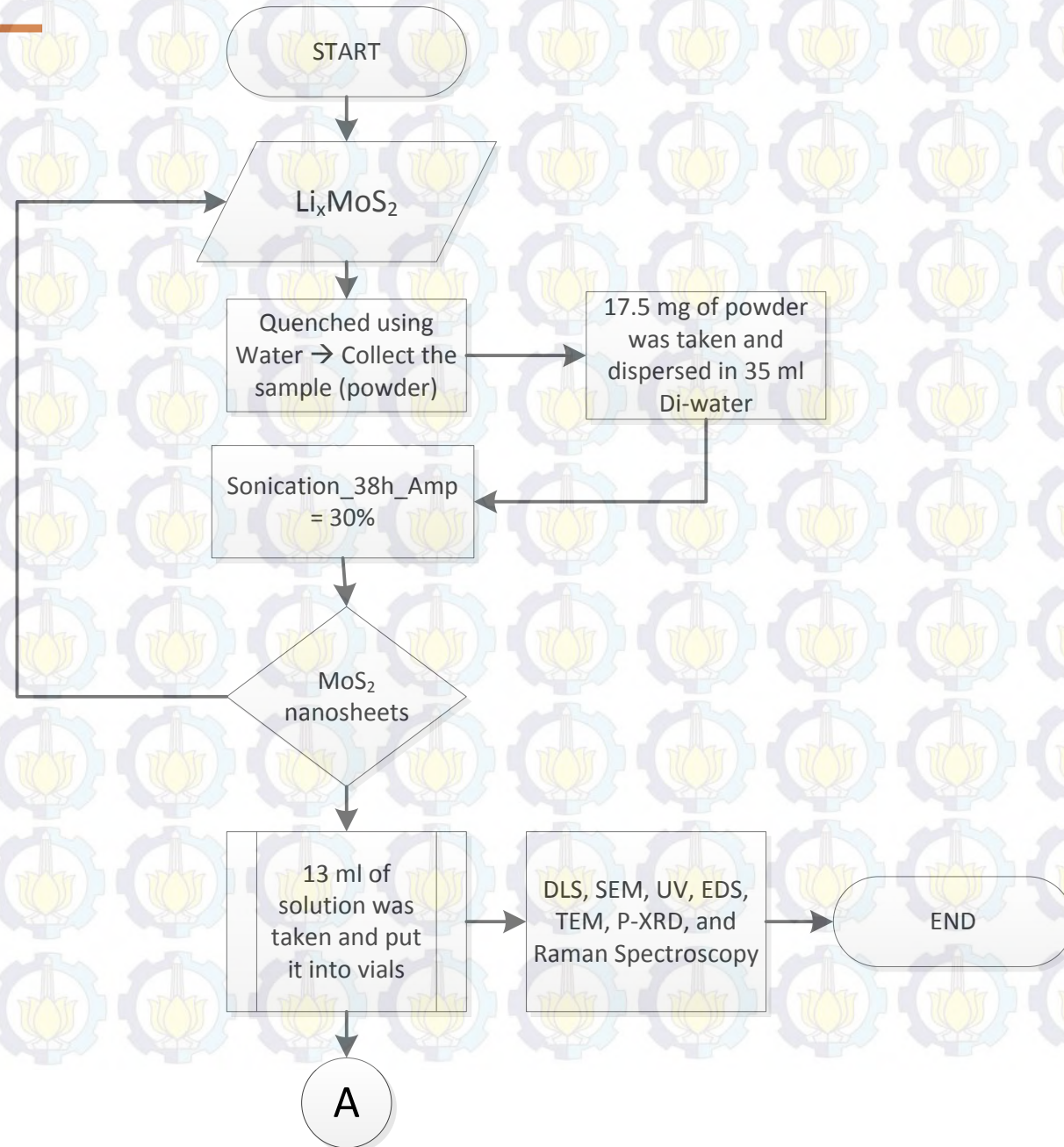
Hydrothermal



# Experimental



## 1<sup>st</sup> Part

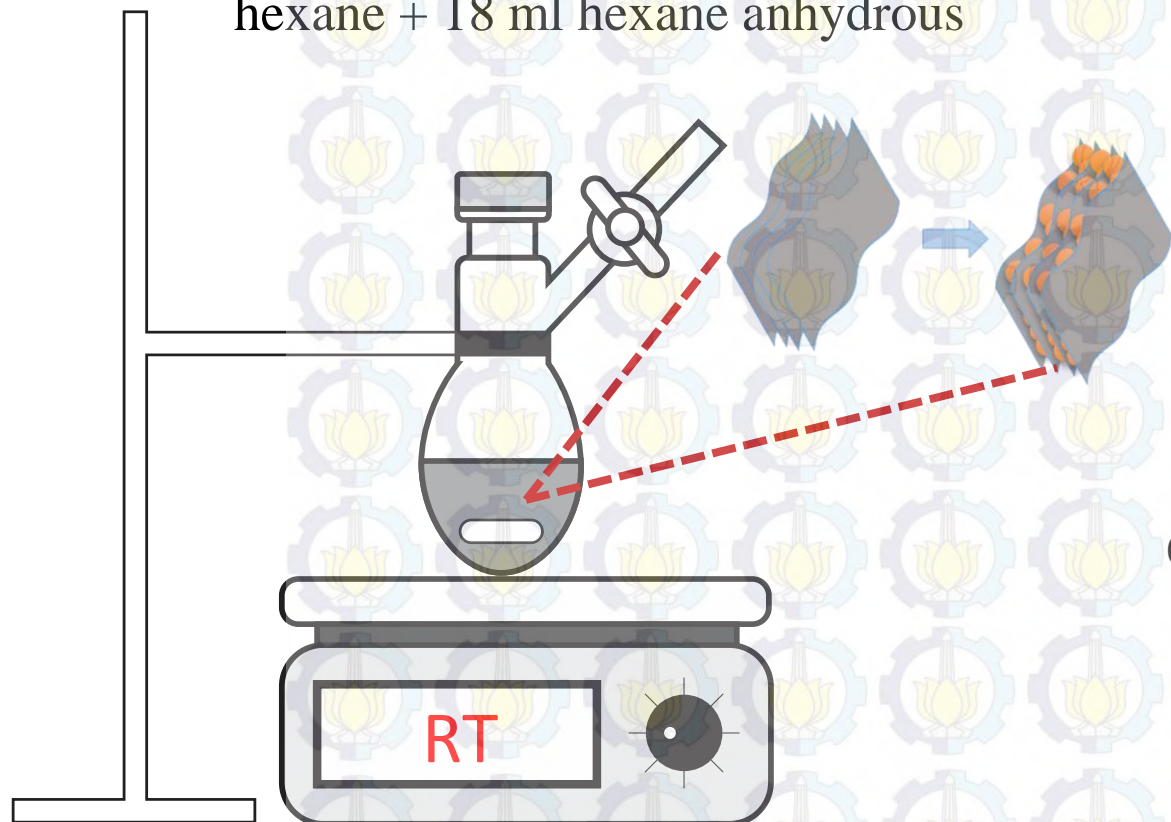


# Experimental (1<sup>st</sup> Part)



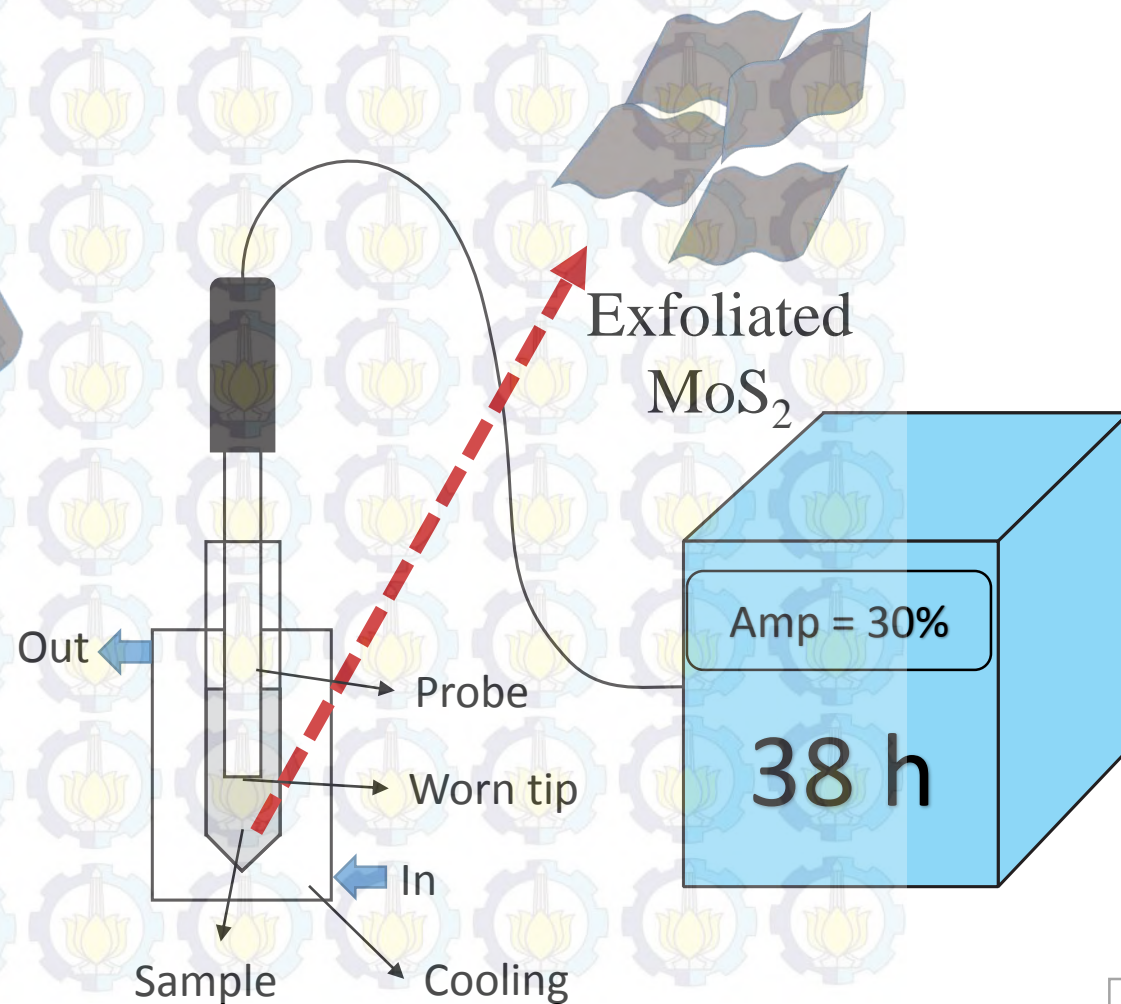
## Intercalation Process

0.3 g Bulk MoS<sub>2</sub> + 2 ml of 2.5 M *n*-BuLi in hexane + 18 ml hexane anhydrous



Stirred for 5 days

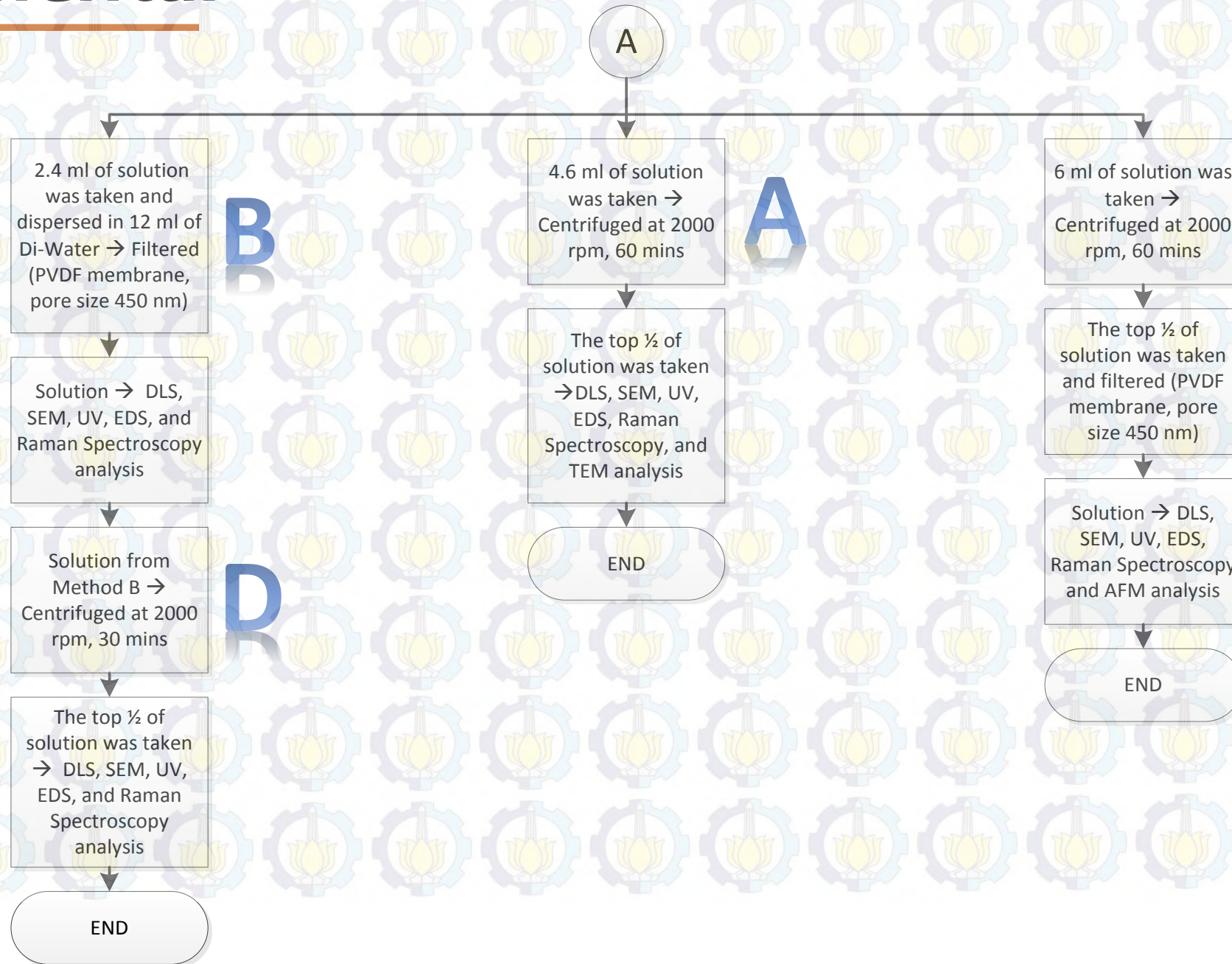
## Exfoliation Process



# Experimental



## 2<sup>nd</sup> Part

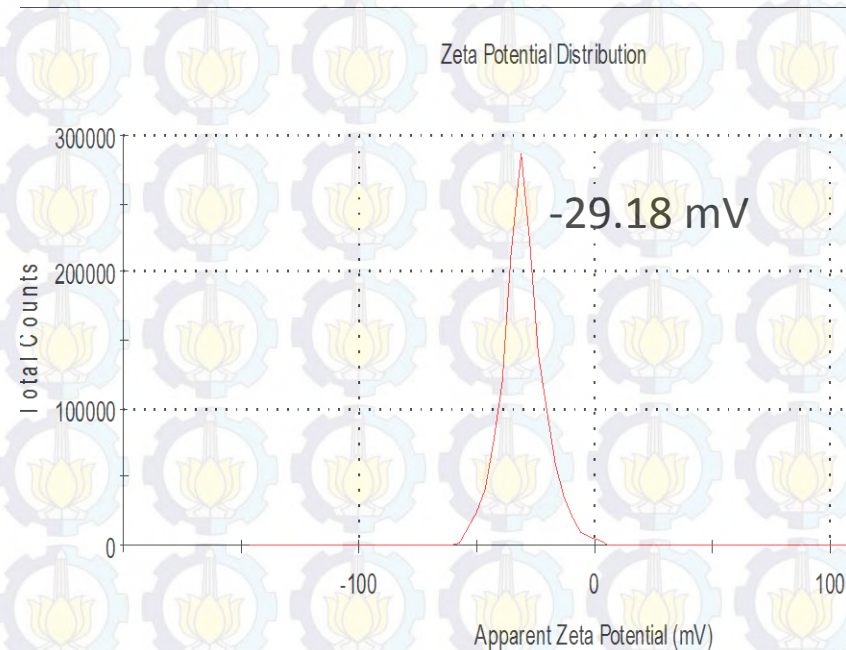
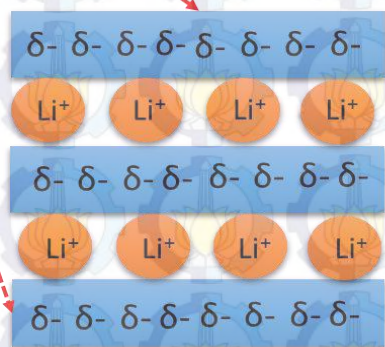
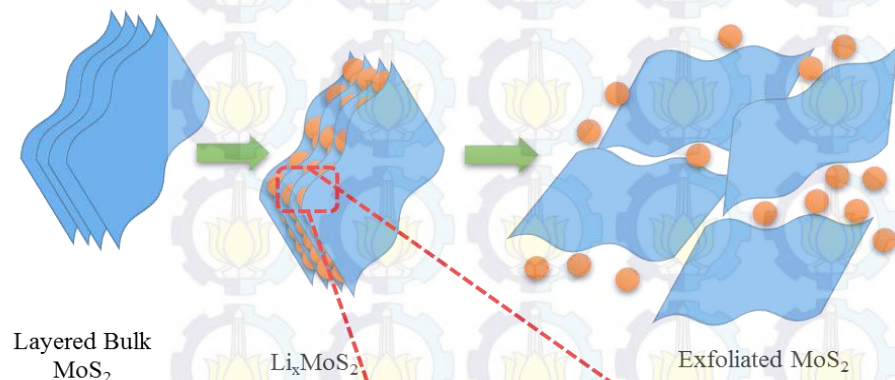




# Results and Discussion

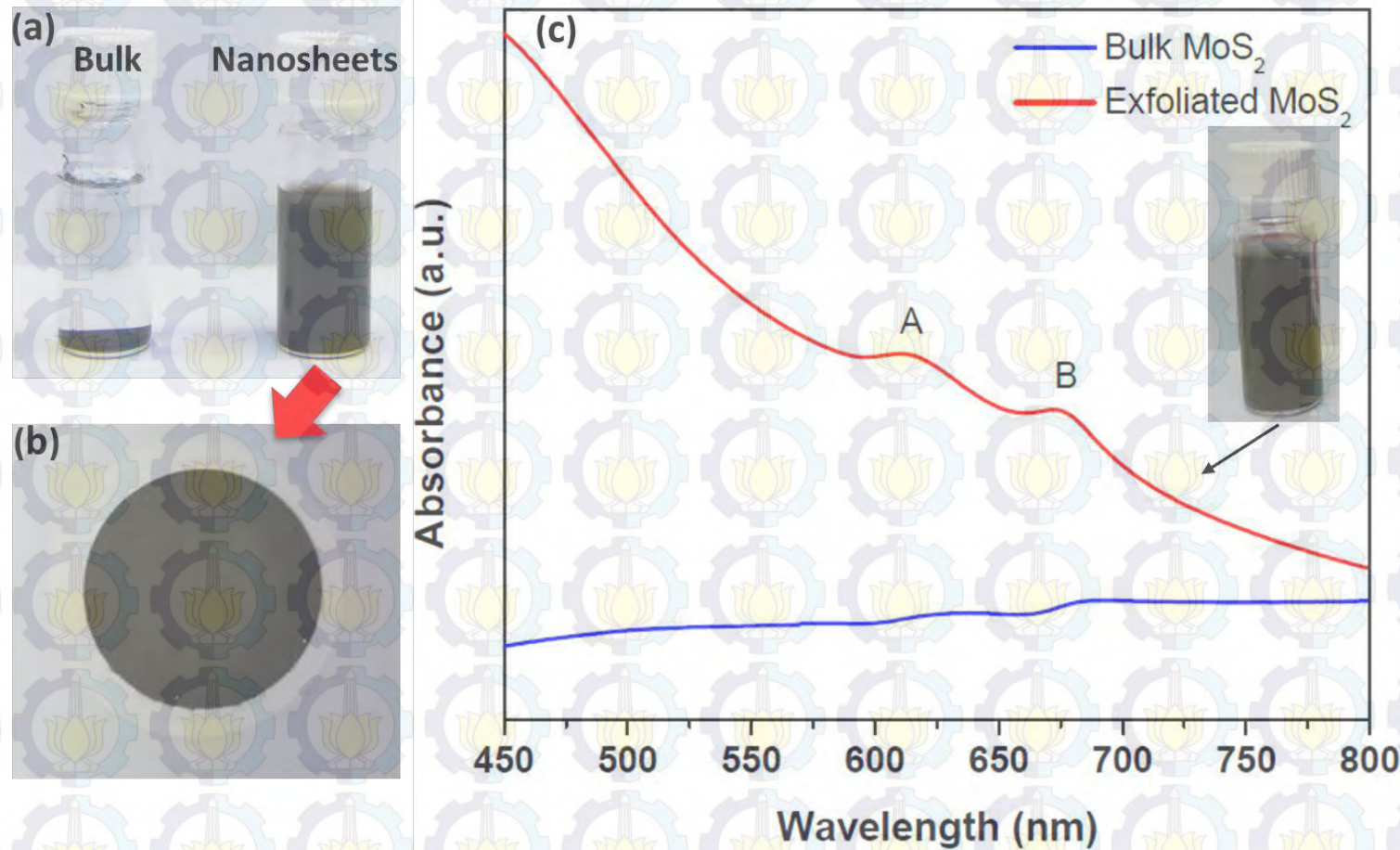


# Results (1st Part)



Experiment	1 <sup>st</sup>	2 <sup>nd</sup>	3 <sup>rd</sup>	4 <sup>th</sup>	5 <sup>th</sup>
Zeta Potential (mV)	-30	-30	-27.9	-29.9	-28.1

# UV – Vis Spectra

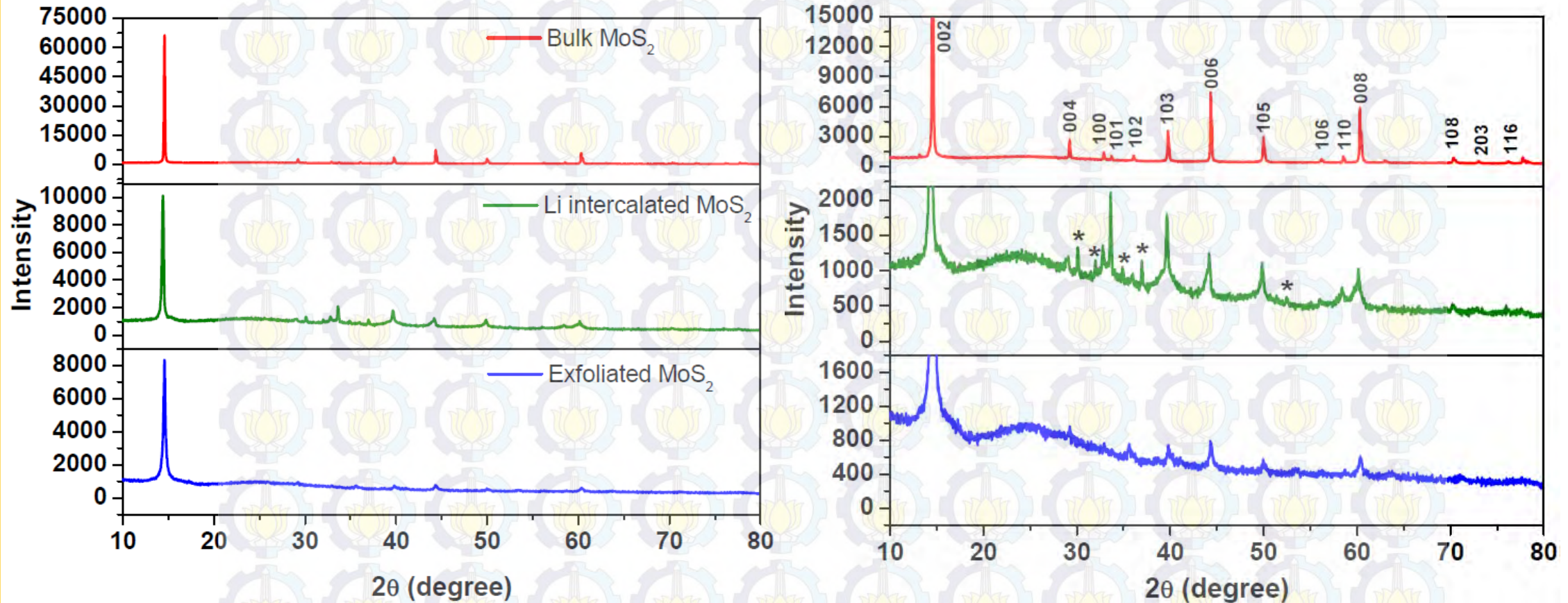


The two peaks centered at 610 nm (2.03 eV) and 673 nm (1.84 eV) can be attributed to the characteristic A and B direct-gap absorptions and excitonic transitions of MoS<sub>2</sub> with energy separation of 0.19 eV<sup>1,2</sup>

1 Benavente, E., et al. *Coord. Chem. Rev.* **2002**, 224, 87–109

2 Bang, G. S., et al. *ACS Appl. Mater. Interfaces.* **2014**, 6, 7084–7089

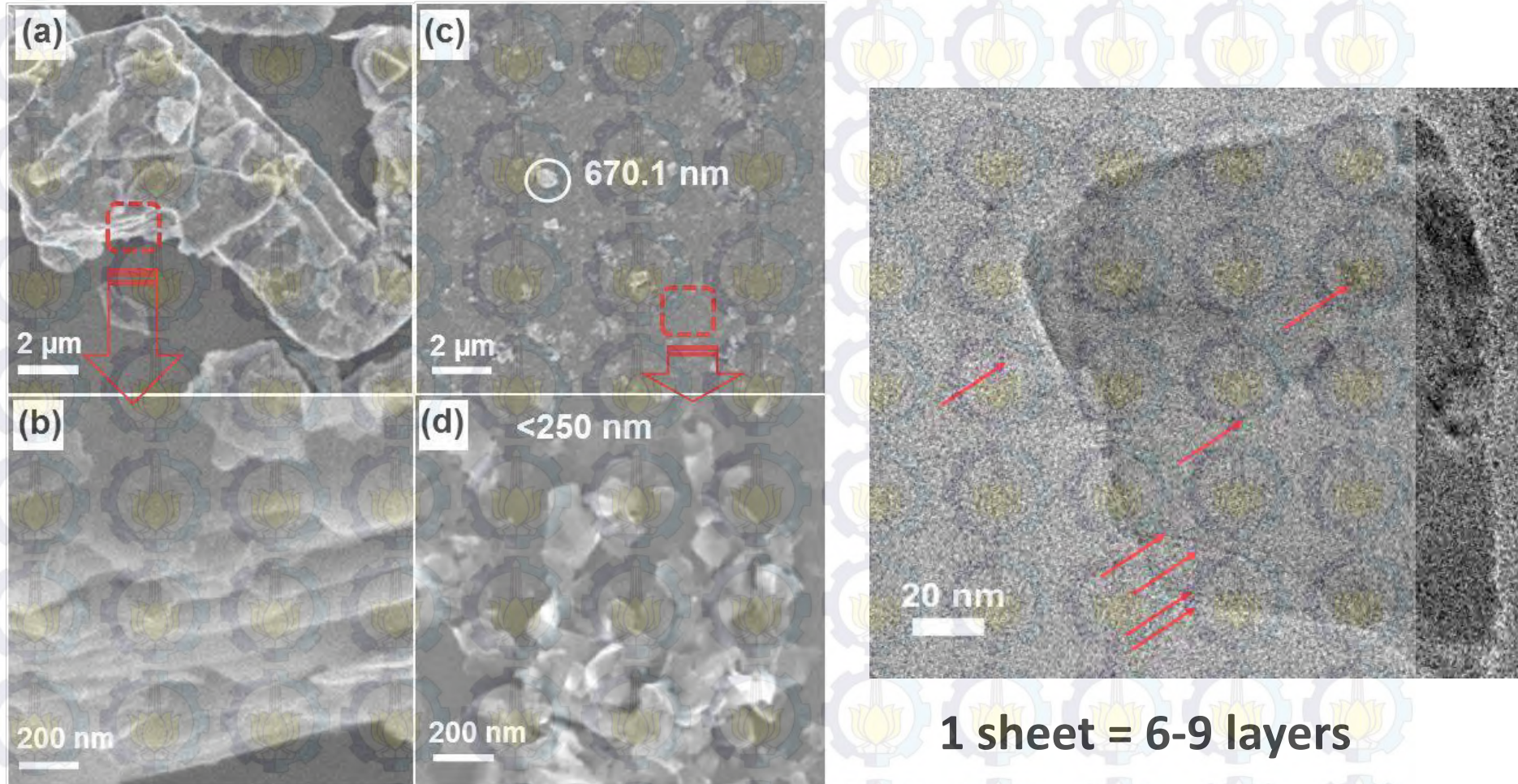
# P-XRD Analysis



All diffraction peaks of the sample were in good agreement with a hexagonal lattice structure of MoS<sub>2</sub> (JCPDS No. 37-1492).

The additional diffraction peaks (stars) at 30°, 32°, 35°, 37° and 52° indicate the lithium intercalated MoS<sub>2</sub>

# SEM & TEM

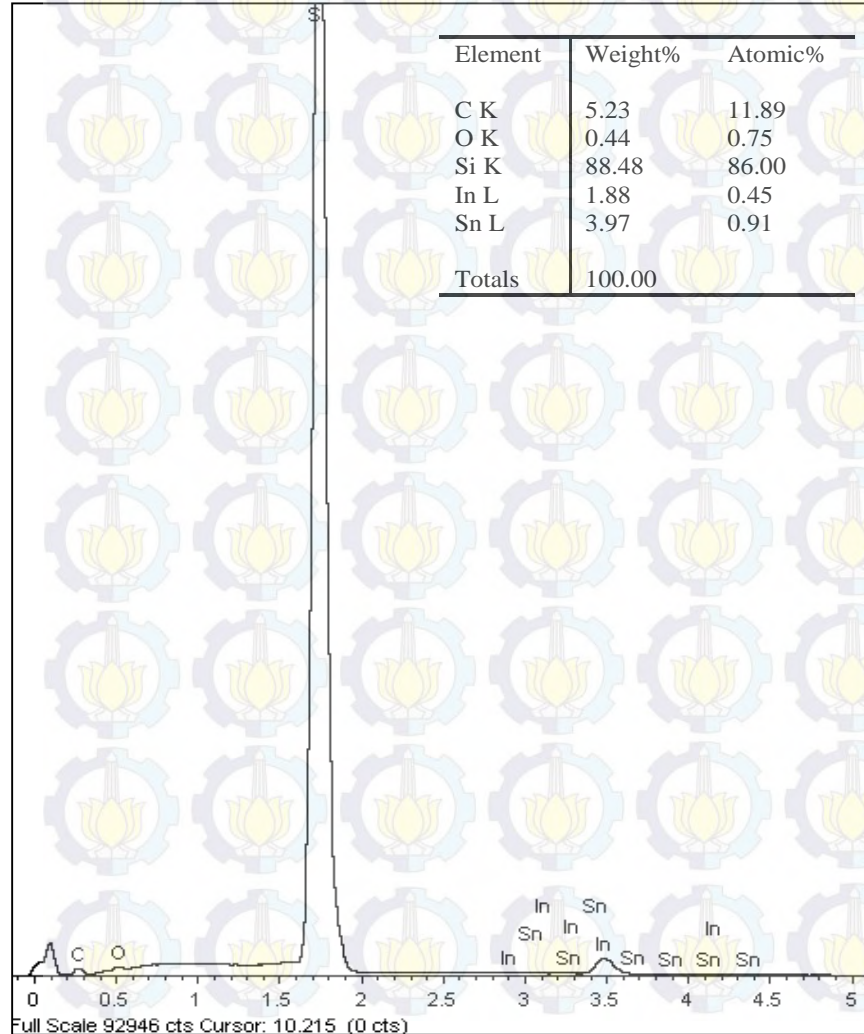


The typical SEM images: (a) and (b) Bulk MoS<sub>2</sub> powder with different resolution; (c) MoS<sub>2</sub> nanosheets with different lateral sizes; (d) MoS<sub>2</sub> nanosheets with lateral size <250 nm.

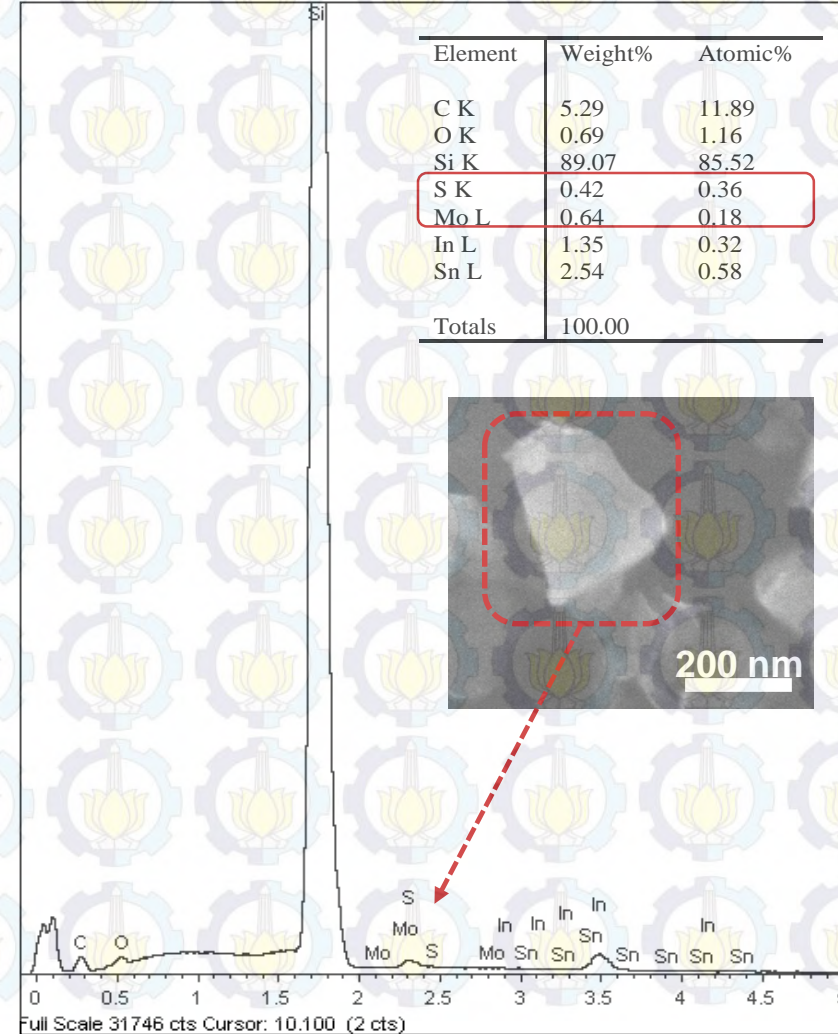




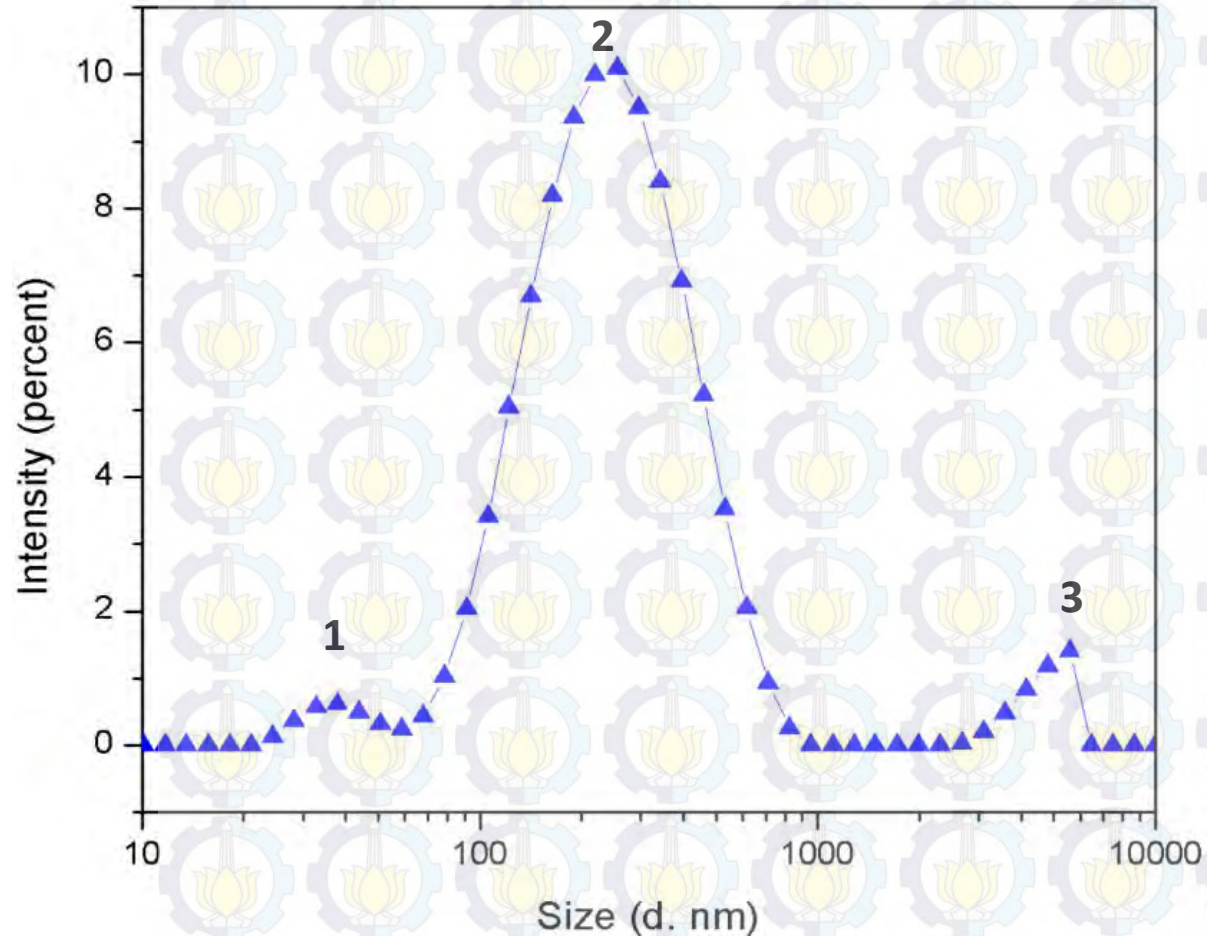
## Background



## After Sonication

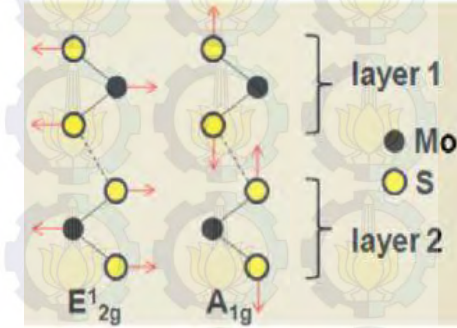
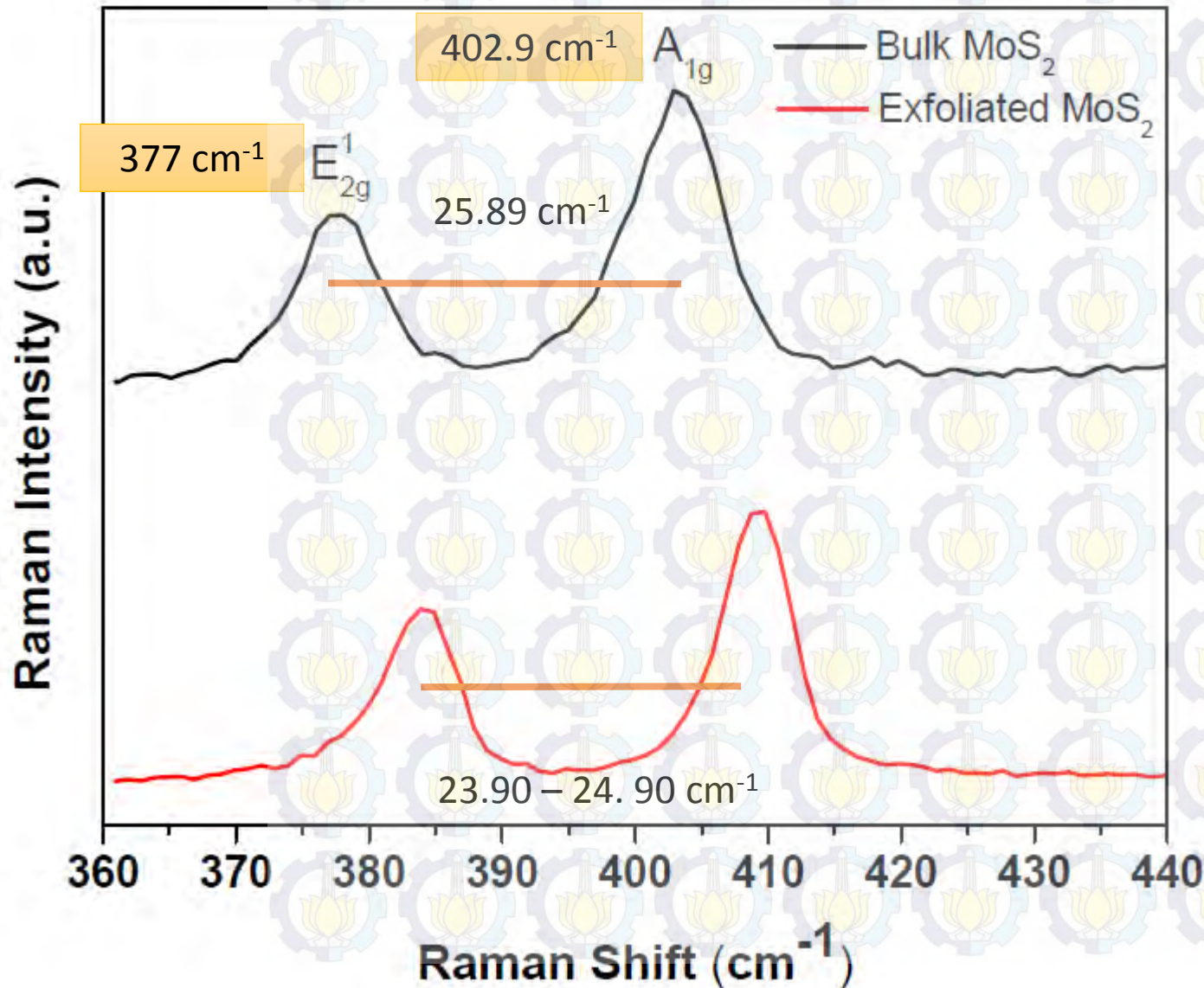


# DLS Analysis



Peak	d. nm
1 <sup>st</sup>	38
2 <sup>nd</sup>	220
3 <sup>rd</sup>	5800

# Raman Spectroscopy



Reported by	$\Delta k$ (A <sub>1g</sub> -E <sup>1</sup> <sub>2g</sub> ) cm <sup>-1</sup>	Layer number of MoS <sub>2</sub>
Korn, T. et al <sup>1</sup>	18	1 layer
Yu, Y. et al <sup>2</sup>	20-21.2	1 layer
Van Thanh, V. et al <sup>3</sup>	21.7	2 layers
Yu, Y. et al <sup>2</sup>	22.4-23.2	2 layers
Yu, Y. et al <sup>2</sup>	23.6-23.9	3 layers
Yu, Y. et al <sup>2</sup>	24.0-24.2	4 layers
Lee, C. et al <sup>4</sup>	24.9	6 layers
Lee, C. et al <sup>4</sup>	25.6	bulk
Van Thanh, D. et al <sup>3</sup>	27.2	bulk

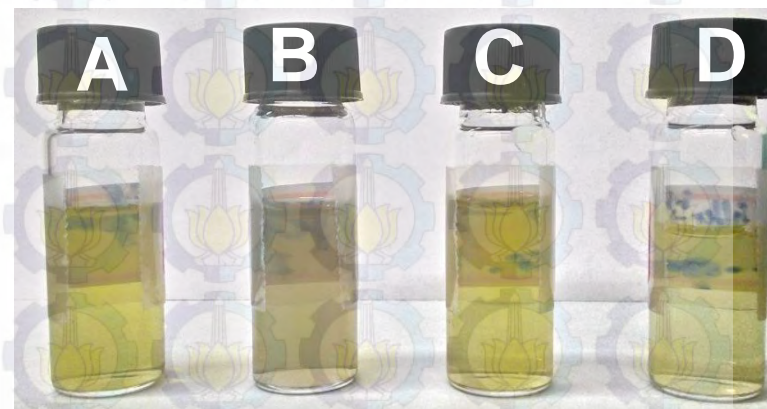
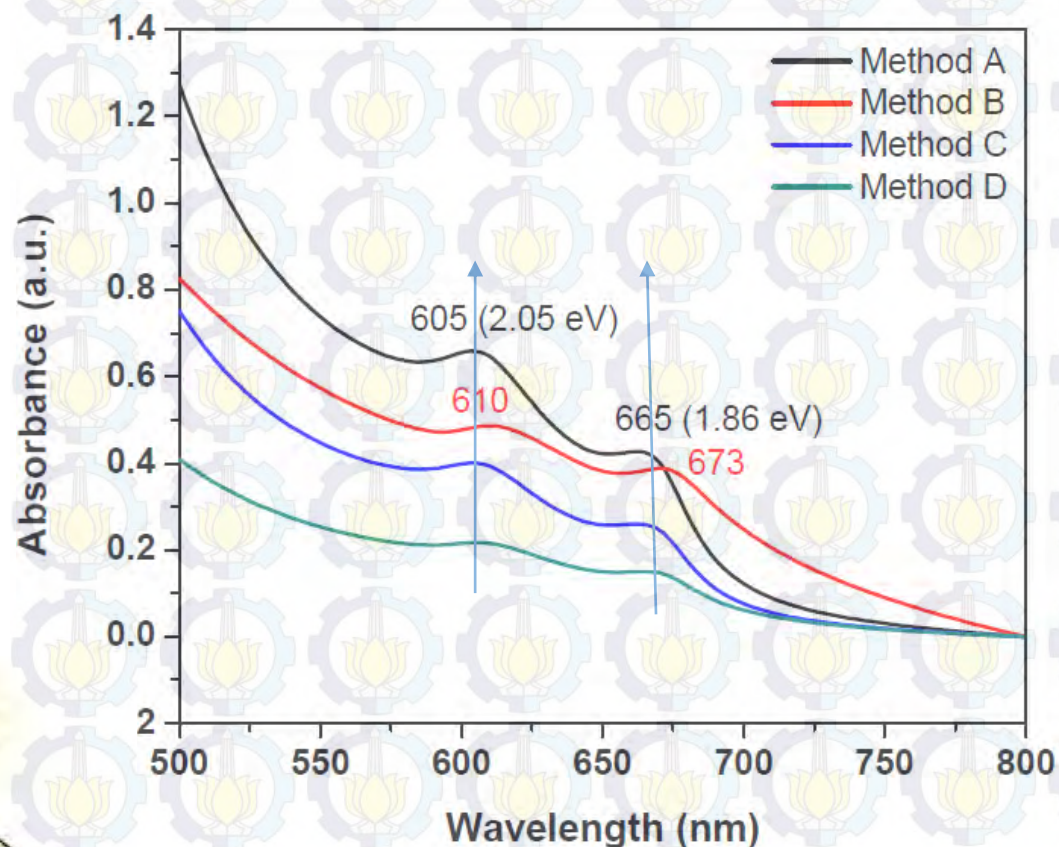
(1) Korn, T. et al., *Applied Physics Letters* **2011**, *99*, 102109.

(2) Yu, Y. et al., *Sci. Rep.* **2013**, *3*, 1866.

(3) Van Thanh, D. et al., *RSC Advances* **2014**, *4*, 15586.

(4) Lee, C. et al., *ACS Nano* **2010**, *4*, 2695.

# Results (2<sup>nd</sup> Part)



- A = Sonic\_38h, 2000 rpm, 60 mins
- B = Sonic\_38h, Filter, Solution
- C = Sonic\_38h, 2000 rpm, 60 mins + Filter, Solution
- D = Sonic\_38h, Filter, Solution + 2000 rpm, 30 mins



The peak positions for electronic transitions are at 605 nm (2.05 eV) and 665 nm (1.86 eV) with energy separation of 0.19 eV<sup>1,2</sup> with smaller lateral dimensions<sup>3,4</sup>

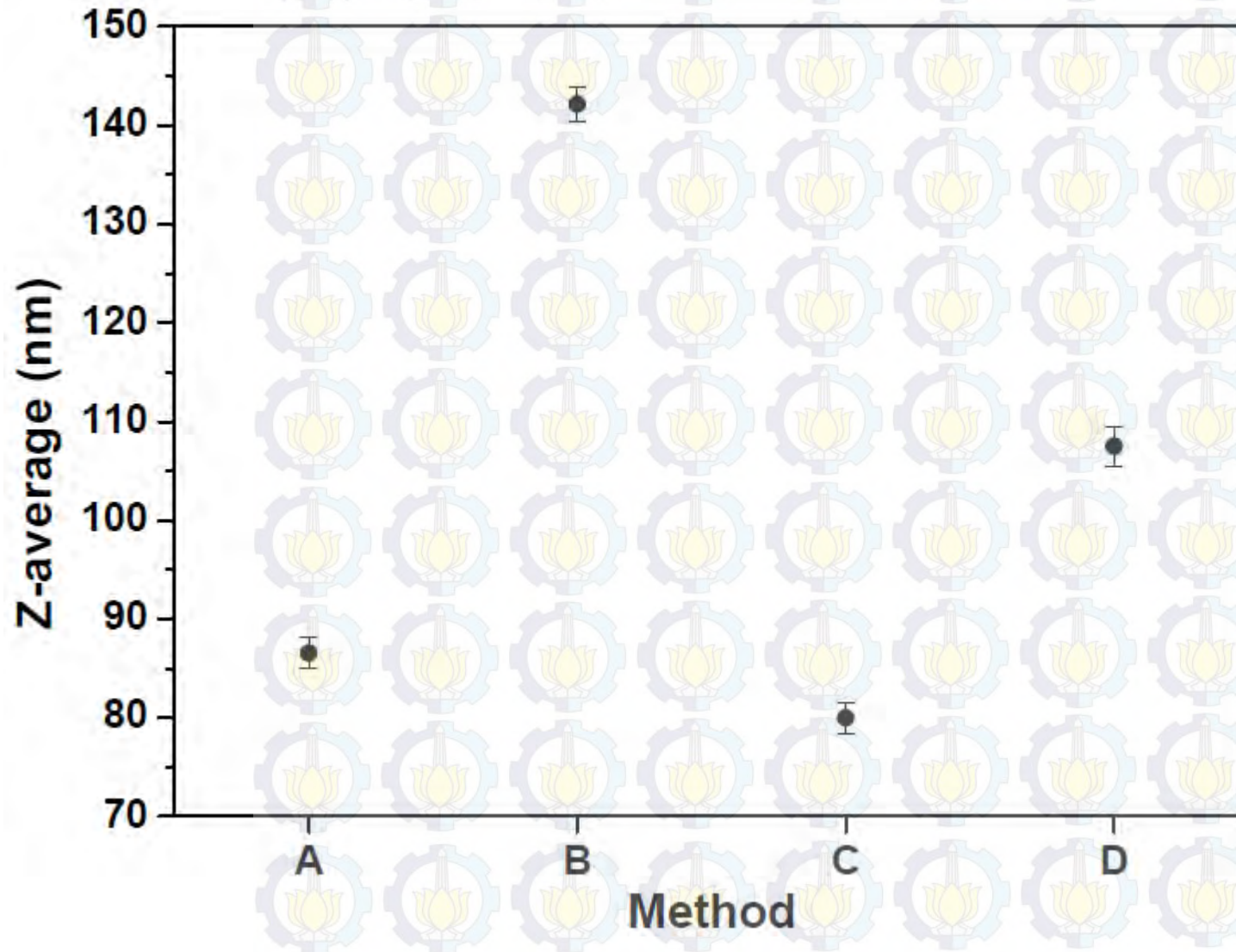
1 Benavente, E., et al. *Coord. Chem. Rev.* **2002**, 224, 87–109

2 Bang, G. S., et al. *ACS Appl. Mater. Interfaces.* **2014**, 6, 7084–7089

3 Bernardi, M., et al. *Nano Letters* **2013**, 13, 3664.

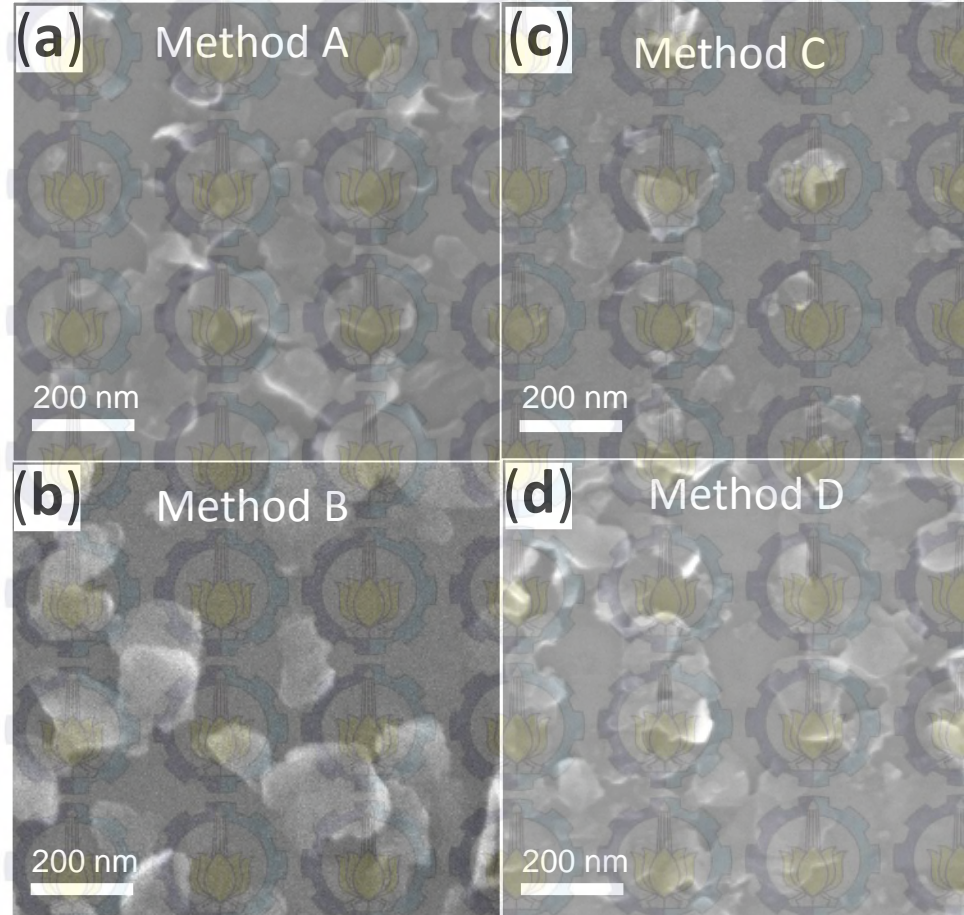
4 Coleman, J. N., et al. *Science* **2011**, 331, 568.

# DLS Analysis



Method	Z-average (d. nm)
A	$87.5 \pm 2.5$
B	$142.5 \pm 2.5$
C	$80.5 \pm 1.5$
D	$107.5 \pm 2.5$

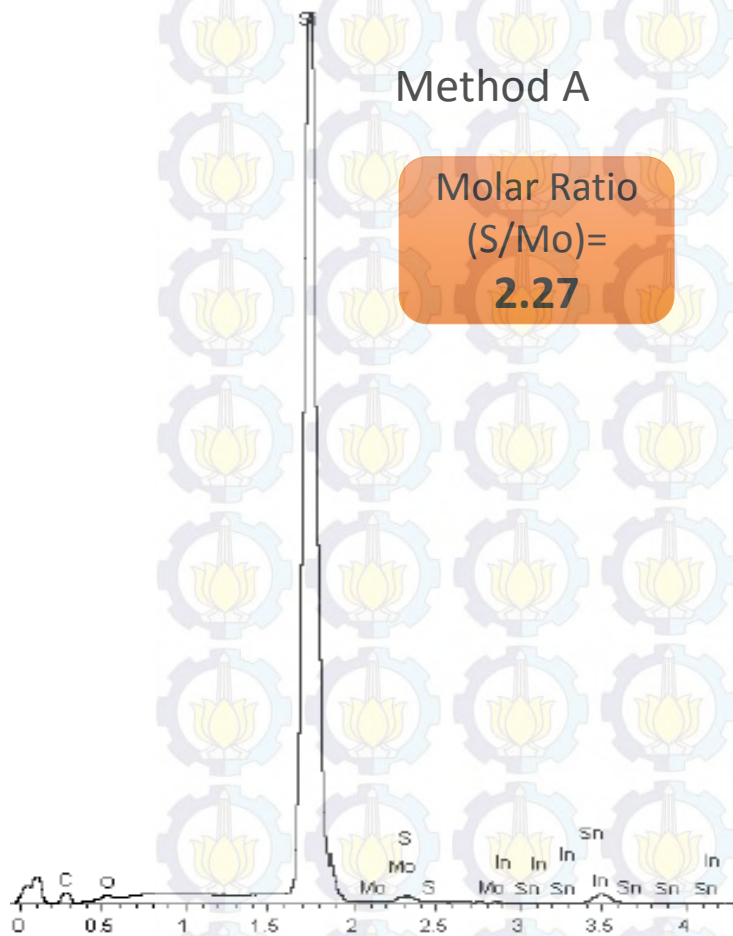
# SEM Images



Sample B  
is Biggest  
one



# EDS-SEM



Method A

Molar Ratio  
(S/Mo)=  
**2.27**

Element	App Conc.	Intensity Corr.	Weight%	Weight% Sigma	Atomic%
C K	0.25	0.2815	7.90	0.21	17.18
O K	0.10	1.0973	0.85	0.06	1.38
Si K	11.75	1.2197	85.80	0.29	79.82
S K	0.06	0.8890	0.61	0.06	0.50
Mo L	0.06	0.6368	0.80	0.18	0.22
In L	0.12	0.7455	1.43	0.09	0.32
Sn L	0.20	0.6688	2.62	0.11	0.58
Totals			100.00		

Method B

Element	App Conc.	Intensity Corr.	Weight%	Weight% Sigma	Atomic%
C K	0.20	0.2767	6.45	0.22	14.28
O K	0.11	1.1055	0.92	0.06	1.53
Si K	11.91	1.2232	87.14	0.31	82.54
S K	0.06	0.8881	0.60	0.06	0.57
Mo L	0.07	0.6362	1.04	0.19	0.29
In L	0.11	0.7460	1.33	0.09	0.31
Sn L	0.19	0.6695	2.53	0.12	0.49
Totals			100.00		

Molar Ratio  
(S/Mo)=  
**1.97**

Method C

Element	App Conc.	Intensity Corr.	Weight%	Weight% Sigma	Atomic%
O K	1.21	1.1649	9.37	0.08	16.38
Si K	10.74	1.2191	79.66	0.22	79.34
S K	0.23	0.9106	2.33	0.07	2.03
Mo L	0.26	0.6523	3.60	0.21	1.05
In L	0.18	0.7541	2.12	0.08	0.52
Sn L	0.22	0.6770	2.93	0.11	0.69
Totals			100.00		

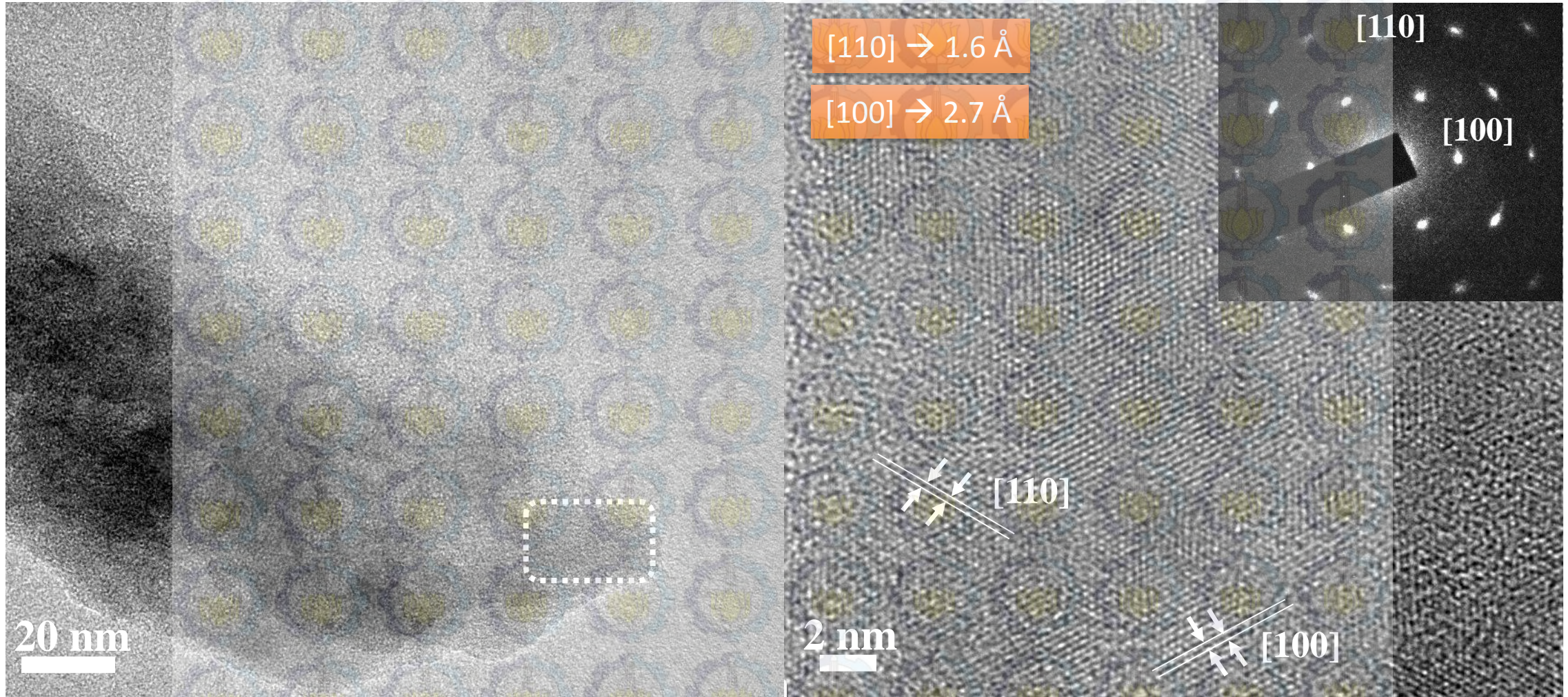
Molar Ratio  
(S/Mo)=  
**1.93**

Method D

Element	App Conc.	Intensity Corr.	Weight%	Weight% Sigma	Atomic%
C K	0.34	0.2896	10.04	0.21	21.32
O K	0.24	1.0872	1.86	0.06	2.96
Si K	11.49	1.2150	80.44	0.29	73.02
S K	0.17	0.8988	1.61	0.07	1.28
Mo L	0.17	0.6438	2.26	0.20	0.60
In L	0.11	0.7452	1.25	0.08	0.28
Sn L	0.20	0.6686	2.55	0.11	0.55
Totals			100.00		

Molar Ratio  
(S/Mo)=  
**2.13**

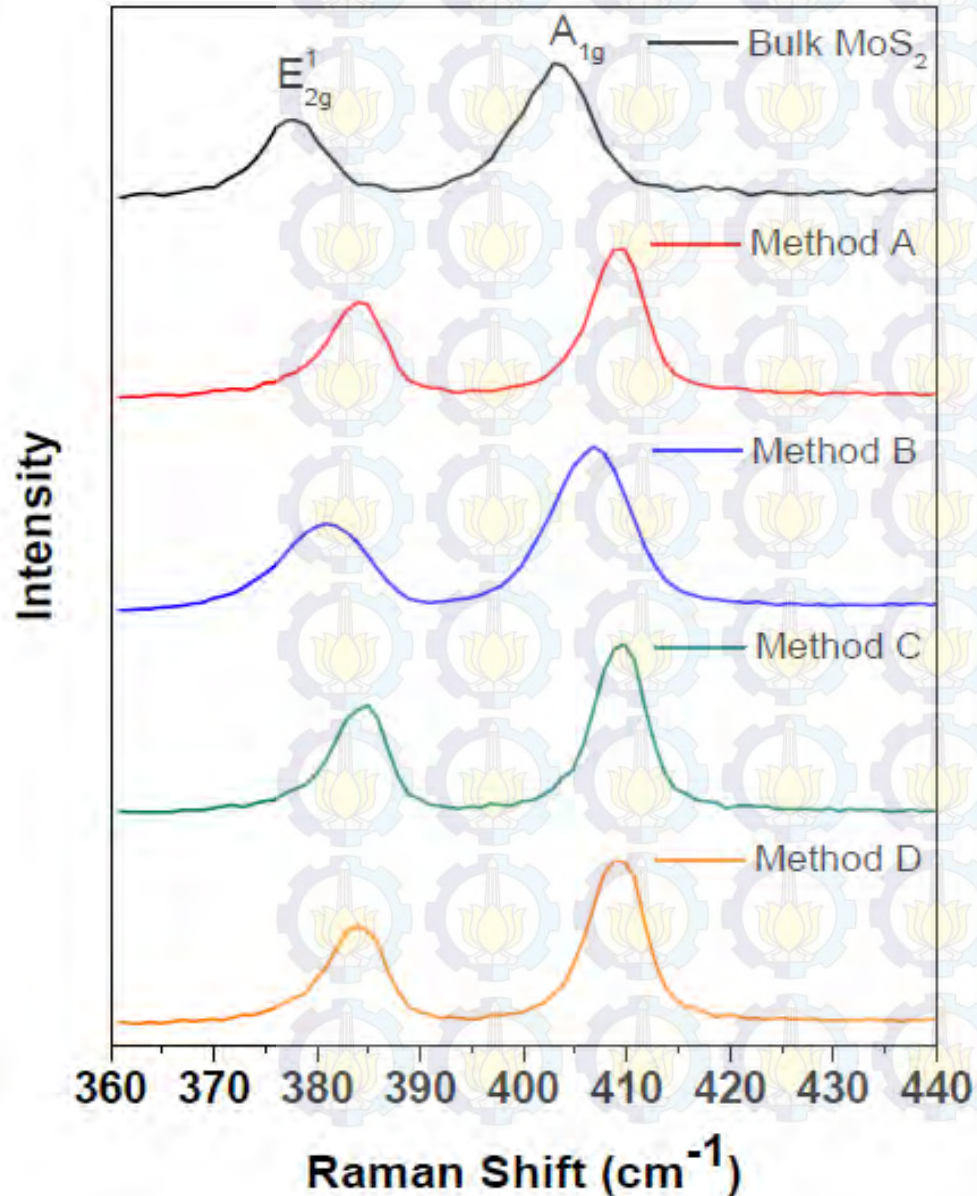
# TEM Analysis



All of images were taken from sample A

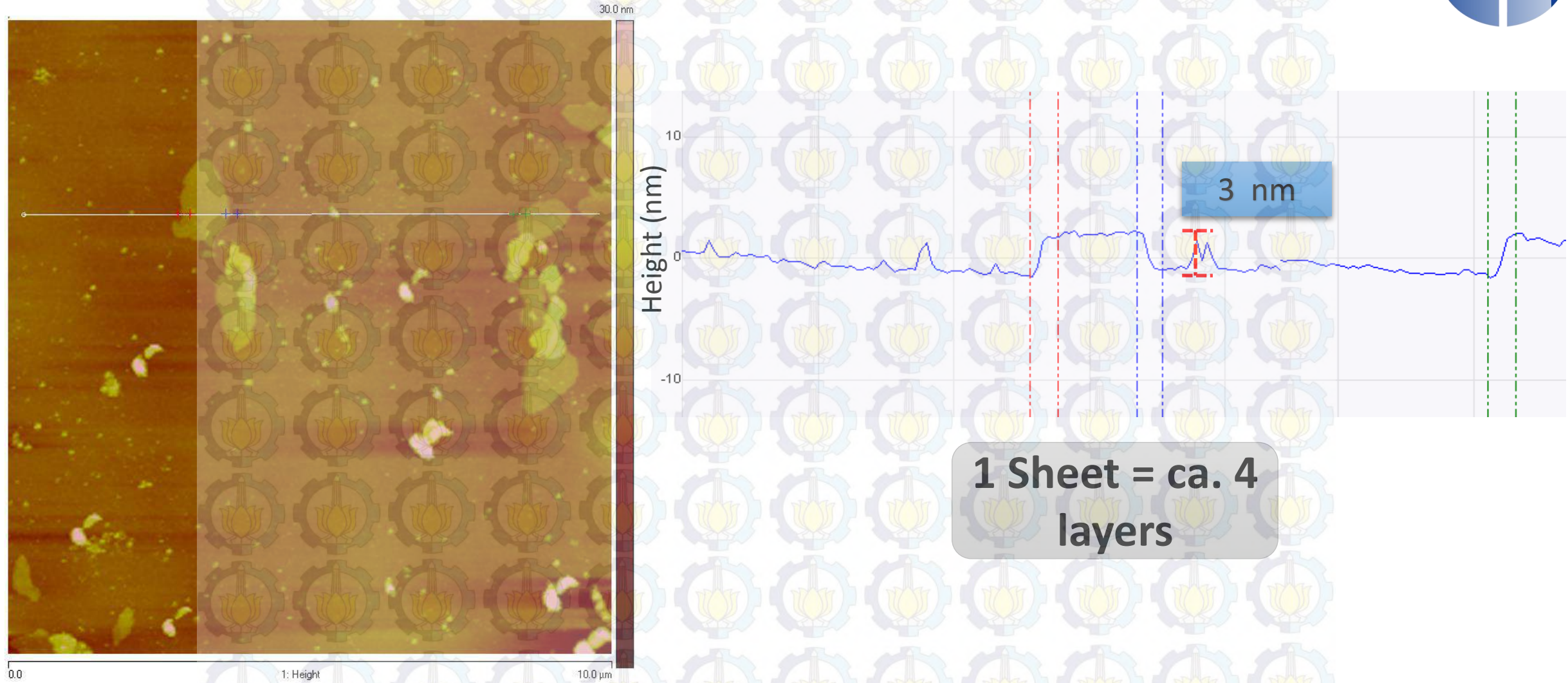


# Raman Spectroscopy



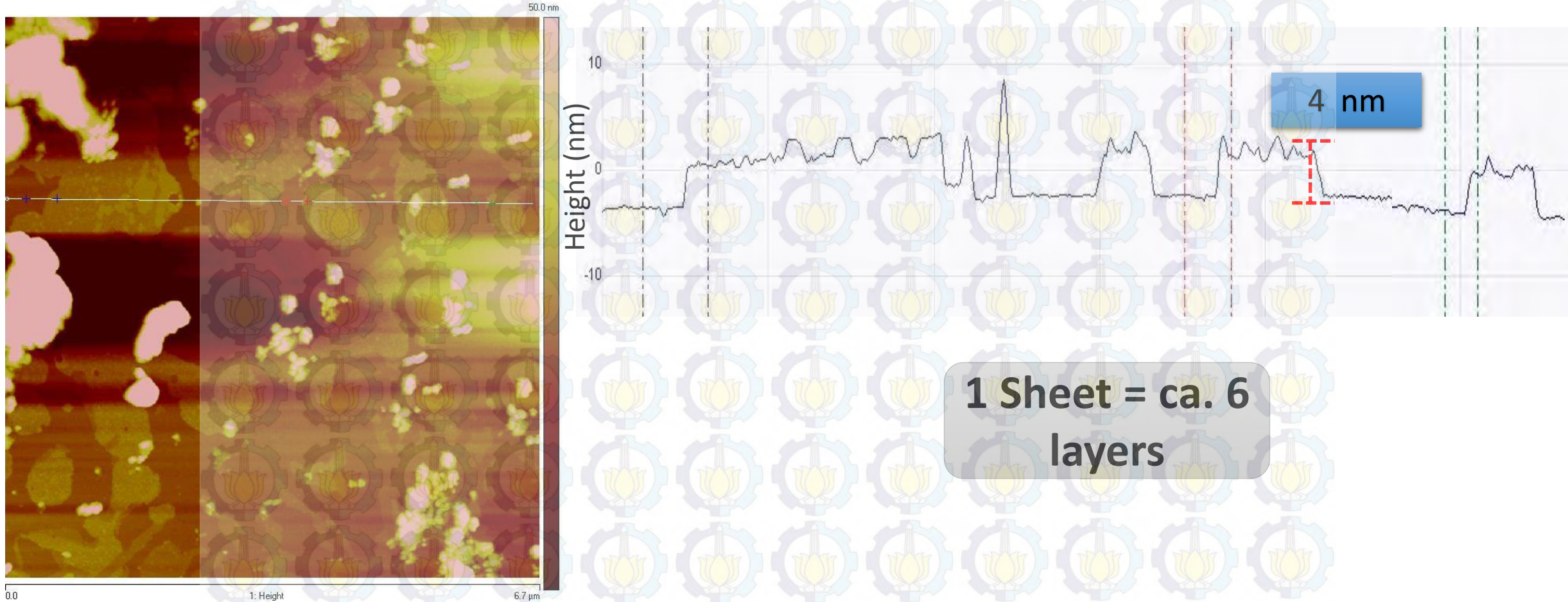
Method	$\Delta k (A_{1g}-E_{2g}^1)$ $\text{cm}^{-1}$	Layer number of $\text{MoS}_2$
A	23.89	3-5 layers
B	24.88	6 layers
C	24.89	6 layers
D	24.88	6 layers

# AFM Analysis



The image was taken from sample A

# AFM Analysis



The image was taken from sample C



# Conclusion

# Conclusion



Few-layer MoS<sub>2</sub> nanosheets have been prepared successfully by the lithium intercalation method.



According to DLS and spectroscopic analysis, the MoS<sub>2</sub> nanosheets have different mean flake lengths ranging 85-145 nm with layer number of MoS<sub>2</sub> is *ca.* 3-6 layers

# Acknowledgement



Prof. Ming-Hsi Chiang  
Prof. Ling-Kang Liu  
Prof. Shawn D. Lin



